1.0

1.1

1.25 1.4

2.8 2.5

2.2

2.0

1.8

1.6

MICROCOPY RESOLUTION TEST CHART

NATIONAL BUREAU OF STANDARDS 1963 A

ARO 13252.6-P

LEVEL

STUDY OF BOUNDARY STRUCTURES

by

RYOICHI KIKUCHI

Covering the Period

May 1, 1976 through April 30, 1979

JUNE 1979

U. S. ARMY RESEARCH OFFICE
Research Triangle Park, NC 27709

DDC
RECEIVED
JUL 26 1979
C

CONTRACT NO. DAAG29—76—C—0026

Hughes Research Laboratories
3011 Malibu Canyon Road
Malibu, California 90265

Approved for public release; distribution unlimited.

The findings in this report are not to be construed as an official Department of the Army position, unless designated by other authorized documents.

79 07 24 045

REPORT DOCUMENTATION PAGE		READ INSTRUCTIONS BEFORE COMPLETING FORM
1. REPORT NUMBER	2. GOVT ACCESSION NO.	3. RECIPIENT'S CATALOG NUMBER
4. TITLE (and Subtitle) STUDY OF BOUNDARY STRUCTURES.		5. TYPE OF REPORT & PERIOD COVERED Final Report. 1 May 1976–30 Apr 1979.
		6. PERFORMING ORG. REPORT NUMBER
7. AUTHOR(s) Ryoichi Kikuchi		8. CONTRACT OR GRANT NUMBER(s) DAAG29-76-C-0026
9. PERFORMING ORGANIZATION NAME AND ADDRESS Hughes Research Laboratories 3011 Malibu Canyon Road Malibu, California 90265		10. PROGRAM ELEMENT. PROJECT, TASK AREA & WORK UNIT NUMBERS
11. CONTROLLING OFFICE NAME AND ADDRESS U.S. Army Research Office P.O. Box 12211 Research Triangle Park, NC 27709		12. REPORT DATE June 1979
		13. NUMBER OF PAGES 163
14. MONITORING AGENCY NAME & ADDRESS(if different from Controlling Office)		15. SECURITY CLASS. (of this report) UNCLASSIFIED
		15a. DECLASSIFICATION DOWNGRADING SCHEDULE NA

16. DISTRIBUTION STATEMENT (of this Report)

Approved for public release; distribution unlimited.

17. DISTRIBUTION STATEMENT (of the abstract entered in Block 20, if different from Report)

18. SUPPLEMENTARY NOTES

The findings in this report are not to be construed as an official Department of the Army position, unless so designated by other authorized documents.

19. KEY WORDS (Continue on reverse side if necessary and identify by block number)

20. ABSTRACT (Continue on reverse side if necessary and identify by block number)

The scalar product (SP) formulation evaluates the boundary free energy σ using the properties of only the two homogeneous phases (without explicitly calculating the boundary profile) that meet at the boundary. The SP method is explored in detail and is now considered ready for further use. — over

The boundary profile can be calculated using the sum method. How to formulate this method using the cluster variation method (CVM) and the natural iteration method (NIM) is presented. Then the sum method is applied to antiphase boundaries (APBs) inside the Cu_3Au phase and to interphase boundaries (IPBs) between Cu_3Au and disordered phases. At a constant composition, σ_{APB} has a maximum at T of about 0.6 of the disordering temperature T_D. At T_D the APB is made of two IPBs separated by the disordered phase in between; this is the complete wetting of the APB at T_D by the disordered phase.

A two-dimensional lattice-gas model was used to study the grain boundary (GB). When the excess entropy S is plotted against $-\log (T_m-T)$, T_m being the melting temperature, the curve is made of two distinctly separated linear portions, indicating the possibility of distinguishing the low-temperature structure from the high-temperature structure of the GB. The transition between the two structures is gradual because of the one-dimensional nature of the GB in this model. The GB at the melting point is completely wet with the liquid phase.

Accession For

NTIS GRA&I	✓
DDC TAB	☐
Unannounced	☐
Justification	

By_____

Distribution/

Availability Codes

Dist	Avail and/or special
A	

TABLE OF CONTENTS

SECTION 1

INTRODUCTION AND SUMMARY

During this contract, three papers were published and two others
are in print. A sixth paper is now being prepared for publication.
These papers (listed in chronological order as Refs. 1 through 6) are
included as Appendices 1 through 6.

These papers fit into two categories: (1) the study of the scalar-
product (SP) expression of the boundary free energy[1,3] and (2) the study
of the structure of the antiphase (APB) and interphase (IPB) boundaries
and grain boundaries using the sum method[2,4,5,6] rather than using the
SP method.

If used with care, the SP method is simpler than the sum method in
obtaining the boundary free energy value. Appendix 1 concludes that the
SP method is reliable, and Appendix 3 extends the original SP formulation
to the case of long-range interaction energy. However, during the three-
year contract period, the SP method has not been used to its full capacity.

The sum method has the advantage that it gives the profile (which
the SP method cannot give) across the boundary; however, the computation
is more lengthy than with the SP method. Appendix 2 introduces a crucial
concept that opens up a way of using the sum method to the boundary
structure, and the procedure is shown with an example in a b.c.c. ordered
structure.

The method developed in Appendix 2 is put to full use in Appendices 4
and 5, in which the APBs within the ordered Cu_3Au phase and the IPBs
between the Cu_3Au phase and the disordered phase are studied. This work
is a revival of cooperation on a similar subject with Dr. John W. Cahn
(now at the National Bureau of Standards). Appendices 4, 5, and 6 rely
heavily on Dr. Cahn's knowledge concerning the metallurgical aspects of
the problems considered.

Three new findings came out of the study of the Cu_3Au phase boundar-
ies. The first is the behavior of the APB free energy σ, which shows
a maximum at a temperature of about 0.6 of the disordering temperature
T_D. The second is the complete wetting of the APB at T_D, and the third

5

is the discovery of a series of second-order phase transitions within the APB slightly below T_D.

The structure of grain boundaries (GBs) was studied during the contract. Although work in this area is not yet complete, preliminary findings are being written up[6] for publication (probably in Physical Review Letters). The main discoveries are first that distinct distinguishable low- and high-temperature structures of the GBs exist, and second that the GB is completely wet at the melting point.

6

SECTION 2

THE NATIONAL ITERATION METHOD WITH CONSTRAINTS

The natural iteration method (NIM) was introduced some time ago[7] in solving high-order simultaneous algebraic equations appearing in the cluster-variation method (CVM). As NIM applications increased, it became necessary to treat cases in which subsidiary conditions were imposed. Appendix 1 shows that these subsidiary conditions can be treated based on a concept similar to the original NIM. Within each iteration step originally designed (which we call the "major" iteration), we do what we call "minor" iterations to satisfy subsidiary conditions. In Ref. 7 we proved that the major iterations always converge; in contrast, we have not proved that the minor iterations converge. However, in all the cases during the last three years in which we used the minor itera-tions, they never failed to converge.

When subsidiary conditions exist, we can classify the variables as independent or dependent. One way of solving the equilibrium state is to minimize the free energy with respect to the independent variables (rather than using Lagrange multipliers for subsidiary conditions). When this is done, the resulting simultaneous equations are not of the form for which the NIM is applicable. In such a case, the Newton-Raphson (N-R) method can certainly be applied, but it is often quite time consuming to find the right initial guess of variables for the N-R method, since otherwise the N-R method does not converge to the desired equilibrium state. In the boundary studies described below in Appendices 2,4,5, and 6, it is practically impossible to use the N-R method because there are several thousand independent variables.

SECTION 3

THE SP FORMULATION OF THE BOUNDARY ENERGY

The scalar-product (SP) formulation of the boundary free energy, first proposed by Clayton and Woodbury,[8] calculates the boundary free energy σ using the formula

$$\exp(-A\sigma/RT) = \sum_{\nu} \left[P_1(\nu)\, P_2(\nu) \right]^{1/2} \quad , \tag{1}$$

where A is the sectional area parallel to the boundary. This formula is written for a lattice structure having phase 1 on the left, phase 2 on the right, and the boundary in between.

We consider a lattice plane parallel to the boundary but far away from it, and well inside the bulk phase i (i = 1 or 2). A configuration within the plane is denoted by ν, and $P_i(\nu)$ is the probability of finding the configuration ν in the plane inside the bulk phase i (i = 1 or 2). Since the right side of Eq. 1 has the form of the SP of two vectors $[P_i(\nu)]^{1/2}$ with i = 1 and 2, we call Eq. 1 the SP formula of the boundary free energy σ.

Eq. 1 is noteworthy in that σ can be calculated by knowing only the properties of the two bulk phases. Expression 1 is reasonable since, when phases 1 and 2 are identical, σ vanishes because $P_i(\nu)$ is normalized to unity and since, when the two bulk phases are very different in their properties, σ is large.

Eq. 1 is rigorous when ν is for the configuration of an infinitely wide plane parallel to the boundary. In Eq. 1, however, approximations must be introduced. In Ref. 9, we had calculated Eq. 1 using the general CVM approach. Another feature of Eq. 1 is that a rigorous proof was lacking; Clayton and Woodbury's proof[8] was not sufficient, and our attempt in Ref. 9 still lacked mathematical rigor. Therefore, to use Eq. 1 with enough confidence, we felt it necessary to use better approximations in the CVM and to compare the result with Onsager's[10] rigorous result in a

9

two-dimensional square lattice Ising model. In Ref. 9, we used the pair
approximation and the square-angle approximateion of the CVM.   In
Appendix 1, we improved the treatment using the double square for the
(1,0)-direction boundary and the W-shaped cluster for the (1,1)-direction
boundary, both for the two-dimensional square Ising lattice. Since the
results are converging to Onsager's rigorous result, we concluded in
Appendix 1 that we can use the general expression (Eq. 1) with
confidence.

The general idea behind the derivation of Eq. 1 is given below.
Consider a three-dimensional system as made up of two-dimensionally
large planes stacked on top of each other. Write the free energy F of
the entire system using the CVM in terms of the probability variables
for two adjoining planes $P_n(\mu,\nu)$, where n indicates the location of the
planes. Minimizing F with respect to $P_n(\mu,\nu)$ yields a relation that
expresses $P_n(\mu,\nu)$ as proportional to $[P_n(\mu) P_{n+1}(\nu)]^{1/2}$. If the system
is homogeneous (i.e., no boundary in it), this procedure leads to the
eigenvalue formulation with which Onsager started.[10] The details of
the derivation of Eq. 1 from this point on are presented in Refs. 3 and 9.

SECTION 4

THE SP EXPRESSION FOR LONG-RANGE INTERACTION

· Eq. 1 considers one lattice plane in each bulk phase. This expression is good when the interaction potential is of the nearest-neighbor type. But it must be modified when the interaction potential goes beyond the nearest neighbor. This problem is worked out in Appendix 3. The resultant formula modifies Eq. 1 as

$$\exp(-A\sigma/RT) = \sum \left[P_1(\nu_1, \nu_2, \ldots, \nu_k) \, P_2(\nu_1, \nu_2, \ldots, \nu_k) \right]^{1/2} \tag{2}$$

$$\times \exp\left[\alpha_1(\nu_1, \nu_2, \ldots, \nu_k) - \alpha_2(\nu_1, \nu_2, \ldots, \nu_k) \right] \;,$$

where $P_i(\nu_1, \nu_2, \ldots, \nu_k)$ is the extension of $P_i(\nu)$ and is the probability that consecutive $1, 2, \ldots, k$ planes inside the bulk phase i take the configurations $\nu_1, \nu_2, \ldots, \nu_k$. The variable $\alpha_1(\nu_1, \nu_2 \ldots, \nu_k)$ is a Lagrange multiplier to guarantee continuity of the form

$$\sum_\mu P_1(\mu, \nu_1, \nu_2, \ldots, \nu_k) = \sum_\xi P_1(\nu_1, \nu_2, \ldots, \nu_k, \xi) \;. \tag{3}$$

Eq. 2 can take into account the long-range interactions up to the interaction between the lattice 1 and the lattice $(k + 1)$. Eq. 2 reduces to Eq. 1 when $k = 1$ and when the symmetry of the lattice

$$P_1(\mu, \nu) = P_1(\nu, \mu) \tag{4}$$

holds.

The general expression, Eq. 2, was tested for the two-dimensional Ising model using a 3 x 2 cluster (i.e., a double-square cluster made of six lattice points) with the "3"-side perpendicular to the boundary.[3] The result agrees well with that of the double square in Appendix 1 when the α terms in Eq. 2 are included.

SECTION 5

THE SUM METHOD OF CALCULATING BOUNDARIES

For lack of a better name, we call this method the sum method in contrast to the SP method. Both methods are based on the CVM mode of thinking,[11] but differ as to the step at which and the method by which they introduce the approximation into the formulation. The two methods produce similar but different results. Although the SP method has the advantage that it can define the transition point within the boundary more clearly,[3] it cannot give the information about the structure across the boundary. The sum method can give the latter information, but usually at the cost of more computer time. Sometimes the approximation used in reducing the SP formulation to the tractable level makes the results unacceptable on a physical basis (such a case is discussed in Appendix 5). A similar trouble has not been encountered with the approximate treatments of the sum method.

When the sum method was used more than ten years ago,[12,13] the NIM was unknown. After the NIM had been devised in 1974,[7] we tried to apply it to the boundary structure. However, a difficulty was encountered in handling the normalization condition for individual planes (parallel to the boundary) until the work of Weeks and Gilmer[14] was noticed.

In Appendix 2, we treat the boundary between the + spin phase and the − spin phase (of the Ising model) in a b.c.c. structure using a tetrahedron (irregular) as the basic cluster. Appendix 2 presents how the idea of Weeks and Gilmer[14] can be incorporated in the CVM-based treatment. The advantages of the latter over the original method in Ref. 14 are that the excess free energy is obtained with ease from the treatment and that it can be extended to larger clusters (e.g., the tetrahedron) systematically.

The result of the tetrahedron treatment in Appendix 2 was compared with that of the pair treatment[12] done many years ago. We also did SP

calculations and compared the results with others. These different
methods compare nicely, and the relations among them are understandable.
As expected, the SP method can pinpoint the transition temperature
within the boundary, but the sum method cannot.

SECTION 6

PHASE BOUNDARY AT T = 0

In Appendix 5, we study the structure of boundaries in the Cu-Au alloy. The work in Appendix 5 was made possible by the previous theoretical calculation of the phase diagram of this alloy worked out by Kikuchi and deFontaine[15,16] extending the work by van Baar.[17]

During the work discussed in Appendix 5, it became evident that many properties of the alloy near $T = 0$ are singular theoretically and hence that more detailed knowledge is needed than that given in Refs. 15 and 16 about the behavior near $T = 0$ of the Cu_3Au phase and also about the phase boundary between Cu_3Au and the disordered phase. Thus, we did the study near $T = 0$ and discussed our results in Appendix 4. The phase diagram of the Cu-Au alloy in Appendix 5 is calculated using the tetrahedron as the basic cluster of CVM and also using the multiatomic interaction potential. The latter means that tetrahedra CuCuCuAu and CuAuAuAu contribute different four-body interaction potentials. The four-body interaction can induce the asymmetry observed in experiments between the Cu-side and the Au-side in the phase diagram.

The four-body effect is represented by two parameters α and β. The range of values of α and β in which the phases Cu_3Au, CuAu, and $CuAu_3$ are stable was investigated. The technique of analysis was the linear programming method, which had been used by Cahn before.[17,18] This part of the work was done by Dr. J.W. Cahn of the National Bureau of Standards, who was cooperating in this project.

In calculating phase diagrams, it is often helpful to know phase boundaries at $T = 0$. There was no theory to treat this problem before. Appendix 4 shows how to do it. At a finite temperature, a phase boundary is calculated by drawing a common tangent to free-energy curves F_1 and F_2 for the two phases plotted against the composition. As discovered in Appendix 4, the phase boundary between the disordered phase and the ordered Cu_3Au phase can be calculated by the following procedure.

Configurations of the tetrahedral cluster are limited to CuCuCuCu and CuCuCuAu only (the rest of the configurations, e.g., CuCuAuAu, having zero probability of appearance). Using these two configurations, we write the entropy expressions for the disordered phase S_D and for the ordered phase S_O as functions of the composition. Figure 7 of Appendix 4 shows an example. Then we draw a common tangent to the S_D and S_O curves. The points of contact of the common tangent to S_D and S_O give the two composition values of the coexisting phases.

The procedure of finding the common tangent to S curves is equivalent to the following. At a finite temperature, constructing the common tangent to the F curves is equivalent to finding the intersection of two grand potential $\hat{G}$ curves for the two phases plotted against the chemical potential μ. When T is infinitesimally small, μ and $\hat{G}$ near the phase boundary can be expanded as

$$\mu = \mu_o + akT + \ldots$$

$$\hat{G} = \hat{G}_o + bkT + \ldots \quad ,$$

(5)

where μ_o and $\hat{G}_o$ are common to the two coexisting phases. The coefficient b is derived when the value of a is assigned. Then two b curves for the two phases are plotted against a to find the intersection, which gives the coexisting phases for the limit $T \to 0$. It is illustrated in Figure 8 of Appendix 4.

SECTION 7

INTERPHASE AND ANTIPHASE BOUNDARIES IN Cu_3Au

The f.c.c. lattice can be separated into four equivalent simple cubic sublattices. When one of the s.c. sublattices is preferentially occupied by Au atoms and the other three s.c. sublattices are equivalent, we obtain the Cu_3Au structure (also called the $L1_2$ structure).

An APB in Cu_3Au is formed when the Au atoms on the left side of the boundary preferentially occupy sublattice 1 and those on the right side preferentially occupy sublattice 2. (See Figures 1, 2, and 3 of Appendix 5.) When the left side of the boundary is the Cu_3Au phase and the right side is a disordered phase, we call the boundary the interphase boundary (IPB).

APBs and IPBs are studied in Appendix 5 using the sum method. The technique is an application of one developed in Appendix 2. We take a tetrahedron as the basic cluster and assign a variable $Z_n(i,j,k,\ell)$ to the configuration (i,j,k,ℓ) of the tetrahedron. The Cu and Au atoms are designated by $i = 1$ and 2, and n indicates the location of the tetrahedron relative to the boundary.

The grand potential

$$\hat{G} = F - (\mu_1 N_1 + \mu_2 N_2) \tag{6}$$

for the entire system including the boundary region is written in terms of $Z_n(i,j,k,\ell)$ and is minimized (keeping T and μ fixed) with respect to the Zs. (We can choose $-\mu_1 = \mu_2 \equiv \mu$.) The resulting equations are solved for $Z_n(i,j,k,\ell)$ using the NIM. The excess free energy σ attributed to the boundary is calculated as the difference between $\hat{G}$ thus calculated and the value of $\hat{G}$ for the homogeneous phase.

The σ curves for the APBs are given in Figure 6 of Appendix 5. The special features are the following:

(1) A σ curve for a constant μ increases monotonically as T decreases. Although in the phase diagram (Figure 5 of Appendix 5) all the μ-constant curves converge to

17

the stoichiometric state $x = 1/4$ as $T \to 0$, the σ curves for different μs tend to different values as $T \to 0$. This is one of the singular behaviors of the Cu_3Au phase near $T = 0$.

(2) The lower two σ curves in Figure 6 of Appendix 5 are for constant composition x, the x being the value for the peak (the congruent point) of the Cu_3Au phase. Different from the μ-constant curves, these two σ curves go through maxima at about 0.6 of the disordering temperature and reduce to zero at $T = 0$.

(3) The general shape of the lower two σ curves in Figure 6 of Appendix 5 resembles that of the shear strength curves of Ni-based superalloys (e.g., Ni_3Al).[19,20] The resemblance implies that the APB behavior is an important factor in understanding the shear strength of these superalloys. The APB and the shear strength are related through the creation of an APB when a dislocation enters a dispersed ordered precipitate within the disordered matrix.

(4) The disorder-Cu_3Au IPBs were calculated and are shown in Figures 7 and 8 of Appendix 5. The noteworthy feature is that the IPB is exactly one-half of the APB at the same point in the phase diagram. In other words, when the disordered phase (D) coexists with the Cu_3Au phase, the APB inside the Cu_3Au phase at this point is made of two D-Cu_3Au IPBs. This property, which is also seen by comparing Figure 11(a) with Figure 11(b) in Appendix 5, means that the APB at this point is completely wet with the disordered phase.

(5) The density profiles across the boundary are shown in Figures 11(a) and 12 of Appendix 5. Although the bulk phase is Cu_3Au ($L1_2$) structure, there is a CuAu ($L1_0$) type region near the center of the boundary. The onset of the $L1_0$ region is interpreted as a second-order phase change from the behavior of the plane next to the center as shown in Figure 14 of Appendix 5.

18

SECTION 8

GRAIN BOUNDARY STUDIES

As the first step in studying the structure of grain boundaries, we worked on a two-dimensional lattice-gas model that is capable of producing gas, liquid, and solid phases and also two different orientations of the solid phase. The region near the grain boundary is shown in Figure 1 of Appendix 6.

The grain boundary free energy σ for a constant chemical potential μ is shown in Figure 3 of Appendix 6. Along with σ, we calculated the excess entropy S due to the grain boundary. A remarkable discovery is that the S curve is clearly made of two portions, as shown in Figure 5 of Appendix 6. For low temperatures, $T < 0.3 \, T_m$ (T_m being the melting temperature for this μ), S is almost equal to $k\ell n2$. For high temperatures, $T > 0.6 \, T_m$, S is linear in $-\log(T_m - T)$, diverging at T_m.

This remarkable property of S, combined with the calculated values of σ for the grain boundary and the IPB (the boundary between the solid phase and the liquid phase), indicates that the grain boundary is completely wet at the melting point.

REFERENCES

1. R. Kikuchi, "Natural Iteration Method and Boundary Free Energy," J. Chem. Phys. <u>65</u>, 4545 (1976).

2. R. Kikuchi, "Structure of Phase Boundaries," J. Chem. Phys. <u>66</u>, 3352 (1977).

3. R. Kikuchi, "The Scalar-Product Expression of Boundary Free Energy for Long-Range Interacting Systems," J. Chem. Phys. <u>68</u>, 119 (1978).

4. J.W. Cahn and R. Kikuchi, " Ground State of F.C.C. Alloys with Multiatom Interactions," Acta Met. (in press).

5. R. Kikuchi and J.W. Cahn, "Theory of Interphase and Antiphase Boundaries in F.C.C. Alloys," Acta Met. (in press).

6. R. Kikuchi and J.W. Cahn, "A Transition in Grain Boundaries (Antiphase Boundaries) in a Two-Dimensional Lattice-Gas Model" (to be published).

7. R. Kikuchi, "Superposition Approximation and Natural Iteration Calculation in Cluster-Variation Method," J. Chem. Phys. <u>60</u>, 1071 (1974).

8. D.B. Clayton and G.W. Woodbury, Jr., "Interface Structure of the Two-Dimensional, Square Ising Model," J. Chem. Phys. <u>55</u>, 3895 (1971).

9. R. Kikuchi, "Boundary Free Energy in the Lattice Model. I. General Formulation," J. Chem. Phys. <u>57</u>, 777 (1972).

10. L. Onsager, "Crystal Statistics. I. A Two-Dimensional Model with an Order-Disorder Transition," Phys. Rev. <u>65</u>, 117 (1944).

11. R. Kikuchi, "The Cluster Variation Method," J. de Physique <u>38</u>, C7-307 (1977).

12. R. Kikuchi and J.W. Cahn, "Theory of Domain Walls in Ordered Structures — II. Pair Approximation for Nonzero Temperatures." J. Phys. Chem. Solids <u>23</u>, 137 (1962).

13. J.W. Cahn and R. Kikuchi, "Theory of Domain Walls in Ordered Structures — III. Effect of Substitutional Deviations from Stoichiometry," J. Phys. Chem. Solids <u>27</u>, 1305 (1966).

14. J.D. Weeks and G.H. Gilmer, "Pair Approximation Equations for Interfaces and Free Surfaces in the Ising Model," J. Chem. Phys. <u>63</u>, 3136 (1975).

15. R. Kikuchi and D. de Fontaine, "Theoretical Calculation of Phase Diagrams Using the Cluster Variation Method," National Bureau of Standards SP-496, 967 (1977).

16. D. de Fontaine and R. Kikuchi, "Fundamental Calculations of Coherent Phase Diagrams," National Bureau of Standards SP-496, 999 (1977).

17. M.J. Richards and J.W. Cahn, "Pairwise Interactions and the Ground State of Ordered Binary Alloys," Acta Met. 19, 1263 (1971).

18. S.M. Allen and J.W. Cahn, "Ground State Structures in Ordered Binary Alloys with Second Neighbor Interactions," Acta Met. 20, 423 (1972).

19. S.M. Copley and B.H. Kear, "Temperature and Orientation Dependence of the Flow Stress in Off-Stoichiometric Ni_3Al (γ' Phase)," Trans. Met. Soc. AIME 239, 977 (1967).

20. S.M. Copley and B.H. Kear, "A Dynamic Theory of Coherent Precipitation Hardening with Application to Nickel-Base Superalloys," Trans. Met. Soc. AIME 239, 984 (1967).

APPENDIX 1

(Reference [1])

NATURAL ITERATION METHOD AND
BOUNDARY FREE ENERGY

by

R. Kikuchi

Natural iteration method and boundary free energy*

Ryoichi Kikuchi

Hughes Research Laboratories, Malibu, California 90265
(Received 23 August 1976)

The natural iteration technique, which was proposed by the author as a method of solving equations of the cluster variation method, is extended to the case in which variables are subject to subsidiary conditions due to symmetry requirements; the subsidiary conditions are treated by minor iterations at each step of the major iteration. The technique of evaluating the second order transition point for such problems is presented; the technique applies, in general, to problems for which the number of variables is large. As examples, cluster variation methods using a five-point W-shaped cluster and a six-point double-square cluster are presented for the two dimensional Ising model. An improved proof of the scalar product (SP) expression for the boundary free energy is given. The results of the examples are used in the SP expression to evaluate the boundary free energy of the Ising model in order to test the accuracy of the approximations involved.

I. INTRODCUTION

This paper has dual purposes. One is to show in the natural iteration (NI) method how to treat subsidiary conditions and how to calculate the second-order transition point, and the other is to report further results obtained by the scalar product expression of the boundary free energy. These two are closely tied, as the results of the former are used in the calculation of the latter.

The cluster variation (CV) method[1,2] for cooperative systems had been in use for many years. One basic difficulty which had prevented wide use of the method had been the step to solve simultaneous algebraic equations of high orders.[3] This difficulty had been dissolved by the natural iteration method.[4] Many applications of the new technique have been and are currently worked out.[5-8]

The applications of the NI method, however, have been limited to either the pair approximation or the tetrahedron approximation (both for the fcc and the bcc lattices), which do not need subsidiary conditions on the probability variables except for the normalization to unity. As the application of the NI method widens, need arises that additional conditions or the probability variables are to be taken into account without damaging the versatility of the NI method. It will be shown in Secs. II and III that subsidiary conditions due to symmetries of variables can be treated by way of iterations of a kind similar to the main NI procedure.

One of the advantages of the NI method is that it is unnecessary to carefully choose the independent variables and then to write the relations among the dependent and independent variables. When we work with first-order phase transitions, there is no particular complication. In the case of the second-order transition, however, the critical point T_c is to be calculated as the point at which a certain determinant vanishes. A method of calculating elements of the determinant, without explicitly listing relations among the dependent and independent variables and hence without spoiling the spirit of the NI technique, is presented in Sec. II. It is believed timely and useful to report on these techniques of handling subsidiary conditions and the determinant for T_c because the interest in the CV method is

growing.[9-13] The iteration method recently proposed by Weeks and Gilmer[14] for studying boundary structures can also be interpreted as a variation of the NI method with subsidiary conditions[15]

When the author wrote a paper on the scalar product (SP) expression of the boundary free energy,[16] supplementing the work by Clayton and Woodbury,[17] the proof of the SP expression was incomplete. For that reason, the surface tension σ of the boundary between two two-dimensional Ising spin phases was calculated using the proposed method and was compared[18] with the exact result due to Onsager. Since the publication, the proof of the SP expression has been improved and it is reported in Sec. IV. Results of Secs. II and III are used in the SP expression to calculate the boundary free energy in Sec. V.

II. THE W-APPROXIMATION

A. Free energy and its minimization

We present discussions on the NI method in this section using the W-approximation of the two-dimensional Ising net as an example. This approximation uses a five-point cluster, A-B-C-D-E of Table IA, as the basic cluster. The degeneracy factor Ω_W for this case was shown in Table I of Ref. 2 and is reproduced in Table IB. Reference 2 is to be consulted for the meaning of the parentheses notation in Ω_W. Expression Ω_W is used in writing the entropy of the system as

$$S = k \ln \Omega_W . \tag{2.1}$$

The plus and minus spins are designated by $i = 1$ and 2, respectively. The probability of finding a spin configuration i-j-k-l-m on A-B-C-D-E points of the cluster is written as w_{ijklm}, as shown in Table IC. Other variables, v, z and y, are also defined in Table IC. Using these variables, the entropy (2.1) for a system of N lattice points can be written explicitly as

$$\frac{S}{kN} = \left[\sum \mathcal{L}(v_{ijkl}) + \sum \mathcal{L}(v_{jklm}) \right] - \sum \mathcal{L}(w_{ijklm}) + \sum \mathcal{L}(z_{ikm}) - \sum \mathcal{L}(y_{jl}) , \tag{2.2}$$

where the $\mathcal{L}$ operator is defined as

4545

TABLE I. The W cluster.

(a) THE W-CLUSTER
A-B-C-D-E

(b) THE Ω_W FACTOR

(c) DEFINITION OF PROBABILITY VARIABLES

$$\mathcal{L}(x) = x \ln x - x . \tag{2.3}$$

Each summation in (2.2) is to be done over the values 1 and 2 of the subscripts in the summand. The two v terms in (2.2) are equal, but are written separately in order to make the subsequent NI formulation symmetric.

In a system of N lattice points, the total number of W-clusters we are interested in, i.e., those lying parallel to each other, is $2N$. The energy of the system is then written as

$$E = 2N \sum \epsilon_{ijklm} w_{ijklm} , \tag{2.4}$$

where ϵ_{ijklm} is the energy per W-cluster and is written, in turn, in terms of pair-wise energy ϵ_{ij} as

$$\epsilon_{ijklm} = \tfrac{1}{4}(\epsilon_{ij} + \epsilon_{jk} + \epsilon_{kl} + \epsilon_{lm}) . \tag{2.5}$$

We define ϵ_{ij} as

$$\epsilon_{ij} = -\epsilon , \quad \text{when } i = j ,$$
$$\epsilon_{ij} = +\epsilon , \quad \text{when } i \neq j . \tag{2.6}$$

Our program is to minimize the free energy with respect to w_{ijklm}'s. The w variables obey not only the normalization:

$$\sum_{i,j,k,l,m} w_{ijklm} = 1 , \tag{2.7}$$

but also two symmetry requirements. One of them is the "mirror" symmetry:

$$w_{ijklm} = w_{mlkji} , \tag{2.8}$$

and the other is the "translational" symmetry:

$$u_{jkl} = \sum_m w_{ijklm} = \sum_m w_{mijkl} . \tag{2.9}$$

The mirror symmetry is easy to take care of because the NI treatment, to be described in detail below, keeps this symmetry intact through the iterations if the initial input w's satisfy the symmetry.

The translational symmetry is taken into account by adding the following Lagrange terms to the free energy expression:

$$L_\alpha = \sum_{i,j,k,l} \alpha_{ijkl} \sum_m (w_{ijklm} - w_{mijkl}) ,$$
$$= \sum_{i,j,k,l,m} (\alpha_{ijkl} - \alpha_{jklm}) w_{ijklm} . \tag{2.10}$$

We can now prove that the Lagrange multipliers α's obey the following symmetry relations:

$$\alpha_{ijkl} = -\alpha_{lkji} . \tag{2.11}$$

The proof is the following. We form

$$\alpha_{ijkl} \sum_m (w_{ijklm} - w_{mijkl}) + \alpha_{lkji} \sum_m (w_{lkjim} - w_{mlkji})$$

$$= \tfrac{1}{2}(\alpha_{ijkl} + \alpha_{lkji}) \sum_m ((w_{ijklm} - w_{mijkl}) + (w_{lkjim} - w_{mlkji}))$$

$$+ \tfrac{1}{2}(\alpha_{ijkl} - \alpha_{lkji}) \sum_m ((w_{ijklm} - w_{mijkl}) - (w_{lkjim} - w_{mlkji})) \tag{2.12}$$

We see that the first summand in $\sum_m$ vanishes when the mirror symmetry (2.8) is satisfied; this allows us to choose $\alpha_{ijkl} + \alpha_{lkji} = 0$, which is (2.11). This relation (2.11) was also proved in (II.9) of Ref. 2 in general notation.

Using relations obtained so far in this section, we can write the free energy $F = E - TS$ as

$$\frac{\beta F}{N} = \frac{\beta E}{N} - \frac{S}{kN}$$
$$- 2 \sum_{ijklm} (\alpha_{ijkl} + \alpha_{mlkj}) w_{ijklm} + \lambda \beta \left(1 - \sum w_{ijklm}\right) , \tag{2.13}$$

where

$$\beta = 1/kT ,$$

and we use E of (2.4) and S/kN of (2.2) in (2.13). We then minimize F in (2.13) with respect to w_{ijklm}. In order to keep the symmetry, we use

$$v_{ijkl} = \sum_m w_{ijklm} ,$$

and

$$v_{jklm} = \sum_i w_{ijklm} , \tag{2.14}$$

for v_{ijkl} and v_{jklm} in (2.2). The differentiation of (2.13) leads to

$$\ln w_{ijklm} = \tfrac{1}{2}\lambda\beta + \ln w_{ijklm}^{(0)} + \alpha_{ijkl} + \alpha_{mlkj} , \tag{2.15a}$$

where

$$\ln w_{ijklm}^{(0)} = -\beta \epsilon_{ijklm} + \tfrac{1}{2}\ln(v_{ijkl} v_{jklm} z_{klm}/y_{jl}) . \tag{2.15b}$$

We have introduced $w_{ijklm}^{(0)}$ for the sake of convenience in

the following discussions.

Equation (2.15) is the "superposition" relation[4] which is ready to be used in the NI treatment. Except for α's, which will be discussed in the next subsection, the NI starts with an input set $\{w_{ijklm}\}$, and calculates the right-hand side of (2.15a) to obtain the output set $\{\hat{w}_{ijklm}\}$. The input v's are derived from w's using (2.14), and the input z's and y's are from

$$z_{ikm} = \sum_{j,l} w_{ijklm} ,$$

$$y_{il} = \sum_{n} z_{jln} .$$

$$(2.16)$$

In order to start the NI procedure, we assign the value of kT/ϵ and initial guess of w_{ijklm}. Instead of specifying all 32 w's independently, it is sufficient to start with giving probabilities of a single spin x_1 and x_2 ($x_1 + x_2 = 1$) and then write w's as a Bragg–Williams-type product:

$$w_{ijklm} = x_i x_j x_k x_l x_m .$$

$$(2.17)$$

This initial assignment works even for low temperatures.

We call the iteration step of going from the input set $\{w_{ijklm}\}$ to the output set $\{\hat{w}_{ijklm}\}$, which is the next input set, the "major" iteration step. Convergence of the major iteration is tested by the following sum for each step:

$$\Delta_{maj} = \sum | \ln w_{ijklm} - \ln \hat{w}_{ijklm} | .$$

$$(2.18)$$

A typical example of Δ_{maj} as a function of the major iteration step is shown in Fig. 1. It is better to use a logarithm in defining Δ_{maj} as in (2.18) than using a simple sum $\sum | w_{ijklm} - \hat{w}_{ijklm} |$ used in Ref. 4, because some of the w's become very small for low temperatures and do not contribute to $| w - \hat{w} |$, although they do to (2.18). We need accurate digits of these small w's, particularly in calculating the boundary free energy using the scalar product expression in Sec. V.

In the present problem, Fig. 1 shows that Δ_{maj} behaves in the same way as was reported in Ref. 4 and $\log \Delta_{maj}$ decreases linearly as the iteration progresses. It is safe to use $\Delta_{maj} = 10^{-7}$ as the criterion of the convergence.

We can prove that when the iteration has converged, the expression (2.13) reduces to

$$\lambda = F/N .$$

$$(2.19)$$

B. The minor iterations

The remaining question in the present case is how to handle α's which are to be determined so that the translational symmetry (2.9) is satisfied. When we substitute (2.15a) in (2.9), we obtain

$$\alpha_{ijkl} = \tfrac{1}{2} \ln(S_{N,ijkl}/S_{D,ijkl}) ,$$

$$(2.20a)$$

where

$$S_{N,ijkl} = \sum_{m} w_{mijkl}^{(0)} \exp(\alpha_{mijk}) ,$$

$$(2.20b)$$

$$S_{D,ijkl} = \sum_{m} w_{ijklm}^{(0)} \exp(\alpha_{mikj}) .$$

Our procedure of satisfying (2.20) is to do a series of "minor" iterations to determine α's at each "major" iteration step.

In the method we propose, we use input α's on the right-hand side of (2.20a) and evaluate α_{ijkl} on the left-hand side as the output of a minor iteration step. This output is used as the next input on the right-hand side. This technique for the minor iteration is of the same spirit as the NI major iteration steps and, although we have not analytically proved convergence of the minor iterations, they do converge in all similar cases we have worked so far. Speaking in qualitative terms, the output α_{ijkl} in (2.20) is derived as a weighted average of input α's on the right-hand side; the averaging process is interpreted as helping convergence.

At each major iteration step, the minor iterations are tested using

$$\Delta_{mnr} = \sum_{ijkl} | \alpha_{ijkl} - \hat{\alpha}_{ijkl} | .$$

$$(2.21)$$

When Δ_{mnr} becomes less than a criterion value $\Delta_{mnr,c}$, the iteration is judged converged. The number of minor iterations for one major iteration step depends on $\Delta_{mnr,c}$ and also on the progress of the major iterations, and gradually reduces to one as the major iteration approaches its convergence. A typical example of the behavior of the minor iteration is shown in Fig. 2.

As an alternative method, the simultaneous nonlinear equations in (2.20) for α's can be solved by the Newton–
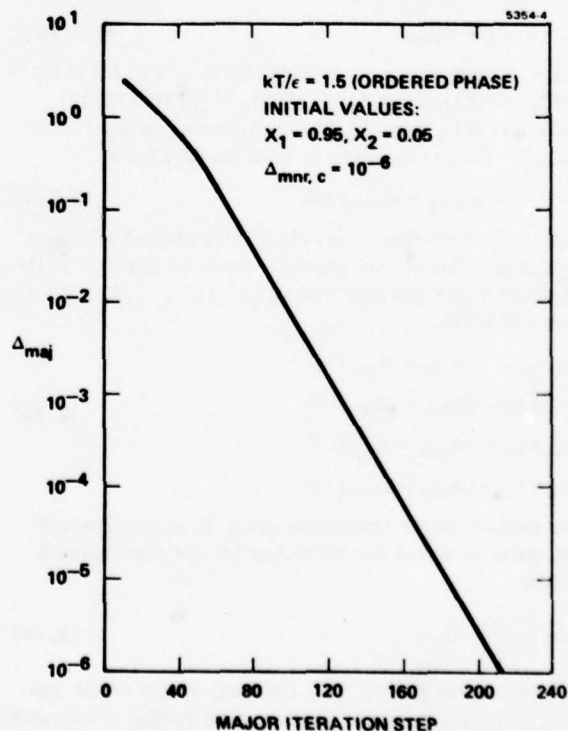

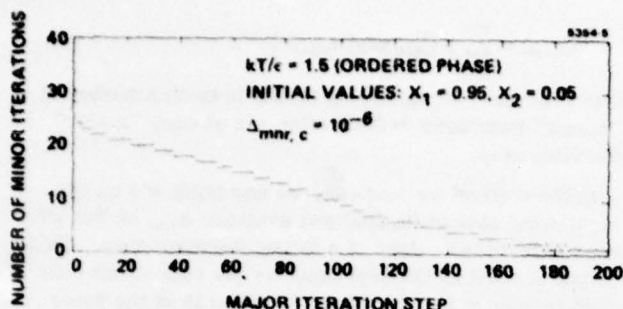FIG. 1. Convergence pattern of the major iterations.

FIG. 2. Convergence pattern of the minor iterations.

Raphson (N-R) method. The convergence is expected to be good because both positive and negative values of α's are allowed and there is no danger of overshooting into unphysical regions. Different from the method we are proposing in this section, however, the N-R procedure needs evaluation of derivatives and an inversion of a matrix. In the present example, the N-R method is not so bad because the number of independent α's is only six in the ordered phase. For problems in which the number of independent α's is larger, the method we are proposing is faster.

C. Determination of T_c

For the sake of convenience, we call a plus spin and a minus spin complements, and write the complement of the subscript i as i' ($i + i' = 3$). The variables w_{ijklm} and $w_{i'j'k'l'm'}$ become identical in the disordered phase and we define their difference as the long-range order parameter ξ_μ. (For ξ we use a different subscript system.) Because of the mirror symmetry, the number of long-range order parameters is ten. An example is

$$\xi_7 \equiv w_{12112} - w_{21221} . \tag{2.22a}$$

The list of subscripts of the first term w's is (11111), (11112), (11121), (11211), (11122), (11212), (12112), (21112), (11221), and (12121) in the order of $\mu = 1$, $2, \ldots, 10$. It is convenient to rewrite (2.22a) as

$$g_7 \equiv \xi_7 - (w_{12112} - w_{21221}) = 0. \tag{2.22b}$$

Beside the differences of w's differences of α's also vanish in the disordered phase and can be defined as the long-range order parameters ξ_μ ($\mu = 11, \ldots, 14$). There are four of them:

$$g_{11} \equiv \xi_{11} - (\alpha_{1112} - \alpha_{2221}) = 0$$
$$g_{12} \equiv \xi_{12} - (\alpha_{1121} - \alpha_{2212}) = 0$$
$$g_{13} \equiv \xi_{13} - (\alpha_{1122} - \alpha_{2211}) = 0 \tag{2.23}$$
$$g_{14} \equiv \xi_{14} - (\alpha_{1212} - \alpha_{2121}) = 0$$

The second-order transition point T_c is determined as the point at which the following 14×14 determinant vanishes:

$$\text{Det} \left| \frac{\partial g_\mu}{\partial \xi_\nu} \right| = 0 . \tag{2.24}$$

Since we are working at T_{c-}, the long-range order parameters ξ_μ are small. Thus we also write, along with ξ's interchangeably,

$$\Delta w_{ijklm} \equiv w_{ijklm} - w_{i'j'k'l'm'} ,$$
$$\Delta \alpha_{ijkl} \equiv \alpha_{ijkl} - \alpha_{i'j'k'l'} . \tag{2.25}$$

The expression g_μ as defined in (2.22b) and (2.23) can be expanded in terms of these Δ's. In other words, we can write in principle

$$g_\mu = \sum_{\nu=1}^{14} c_{\mu\nu} \xi_\nu . \tag{2.26}$$

The coefficient $c_{\mu\nu}$ is $\partial g_\mu / \partial \xi_\nu$, which we want in (2.24). In order to evaluate $c_{\mu\nu}$, we do not need to derive the expression (2.26) analytically but can use the following trick. We simply choose $\xi_\nu = 1$ and $\xi_\kappa = 0$ for $\kappa \neq \nu$ and using substitutions (which we explain below) of many steps, we finally calculate g_μ. However complicated the substitutional steps may be, the value of g_μ thus calculated is equal to $c_{\mu\nu}$.

We show the substitutional steps using g_7 of (2.22b) as an example. For the quantity Δw_{12112} in the parentheses in (2.22b), we use the relation derived from (2.15)

$$\Delta w_{12112} = w_{12112} \left(\frac{\Delta w_{12112}^{(0)}}{w_{12112}} + \Delta \alpha_{1211} + \Delta \alpha_{2112} \right) . \tag{2.27a}$$

In deriving this expression from (2.15a), we left out $\Delta(\lambda\beta)$ because $\lambda\beta$ changes smoothly across T_c and hence $|\partial(\lambda\beta)/\partial T| \ll |\partial\xi_\mu/\partial T|$ at T_{c-}. The first term in the parentheses in (2.27a) is calculated from (2.15b) as, again leaving out $\Delta\beta$,

$$\frac{\Delta w_{12112}^{(0)}}{w_{12112}^{(0)}} = \frac{1}{2} \left(\frac{\Delta v_{1211}}{v_{1211}} + \frac{\Delta v_{2112}}{v_{2112}} + \frac{\Delta z_{112}}{z_{112}} - \frac{\Delta y_{21}}{y_{21}} \right), \tag{2.27b}$$

where we use differentiations of (2.14) and (2.16) for Δv's, Δz's, and Δy's to write them as linear combinations of Δw's. For $\Delta \alpha_{1211}$ and $\Delta \alpha_{2112}$ in (2.27a), we use the differentiation of (2.20)

$$\Delta \alpha_{ijkl} = \frac{1}{2} \left(\frac{\Delta S_{N,ijkl}}{S_{N,ijkl}} - \frac{\Delta S_{D,ijkl}}{S_{D,ijkl}} \right), \tag{2.28a}$$

$$\Delta S_{N,ijkl} = \sum_m \left(\Delta w_{mijkl}^{(0)} + w_{mijkl}^{(0)} \Delta \alpha_{mijk} \right) \exp(\alpha_{mijk}) ,$$

$$\Delta S_{D,ijkl} = \sum_m \left(\Delta w_{ijklm}^{(0)} + w_{ijklm}^{(0)} \Delta \alpha_{mikl} \right) \exp(\alpha_{mikl}) . \tag{2.28b}$$

The transition point thus determined from the vanishing of the determinant in (2.24) is

$$kT_c/\epsilon = 2.36483 , \tag{2.29}$$

which is the same as the value reported in Ref. 2 except for the last digit 3 which was reported as 0 previously.

III. THE DOUBLE-SQUARE APPROXIMATION

A. Free energy and its minimization

As was discussed at length in Ref. 2, the W-approximation treatment in Sec. II looks at the square net from the [11] direction, and is appropriate in calculating the $\langle 11 \rangle$ boundary free energy. When we treat the lattice from the [10] direction, the basic cluster which is one step larger than the square is a double square as shown by $A-B-C-D-E-F$ in Table IIA. This cluster is ap-

(a) THE DOUBLE SQUARE CLUSTER

A-B-C-D-E-F

(b) THE Ω_{OS} FACTOR

$$\Omega_{OS} = \frac{\left[\begin{smallmatrix}A&—&C\\|&&|\\B&—&D\end{smallmatrix}\right]\left\{A—C—E\right\}}{\left[\begin{smallmatrix}A&—&C&—&E\\|&&|&&|\\B&—&D&—&F\end{smallmatrix}\right]\left\{A—C\right\}}$$

(c) DEFINITION OF PROBABILITY VARIABLES

SPIN CONFIGURATION OF	
$\begin{smallmatrix}A&—&C&—&E\\|&&|&&|\\B&—&D&—&F\end{smallmatrix}$	PROBABILITY VARIABLES
$\begin{smallmatrix}i&—&k&—&m\\|&&|&&|\\j&—&l&—&n\end{smallmatrix}$	w_{ijklmn}
$\begin{smallmatrix}i&—&k\\|&&|\\j&—&l\end{smallmatrix}$	v_{ijkl}
$i—k—m$	z_{ikm}
$i—k$	y_{ik}

TABLE II. The double-square cluster.

propriate in calculating the $\langle 10 \rangle$ boundary. The Ω_{DS} factor for this case is also shown in Table IIB. This cluster was studied independently by Allegra and Delise in Politechnico di Milano.[19]

The probability variables are defined in Table IIC. As in Sec. II, $i = 1$ and 2 denote plus and minus spins, respectively. Using these variables and the Ω_{DS} factor, we can write the entropy S for a system of N lattice points as

$$\frac{S}{kN} = \frac{1}{2}\left(\sum \mathcal{L}(v_{ijkl}) + \sum \mathcal{L}(v_{klmn})\right)$$
$$- \sum \mathcal{L}(w_{ijklmn}) + \frac{1}{2}\left(\sum \mathcal{L}(z_{ikm}) + \sum \mathcal{L}(z_{jln})\right)$$
$$- \frac{1}{4}\left(\sum \mathcal{L}(y_{ik}) + \sum \mathcal{L}(y_{km}) + \sum \mathcal{L}(y_{jl}) + \sum \mathcal{L}(y_{ln})\right),$$
$$(3.1)$$

where the $\mathcal{L}$ operator is defined in (2.3) and the summation of each term goes over the values 1 and 2 of the subscripts in the summand.

In a system of N lattice points, the number of double-square clusters is N. Thus the energy of the system is written as

$$E = N \sum \epsilon_{ijklmn} w_{ijklmn} , \qquad (3.2a)$$

where ϵ is now

$$\epsilon_{ijklmn} = \tfrac{1}{3}(\epsilon_{ij} + \epsilon_{kl} + \epsilon_{mn}) + \tfrac{1}{4}(\epsilon_{ik} + \epsilon_{jl} + \epsilon_{km} + \epsilon_{ln}) . \qquad (3.2b)$$

The pair energy ϵ_{ij} is defined in (2.6).

We now examine subsidiary conditions on w's. The normalization is

$$\sum w_{ijklmn} = 1 . \qquad (3.3)$$

There are two "mirror" symmetries:

$$w_{ijklmn} = w_{mnklij} ,$$

and

$$w_{ijklmn} = w_{jiklnm} . \qquad (3.4)$$

These two symmetries in (3.4) can be kept through the iterations, if they are satisfied in the starting input w's. There are two more symmetries. One is the "translational" symmetry:

$$v_{ijkl} = \sum_{m,n} w_{ijklmn} = \sum_{m,n} w_{mnijkl} . \qquad (3.5)$$

and the other is the "rotational" symmetry of v's;

$$v_{ijkl} = v_{ikjl} . \qquad (3.6)$$

The last one is to guarantee that the probability for the spin configuration

$$\begin{pmatrix} 1 & 2 \\ 1 & 2 \end{pmatrix}$$

is equal to that of

$$\begin{pmatrix} 1 & 1 \\ 2 & 2 \end{pmatrix}$$

and hence the isotropy of the system.

The translational symmetry is taken into account by Lagrange terms similar to L_α in (2.10):

$$L_\alpha = \sum_{ijkl} (\alpha_{ijkl} + \alpha_{mnkl}) w_{ijklmn} , \qquad (3.7)$$

where we have used the symmetry of α's:

$$\alpha_{ijkl} = -\alpha_{klij} . \qquad (3.8a)$$

This relation can be proved by an argument similar to (2.12). We may note that α's obey another symmetry relation:

$$\alpha_{ijkl} = \alpha_{jilk} , \qquad (3.8b)$$

which corresponds to the second symmetry of w's in (3.4). Because of these two symmetry requirements, the independent α's are three: α_{1112}, α_{1122}, and α_{1222}. Six α's vanish.

The rotation symmetry (3.6) needs the following Lagrange terms:

$$L_\gamma = \sum_{ijkl} (\gamma_{ijkl} + \gamma_{mnkl}) w_{ijklmn} , \qquad (3.9)$$

where γ's satisfy the symmetry relations:

$$\gamma_{ijkl} = -\gamma_{ikjl} ,$$

and

$$\gamma_{ijkl} = \gamma_{jilk} . \qquad (3.10)$$

Because of these relations, 12 γ's vanish and there is only one independent γ_{ijkl}:

$$\gamma_{1212} = \gamma_{2121} = -\gamma_{1122} = -\gamma_{2211} . \qquad (3.11)$$

The free energy expression corresponding to (2.13) is

$$\frac{\beta F}{N} = \frac{\beta E}{N} - \frac{S}{kN} - \sum(\alpha_{ijkl} + \alpha_{mnkl} + \gamma_{ijkl} + \gamma_{mnkl}) w_{ijklmn}$$

$$+ \lambda\beta\left(1 - \sum w_{ijklmn}\right), \qquad (3.12)$$

where we use E of (3.2) and S/kN of (3.1). When we minimize (3.12) with respect to w_{ijklmn}, we obtain

$$\ln w_{ijklmn} = \lambda\beta + \ln w^{(0)}_{ijklmn} + \alpha_{ijkl} + \alpha_{mnkl} + \gamma_{ijkl} + \gamma_{mnkl},$$

$$(3.13a)$$

where

$$\ln w^{(0)}_{ijklmn} = -\beta\epsilon_{ijklmn}$$

$$+ \tfrac{1}{2}\ln(v_{ijkl} v_{klmn} z_{ikm} z_{jln}) - \tfrac{1}{4}\ln(y_{ik} y_{km} y_{jl} y_{ln}).$$

$$(3.13b)$$

Except for the minor iterations to be shown in the next subsection, the natural iteration step starts with an input set $\{w_{ijklmn}\}$, calculates the output set $\{\hat{w}_{ijklmn}\}$ using (3.13), and then uses $\hat{w}$'s as the next input. The input v's are calculated from w's in (3.5), and the input z's and y's are from the following

$$z_{ikm} = \sum_{j,l,n} w_{ijklmn},$$

$$(3.14)$$

$$y_{ik} = \sum_{m} z_{ikm}.$$

We will call the iteration step from the input set $\{w_{ijklmn}\}$ to the next input set the major iteration. We can use an expression similar to (2.18) as the test value Δ_{maj}, naturally with the six subscripts $(ijklmn)$ in the present section rather than five in (2.18). The convergence behavior in the present section is similar to Fig. 1, but slightly faster.

When the iteration converges, the value of λ is again equal to F/N as was the case in (2.19).

B. The minor iterations

For each major iteration step, the output $\hat{w}$'s have to satisfy the "translational" and the "rotational" symmetry relations (3.5) and (3.6). We have to solve the following two sets of equations for three α's and γ_{1212}:

$$\alpha_{ijkl} = \tfrac{1}{2}\ln(S_{N,ijkl}/S_{D,ijkl}), \qquad (3.15a)$$

where

$$S_{N,ijkl} = \sum_{mn} w^{(0)}_{mnijkl} \exp(\alpha_{mnij} + \gamma_{mnij}),$$

$$(3.15b)$$

$$S_{D,ijkl} = \sum_{mn} w^{(0)}_{ijklmn} \exp(\alpha_{mnkl} + \gamma_{mnkl}),$$

and

$$\gamma_{1212} = \tfrac{1}{2}\ln(R_N/R_D), \qquad (3.16a)$$

where

$$R_N = \sum_{mn} w^{(0)}_{mn2211} \exp(\alpha_{1122} + \alpha_{mn22} + \gamma_{mn22}),$$

$$R_D = \sum_{mn} w^{(0)}_{1212mn} \exp(\alpha_{1212} + \alpha_{mn12} + \gamma_{mn12}). \qquad (3.16b)$$

In the iteration technique we are proposing, the input set $\{\alpha,\gamma\}$ is used on the right-hand side of (3.15) and

(3.16) to evaluate the output set $\{\hat{\alpha},\hat{\gamma}\}$ and repeat the cycle until the iteration converges. At each major iteration step, the minor iterations are tested using Δ_{mnr} similar to (2.21) but including the γ term. The minor iterations behave somewhat similar to Fig. 2, but reduce faster to one; in the example of the same temperature, the points reduce to one in Fig. 2 around 80–100 major iterations.

C. Determination of T_c

We can determine T_c using the method similar as Sec. IIC. Corresponding to (2.22), there are ten equations of the form

$$g_\mu \equiv \xi_\mu - (w_{ijklmn} - w_{i'j'k'l'm'n'}) = 0. \qquad (3.17)$$

The equations corresponding to (2.23) reduce to two:

$$g_{11} \equiv \xi_{11} - (\alpha_{1112} - \alpha_{2221}),$$

$$g_{12} \equiv \xi_{12} - (\alpha_{1122} - \alpha_{2211}), \qquad (3.18)$$

and the determinant (2.24) now becomes 12×12. The "rotational" symmetry parameter γ_{1212} does not contribute to this determinant because $\gamma_{1212} - \gamma_{2121} = 0$ even in the ordered phase as is seen in (3.11). The value of T_c we obtain from vanishing of the determinant is

$$kT_c/\epsilon = 2.37619. \qquad (3.19)$$

It is of interest to see the calculation for which the "rotation" symmetry is not imposed. We find the difference is relatively small. The value of kT_c/ϵ for this case is almost the same as (3.19) except that the last digit 9 is replaced by 3. As far as the values of v's are concerned, we have the following example. At $kT/\epsilon = 2.38$ which is just above T_c, the disordered phase values are

$$v_{1122} = v_{1212} = 0.031227, \qquad (3.20a)$$

when the rotation symmetry is imposed, and

$$v_{1122} = 0.031373,$$

$$v_{1212} = 0.031075, \qquad (3.20b)$$

when it is not.

When we compare T_c in (3.19) for the double-square case with (2.29) for the W approximation, we find the W-value is about 0.5% lower. Based on the generally accepted rule, this means that the W-approximation is slightly better than the D–S approximation. This difference is information which was not available when Table I of Ref. 2 was written.

D. Comment on the double-square approximation

The Ω_{DS} expression in Table II is the case C_2 of Table I in Ref. 2, and treats the two-dimensional net layer wise. Explaining in detail, this Ω_{DS} is the number of ways the lattice can be constructed in such a way that all the *horizontally* placed double squares (like $A-B-C-D-E-F$ in Table III) have the assigned distribution of spin configurations. It is important to note that this Ω_{DS} does not pay attention to *vertically* placed double squares (like $A-B-G-H-D-C$ in Table III).

TABLE III. The 2×3 and 3×3 clusters.
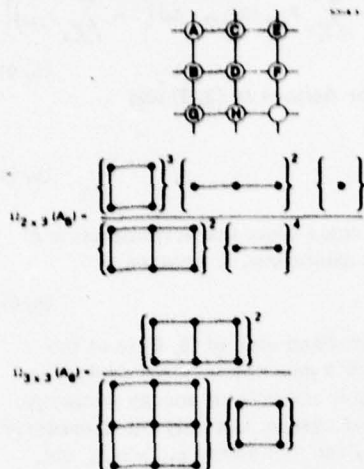
When the interaction energy is limited to the nearest neighbor $A-B$ and the second neighbor $A-D$, then this Ω_{DS} expression is valid. However, when the third neighbor (like $A-E$) interaction is to be taken into account, the Ω_{DS} expression in Table II fails. The reason is that the distribution of the vertical third neighbor $A-G$ is not taken into account in the theory. In Table V of his article,[3] Burley applied the Ω_{DS} expression in Table II to the problem in which the third neighbor interaction comes into play. His example, therefore, is an example in which the method was not expected to work, as Burley agreed with the author privately later.

If the third neighbor (like $A-G$) and the fourth neighbor (like $A-H$) interactions are to be included, the A_6 expression of the Ω factor in Table I of Ref. 2 should be used. It is reproduced as $\Omega_{3 \times 3}(A_6)$ in Table III. This Ω treats both horizontal and vertical double squares equally, and is applicable to the third and fourth neighbor interactions.

As was listed in Table I of Ref. 2, however, if the interaction is nearest neighbor only, then Ω_{DS} of Table II gives a better result than $\Omega_{3 \times 3}(A_6)$ of Table III. This indicates that although the latter works with the third and fourth neighbor interactions, the approximation may not be as good as expected. We certainly expect a good approximation when a 3×3 cluster made of circled points in Table III is used. For this case the Ω factor is given in A_6 of Table I in Ref. 2 and is reproduced in Table III here also.

The same kind of argument about the horizontal and vertical holds for the W approximation of Sec. II.

IV. PROOF OF THE BOUNDARY FREE ENERGY EXPRESSION

In Ref. 16 the scalar product expression for the boundary excess free energy was derived. The proof of the expression, however, contained a weakness. In this section we present an improvement of the proof. It will be done using a three-dimensional nomenclature. First, we briefly summarize Sec. II of Ref. 16.

We consider an ith crystalline plane parallel to the boundary and designate by ν_i a configuration of the entire plane. The probability that the ith plane takes the configuration ν_i is written as $p(\nu_i)$. We define the quantities:

$$g_i(\nu_i) = [p(\nu_i)]^{1/2} \exp[+\beta \alpha(\nu_i)] ,$$
$$h_i(\nu_i) = [p(\nu_i)]^{1/2} \exp[-\beta \alpha(\nu_i)] , \qquad (4.1)$$

which can be regarded as a column vector g_i and a row vector h_i, whose components are indexed by ν_i. The $\alpha(\nu_i)$ takes care of the continuity condition and vanishes when the system is homogeneous. Because of the normalization of the probability distribution $p(\nu_i)$, the scalar product of g_i and h_i is unity:

$$h_i \cdot g_i = 1 . \qquad (4.2)$$

In Ref. 16 we showed that g_i and h_i obey the recurrence relations:

$$g_i = \exp(\beta \lambda_{i+1/2}) P \cdot g_{i+1} , \qquad (4.3a)$$
$$h_i = \exp(\beta \lambda_{i-1/2}) h_{i-1} \cdot P , \qquad (4.3b)$$

where P is the transfer matrix and depends on the interaction energies. The parameter $\lambda_{i+1/2}$ is related to the free energy F of the entire system as

$$F = \sum_i \lambda_{i+1/2} . \qquad (4.4)$$

When the system is homogeneous, $g_i = g_{i+1} = g^{(0)}$ so that (4.3a) reduces to

$$g^{(0)} = \exp(\beta \lambda^{(0)}) P \cdot g^{(0)} . \qquad (4.5)$$

This is the eigenvalue equation. The excess free energy $A\sigma$ attributed to the boundary (A is the cross-sectional area of the system) is written as

$$A\sigma = \lim_{m \to \infty} \sum_{i=-m}^{m} (\lambda_{i+1/2} - \lambda^{(0)}) , \qquad (4.6)$$

when the boundary region lies between $i = -m$ and $+m$.

From now on, we deviate from Ref. 16. In order to calculate σ, we consider a region between $i = +m$ and $+3m$ outside of the boundary, in order to compare with the boundary region. We assume m large enough so that the region $m < i < 3m$ is sufficiently close to the homogeneous phase. This assumption allows us to write

$$h_m \cdot g_{3m} = 1 , \qquad (4.7)$$

which is a modification of (4.2). We can also write

$$g_m = \exp(\beta 2m \lambda^{(0)}) P^{2m} \cdot g_{3m} , \qquad (4.8)$$

which is obtained by applying (4.3a) or (4.5) $2m$ times.

The boundary excess free energy can be derived as follows. Operating (4.3b) between $-m$ and m, we derive

$$h_{-m} = \exp\left(-\beta \sum_{i=-m+1}^{m} \lambda_{i-1/2}\right) h_m \cdot P^{-2m} . \qquad (4.9)$$

We form the scalar product of (4.9) and (4.8), and use (4.6) and (4.7) to arrive at

$$\lim_{m \to \infty} h_{-m} \cdot g_m = \exp(-\beta A \sigma) . \qquad (4.10)$$

Going back to $p(\nu_i)$ in (4.1), we can write (4.10) as

$$\exp(-\beta A \sigma) = \sum_{\nu} \{p_{\text{I}}(\nu) p_{\text{II}}(\nu)\}^{1/2} , \qquad (4.11)$$

where the subscripts I and II denote the first and second phases which meet at the boundary.

Although this proof is not written in mathematical rigor, and still contains some implicit, albeit reasonable, assumptions how h_m and g_m behave away from the boundary, it is an improvement over the proof in Ref. 16, and is applicable to two-dimensional boundaries for which the location of the boundary cannot be specified,[20] as well as to three-dimensional boundaries.

V. CALCULATIONS OF THE BOUNDARY FREE ENERGY

When we apply the scalar product expression (4.11) to the present problem, we can write for the $\langle 10 \rangle$ boundary

$$\exp(-n\sigma_{\langle 10 \rangle} a \beta) = \sum_{\{z_{ijk}\}} \Omega\{z_{ijk}\} (p_{\text{I}}\{z_{ijk}\} p_{\text{II}}\{z_{ijk}\})^{1/2} , \qquad (5.1)$$

where a is the lattice constant and n is the number of lattice points in a line parallel to the boundary. The quantity z_{ijk} on the right-hand side is the probability for a three-point cluster as is defined in Table II.

The sum over all configurations $\sum_{\nu}$ in (4.11) is now written as the sum over the set $\{z_{ijk}\}$ with the weight factor $\Omega\{z_{ijk}\}$. This factor is the number of different ways the line (composed of n lattice points) can take the configuration specified by the distribution $\{z_{ijk}\}$, and is written following the cluster-variation method[1] for a one-dimensional system as

$$\Omega\{z_{ijk}\} = \prod_{i,j}(ny_{ij})! \Big/ \prod_{i,j,k}(nz_{ijk})! . \qquad (5.2)$$

In accordance with the sum over $\{z_{ijk}\}$ in (5.1), the probability factor $p_{\text{I}}(\nu)$ in (4.11) is changed into $p_{\text{I}}\{z_{ijk}\}$, which is the probability that a line of n lattice points imbedded in the equilibrium homogeneous bulk phase I takes a configuration specified by the set $\{z_{ijk}\}$. The conditional probability that a spin k is found next to a pair of spins i–j is $z_{ijk}^{(\text{I})}/y_{ij}^{(\text{I})}$ in the phase I. Making use of this property, we can write p_{I} as

$$p_{\text{I}}\{z_{ijk}\} = \prod_{i,j,k}(z_{ijk}^{(\text{I})}) ** (nz_{ijk}) \Big/ \prod_{i,j}(y_{ij}^{(\text{I})}) ** (ny_{ij}) , \qquad (5.3)$$

where a double asterisk is the FORTRAN notation meaning "raised to the power of." In this expression, $z_{ijk}^{(\text{I})}$ with a superscript (I) is the value in the equilibrium homogeneous bulk phase, and is to be distinguished from z_{ijk} which is the summing variable in (5.1). The other factor p_{II} in (5.1) can be written by changing (I) in (5.3) into (II).

We are now ready to calculate σ from (5.1). Using the standard technique of statistical mechanics, we replace the summation in (5.1) by the maximum term. For that purpose we write from (5.1)

$$\sigma_{\langle 10 \rangle} a \beta = \min_{\{z_{ijk}\}} \Bigg[\sum_{i,j,k} \mathcal{L}(z_{ijk}) - \sum_{i,j} \mathcal{L}(y_{ij})$$

$$+ \sum_{i,j} y_{ij} \ln \hat{y}_{ij} - \sum_{i,j,k} z_{ijk} \ln \hat{z}_{ijk} + \lambda \beta \left(1 - \sum_{i,j,k} z_{ijk} \right) \Bigg] , \qquad (5.4)$$

where $\mathcal{L}$ is the operator defined in (2.3) and

$$\hat{y}_{ij} \equiv (y_{ij}^{(\text{I})} y_{ij}^{(\text{II})})^{1/2} ,$$
$$\hat{z}_{ijk} \equiv (z_{ijk}^{(\text{I})} z_{ijk}^{(\text{II})})^{1/2} . \qquad (5.5)$$

The $\lambda \beta$ terms in (5.4) come from the normalization of z_{ijk}, and when (5.4) is minimized it reduces to

$$\sigma_{\langle 10 \rangle} a \beta = \lambda \beta . \qquad (5.6)$$

We note that the right-hand side of (5.4) is of the form of a free energy of a one-dimensional system in which $\ln \hat{y}_{ij}$ and $\ln \hat{z}_{ijk}$ play the role of energy (times β). Since a one-dimensional system has only the disordered phase, z's and y's obey the symmetry $z_{112} = z_{221}$, etc. Minimization of (5.4) leads to an eigenvalue equation, $e^{-\lambda\beta}$ being the eigenvalue. It is solved as

$$e^{-\lambda\beta} = \frac{1}{2} \left\{ \frac{\hat{z}_{111}}{\hat{y}_{11}} + \frac{\hat{z}_{121}}{\hat{y}_{12}} + \left[\left(\frac{\hat{z}_{111}}{\hat{y}_{11}} - \frac{\hat{z}_{121}}{\hat{y}_{12}} \right)^2 + \frac{4\hat{z}_{112}^2}{\hat{y}_{11}\hat{y}_{12}} \right]^{1/2} \right\} \qquad (5.7)$$

As a check of this equation, we examine the high-temperature case when the homogeneous bulk phase is disordered. In such a case, $\hat{y}_{ij}$ and $\hat{z}_{ijk}$ of (5.5) reduce to

$$\hat{y}_{ij} = y_{ij}^{(\text{I})} = y_{ij}^{(\text{II})} , \text{ and } \hat{z}_{ijk} = z_{ijk}^{(\text{I})} = z_{ijk}^{(\text{II})} , \qquad (5.8)$$

and we can show that $e^{-\lambda\beta}$ of (5.7) reduces to unity and hence $\sigma_{\langle 10 \rangle} = 0$.

The boundary excess free energy $\sigma_{\langle 10 \rangle}$ for the $\langle 10 \rangle$ boundary is then calculated from (5.5), (5.6), and (5.7) using the results of the equilibrium homogeneous bulk phase of Sec. III. The dimensionless quantity $\sigma_{\langle 10 \rangle} a/\epsilon$ is plotted in Fig. 3 by a solid curve marked as double square. It is compared with the exact result of Onsager[21] and the results based on the pair and the square approximations which are reported previously.[18]

The boundary free energy $\sigma_{\langle 11 \rangle}$ of the $\langle 11 \rangle$ boundary can be calculated using (5.5) and (5.7) again, but replacing (5.6) by

$$\sigma_{\langle 11 \rangle} \sqrt{2} \, a\beta = \lambda \beta , \qquad (5.9)$$

since the distance between two neighboring lattice points on a $\langle 11 \rangle$ line is $\sqrt{2} \, a$. For this boundary, y_{ij} and z_{ijk} in (5.5) are those defined in Table I. Section II is used to calculate $\sigma_{\langle 11 \rangle}$ through (5.5), (5.7), and (5.9). The result is shown by the broken curve marked with W in Fig. 3; it is to be compared with the exact result by Fisher and Ferdinand[22] and also with the angle approximation result[18] which are also plotted in Fig. 3 with broken curves.

The curves in Fig. 3 support the correctness of the scalar product expression of the boundary free energy as well as effectiveness of the W- and double-square-approximations of Secs. II and III.

VI. SUMMARY AND CONCLUSION

This paper can be regarded as the follow on of or a supplement to the several papers published previously,
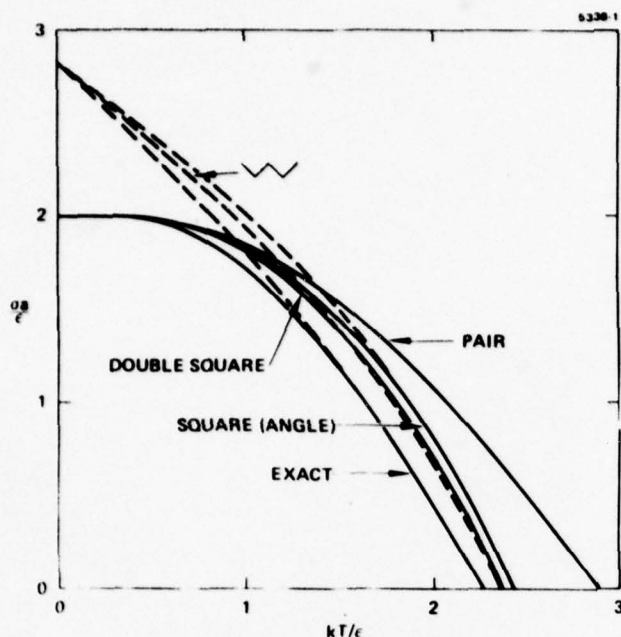
FIG. 3. Boundary excess free energies $\sigma_{\langle 10 \rangle}$ and $\sigma_{\langle 11 \rangle}$ for the two-dimensional Ising model. The solid curves are for $\sigma_{\langle 10 \rangle}$ and the broken curves are $\sigma_{\langle 11 \rangle}$. The kinds of approximation used in evaluation are indicated in the figure.

the paper[2] on the improvement of the cluster variation method, the natural iteration paper,[4] and the boundary free energy papers,[16,18] particularly the latter two, and answers questions left unanswered or having come up after the publications, in order to pave a way for further applications of the techniques.

In computing the equilibrium state of a cooperative system using the cluster variation method,[2] it is necessary in general except for simple cases that subsidiary conditions are to be satisfied among variables. Sections II and III show that these subsidiary conditions can be treated in minor iterations for each major iteration step of the natural iteration (NI) technique.

These sections also present computational details of calculating the second-order transition point without losing the spirit of the NI method. This technique

makes most use of the superposition expressions which form the starting point of the NI treatment.

The scalar product (SP) expression of boundary free energy[16] has lacked a rigorous proof. Section IV presents an improvement of the proof. The SP expression is combined in Sec. V with the results of Secs. II and III for the W- and double-square-approximations to calculate boundary free energies $\sigma_{\langle 10 \rangle}$ and $\sigma_{\langle 11 \rangle}$ for the two-dimensional Ising model. The resulting curves in Fig. 3 leave no doubt that the σ values calculated by the SP expression converge to the exact results of Onsager and Fisher Ferdinand as the approximation is improved. This convergence supports the correctness of the implicit assumptions still left in the analytic proof in Sec. V, and now guarantees that the SP expression can be safely used for further studies of the boundary structures.

[1]R. Kikuchi, Phys. Rev. 81, 988 (1951).
[2]R. Kikuchi and S. G. Brush, J. Chem. Phys. 47, 195 (1967).
[3]D. M. Burley, in Phase Transitions and Critical Phenomena, edited by C. Domb and M. S. Green (Academic, New York, 1972), Vol. 2, Chap. 9.
[4]R. Kikuchi, J. Chem. Phys. 60, 1071 (1974).
[5]R. Kikuchi and H. Sato, Acta Met. 22, 1099 (1974).
[6]R. Kikuchi and C. M. van Baal, Scripta Met. 8, 425 (1974).
[7]R. Kikuchi and H. Sato, AIP Conf. Proc. 18, 605 (1974).
[8]R. Kikuchi, D. de Fontaine, M. Murakami, and T. Nakamura, Acta Met. (in press).
[9]N. S. Golosov, L. Ya. Pudan, G. S. Golosova, and L. E. Popov, Sov. Phys. Solid State 14, 1280 (1972).
[10]N. S. Golosov and A. M. Tolstik, J. Phys. Chem. Solids 35, 1575 and 1581 (1974).
[11]C. M. van Baal, Physica (Utrecht) 64, 571 (1973).
[12]P. C. Clapp, Phys. Rev. B 4, 255 (1971).
[13]W. E. Case, J. Phys. Chem. Solids 37, 353 (1976).
[14]J. D. Weeks and G. H. Gilmer, J. Chem. Phys. 63, 3136 (1975).
[15]R. Kikuchi (to be published).
[16]R. Kikuchi, J. Chem. Phys. 57, 777 (1972).
[17]D. B. Clayton and G. W. Woodbury, Jr., J. Chem. Phys. 55, 3895 (1971).
[18]R. Kikuchi, J. Chem. Phys. 57, 783 (1972).
[19]G. Allegra and P. Delise (unpublished).
[20]G. Gallavotti, Riv. Nuovo Cimento 2, 133 (1972).
[21]L. Onsager, Phys. Rev. 65, 117 1944).
[22]M. E. Fisher and A. E. Ferdinand, Phys. Rev. Lett. 19, 169 (1967).

APPENDIX 2

(Reference [2])

STRUCTURE OF PHASE BOUNDARIES

R. Kikuchi

J. Chem. Phys. <u>66</u>, 3352 (1977)

Structure of phase boundaries*

Ryoichi Kikuchi

Hughes Research Laboratories, Malibu, California 90265
(Received 4 January 1977)

The boundary between plus and minus spin phases of the Ising model is studied for the bcc ⟨110⟩ boundary. The iterative calculation due to Weeks and Gilmer is interpreted as a modification of the Natural Iteration computation (with subsidiary conditions) for deriving a free energy minimum. A tetrahedron is used as the basic cluster in the cluster-variation scheme for this problem. Two formulations are presented: one uses the scalar-product formulation and the other the boundary sum method. Previous results of an order–disorder type phase transition within the boundary are confirmed. Results of calculations on the boundary excess free energy and the boundary profile are compared for the pair and the tetrahedron treatments.

I. INTRODUCTION

In a recent publication, Weeks and Gilmer[1] proposed a novel iterative technique for numerically solving the density profile across a phase boundary. They presented their idea based on the original Bethe[2] method of treating cooperative systems using consistency relations. In Sec. II of the present paper, we point out that the Weeks–Gilmer (WG) technique fits well with the cluster-variation method of formulating the boundary structure by Cahn and the present author,[3,4] and that the WG iteration technique supplements the Natural Iteration (NI) technique recently proposed by the present author.[5,6] The iterative technique of Sec. II can be generalized to larger clusters. In Sec. IV we calculate the boundary profile of the bcc ⟨110⟩ boundary using a tetrahedron as the basic cluster.

Along with the boundary profiles, the excess free energy of the boundary is calculated in Secs. II and IV. In order to compare these results with those obtained by the scalar-product formulation,[6,7] Sec. III reports the latter using the tetrahedron as the basic cluster. Particular emphasis is placed on the phase transition within the phase boundary. Examples are limited to the ⟨110⟩ boundary of the bcc Ising model.

II. ITERATIVE COMPUTATION OF THE PROFILE

The pair approximation formulation

In this section we use the pair approximation of the cluster-variation method to calculate the density (spin) profile across the bcc ⟨110⟩ boundary and show where the WG idea fits into the formulation and how their idea facilitates numerical computations. We work with the nearest-neighbor interaction as in WG and use the Ising model terminology, rather than ordered alloys.

The crystal structure is illustrated in Fig. 1. We consider the plane of the lattice points i–j–l to be parallel to the boundary, and phase I to be on the left and phase II on the right. A lattice plane parallel to the boundary is called a "parallel" plane for short and is numbered by ν, as in Fig. 1.

Two kinds of nearest-neighbor bonds are to be distinguished, to be called the B bond and the C bond for short. A B bond is within a parallel plane and examples are i–l and j–l in Fig. 1. A C bond, such as i–m in Fig. 1, connects two lattice points on adjacent parallel planes. A B bond on the νth plane will be called a $B\nu$ bond, and a C bond connecting points on the νth plane and

the $(\nu+1)$th plane will be called a $C\mu$ bond. The numbering system μ for bonds is indicated in Fig. 1. Actually, we use $\mu = \nu$ in numerical computations, but it is better to distinguish them in the presentation.

Plus and minus spins are denoted by $i=1$ and 2, respectively. The distributions of spin configurations over a lattice plane and over bonds are defined as in Table I. We use distributions of nearest-neighbor pairs only in this section.

There are three kinds of constraints for these variables: first, the set of normalizations

$$\sum_{i,l} y_{B\nu,il} = \sum_{j,m} y_{C\mu,jm} = 1 \quad \text{for all } \nu\text{'s and } \mu\text{'s;} \quad (2.1)$$

second, the symmetry relations

$$y_{B\nu,il} = y_{B\nu,li} \quad \text{for all } \nu\text{'s;} \quad (2.2)$$

and third, the consistency relations

$$x_{\nu,i} = \sum_l y_{B\nu,il}, \quad x_{\nu,l} = \sum_i y_{B\nu,il} \quad (2.3a)$$

$$x_{\nu,j} = \sum_m y_{C\mu,jm}, \quad x_{\nu+1,m} = \sum_u y_{C\mu,jm} \quad (2.3b)$$

In Eqs. (2.3b), remember that the $C\mu$ bond connects lattice points between the νth plane and the $(\nu+1)$th plane, as shown in Table I and Fig. 1.

The cluster-variation method starts with the free energy expression. The energy of the system is written as
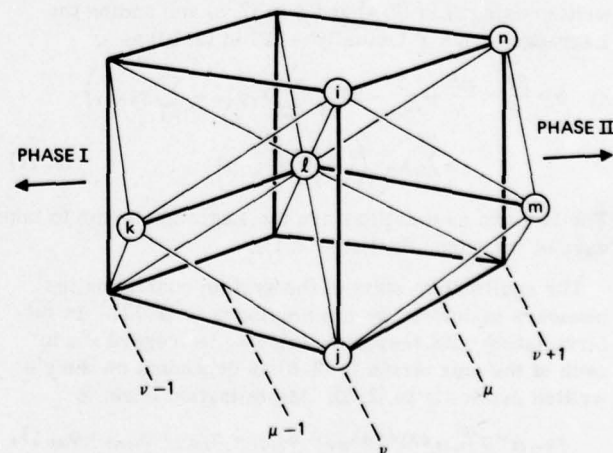

FIG. 1. Geometry of the bcc lattice and the nomenclature used in defining variables. Thin lines are nearest-neighbor bonds, and thick lines are second-neighbor bonds. Section II uses only thin line bonds.

TABLE I. Definition of the distribution variables. The subscripts il in $y_{Bv,il}$ are symmetric as seen in (2.2). For $y_{C\mu,im}$ the first subscript i refers to the left side of the bond as shown in Fig. 1.

Configuration	Distribution variable
i-spin on the vth plane	$x_{v,i}$
i-l on a Bv bond	$y_{Bv,il}$
i-m on a $C\mu$ bond, i on the vth plane, and m on the $(v+1)$th plane	$y_{C\mu,im}$

$$E = 2n \sum_{i,j} \epsilon_{ij} \left[\sum_{v=1}^{v_s} y_{Bv,ij} + \sum_{\mu=1}^{\mu_s} y_{C\mu,ij} \right] , \qquad (2.4)$$

where n is the number of lattice points on each of the parallel planes. The energy parameter ϵ_{ij} for the Ising model is

$$\epsilon_{ij} = +\epsilon \quad \text{when } i \neq j,$$
$$\epsilon_{ij} = -\epsilon \quad \text{when } i = j. \qquad (2.5)$$

In (2.4), the parallel planes go from $v=1$ through v_s, and the bonds go from $\mu=1$ through $\mu_s = v_s - 1$.

The entropy of the pair approximation of the cluster-variation method is written for a homogeneous phase of N lattice points as[8,9]

$$S = kN \left[(2\omega - 1) \sum_i \mathcal{L}(x_i) - \omega \sum_{ij} \mathcal{L}(y_{ij}) + (\omega - 1) \right], \quad (2.6)$$

$$\Gamma = \sum_{v=1}^{v_s} \left\{ \sum_i \alpha_{Lv,i} \left[\sum_l (y_{Bv,il} + y_{Bv,li}) - 2 \sum_m y_{C\mu,im} \right] + \sum_i \alpha_{Rv,i} \left[2 \sum_h y_{C(\mu-1),hi} - \sum_l (y_{Bv,il} + y_{Bv,li}) \right] \right\}$$
$$= \sum_{v=1}^{v_s} \left\{ \sum_{i,l} (\alpha_{Lv,i} + \alpha_{Lv,l} - \alpha_{Rv,i} - \alpha_{Rv,l}) y_{Bv,il} + 2 \sum_{j,m} (\alpha_{R(v+1),m} - \alpha_{Lv,j}) y_{C\mu,jm} \right\} . \qquad (2.10)$$

In the first line of this expression, $y_{Bv,il} + y_{Bv,li}$ guarantees that $y_{Bv,il}$ is invariant under the interchange of i and l.

The free energy of the entire system $F = E - TS$ is written using E in (2.4) and S in (2.8) and adding the Lagrange terms Γ (actually -2Γ) in (2.10) as

$$\Phi \equiv \frac{\beta F}{n} = \frac{\beta E}{n} - \frac{S}{kn} - 2\Gamma + \beta \sum_{v=1}^{v_s} \lambda_{Bv} \left(1 - \sum_{i,l} y_{Bv,il} \right)$$
$$+ \beta \sum_{\mu=1}^{\mu_s} \lambda_{C\mu} \left(1 - \sum_{j,m} y_{C\mu,jm} \right) . \qquad (2.11)$$

The last two summations are the Lagrange terms to take care of the normalizations (2.1).

The equilibrium state of the system containing the boundary is derived by minimizing Φ in (2.11). In differentiating with respect to the y's, we regard x's in each of the four terms in (2.8) as dependent on the y's written explicitly in (2.3). Minimization leads to

$$y_{Bv,il} = y_{Bv,il}^{(0)} \exp(\tfrac{1}{2}\beta\lambda_{Bv} - \alpha_{Lv,i} - \alpha_{Lv,l} + \alpha_{Rv,i} + \alpha_{Rv,l}),$$
$$y_{C\mu,jm} = y_{C\mu,jm}^{(0)} \exp(\tfrac{1}{2}\beta\lambda_{C\mu} + 2\alpha_{Lv,j} - 2\alpha_{R(v+1),m}),$$
$$\qquad (2.12)$$
where
$$y_{Bv,il}^{(0)} = (x_{v,i} x_{v,l})^{7/8} \exp(-\beta\epsilon_{il}),$$

where the $\mathcal{L}$ operator originates from the Stirling approximation of a factorial and is defined as

$$\mathcal{L}(x) \equiv x \ln x - x . \qquad (2.7)$$

In (2.6), N is the number of lattice points in the system and 2ω is the coordination number. For an inhomogeneous system in a bcc lattice ($\omega = 4$), which is what we are interested in, we modify (2.6) and write the entropy as

$$\frac{S}{kn} = \frac{7}{4} \sum_{v=1}^{v_s} \left[\sum_i \mathcal{L}(x_{v,i}) + \sum_i \mathcal{L}(x_{v,i}) \right]$$
$$+ \frac{7}{4} \sum_{\mu=1}^{\mu_s} \left[\sum_j \mathcal{L}(x_{v,j}) + \sum_m \mathcal{L}(x_{v+1,m}) \right] \qquad (2.8)$$
$$- 2 \sum_{v=1}^{v_s} \left[\sum_{i,l} \mathcal{L}(y_{Bv,il}) - \tfrac{3}{4} \right] - 2 \sum_{\mu=1}^{\mu_s} \left[\sum_{j,m} \mathcal{L}(y_{C\mu,jm}) - \tfrac{3}{4} \right].$$

The four x terms in (2.8) are equal, except for the end terms, but are written separately to make the treatment symmetric. The $-\tfrac{3}{4}$ terms in (2.8) take case of $(\omega - 1)$ in (2.6).

In minimizing the free energy, we want to treat all y's as independent. For that purpose we need Lagrange multipliers for the following relations:

$$x_{v,i} = \sum_l y_{Bv,il} = \sum_m y_{C\mu,im} ,$$
$$x_{v,i} = \sum_h y_{C(\mu-1),hi} = \sum_l y_{Bv,il} . \qquad (2.9)$$

We write the Lagrange terms as

$$y_{C\mu,jm}^{(0)} = (x_{v,j} x_{v+1,m})^{7/8} \exp(-\beta\epsilon_{jm}) . \qquad (2.13)$$

Note that the il exchange symmetry of $y_{Bv,il}$ in (2.2) is demonstrably satisfied by the expressions in (2.12) and (2.13).

When Φ in (2.11) is a minimum and (2.12) and (2.13) hold, we can show that Φ reduces to

$$F/n = \sum_{v=1}^{v_s} \lambda_{Bv} + \sum_{\mu=1}^{\mu_s} \lambda_{C\mu} \qquad (2.14)$$

This F is the free energy of the entire system including the boundary region.

The Lagrange multiplier α's are determined from (2.9). Let us define

$$S_{Bv,i} \equiv \sum_l y_{Bv,il}^{(0)} \exp(-\alpha_{Lv,l} + \alpha_{Rv,l}) ,$$
$$S_{CRv,i} \equiv \sum_m y_{C\mu,im}^{(0)} \exp(-2\alpha_{R(v+1),m}) ,$$
$$S_{CLv,i} \equiv \sum_h y_{C(\mu-1),hi}^{(0)} \exp(2\alpha_{L(v-1),h}) . \qquad (2.15)$$

Substituting these in (2.9), we obtain

$$\exp(\tfrac{1}{2}\beta\lambda_{B\nu} - \alpha_{L\nu,i} + \alpha_{R\nu,i})S_{B\nu,i} = \exp(\tfrac{1}{2}\beta\lambda_{C\mu} + 2\alpha_{L\nu,i})S_{CR\nu,i} ,$$

$$\exp(\tfrac{1}{2}\beta\lambda_{C(\mu-1)} - 2\alpha_{R\nu,i})S_{CL\nu,i}$$

$$= \exp(\tfrac{1}{2}\beta\lambda_{B\nu} - \alpha_{L\nu,i} + \alpha_{R\nu,i})S_{B\nu,i} . \qquad (2.16)$$

The novel idea of Weeks and Gilmer[1] is to eliminate the λ's from (2.16) by forming ratios of $i=1$ and $i=2$ cases:

$$\frac{\exp(-\alpha_{L\nu,1} + \alpha_{R\nu,1})S_{B\nu,1}}{\exp(-\alpha_{L\nu,2} + \alpha_{R\nu,2})S_{B\nu,2}} = \frac{\exp(2\alpha_{L\nu,1})S_{CR\nu,1}}{\exp(2\alpha_{L\nu,2})S_{CR\nu,2}} ,$$

$$\frac{\exp(-2\alpha_{R\nu,1})S_{CL\nu,1}}{\exp(-2\alpha_{R\nu,2})S_{CL\nu,2}} = \frac{\exp(-\alpha_{L\nu,1} + \alpha_{R\nu,1})S_{B\nu,1}}{\exp(-\alpha_{L\nu,2} + \alpha_{R\nu,2})S_{B\nu,2}} . \quad (2.17)$$

From these we can solve

$$\alpha_{R\nu,1} - \alpha_{R\nu,2} = (3A_{L,\nu} - A_{R,\nu})/8 ,$$

$$\alpha_{L\nu,1} - \alpha_{L\nu,2} = (A_{L,\nu} - 3A_{R,\nu})/8 , \qquad (2.18)$$

where the A's are defined using the S's in (2.15) as

$$A_{R,\nu} \equiv \ln(S_{CR\nu,1}S_{B\nu,2}/S_{CR\nu,2}S_{B\nu,1}) ,$$

$$A_{L,\nu} \equiv \ln(S_{CL\nu,1}S_{B\nu,2}/S_{CL\nu,2}S_{B\nu,1}) . \qquad (2.19)$$

Since the y's satisfy the normalizations, we can choose, for example,

$$\alpha_{L\nu,2} = \alpha_{R\nu,2} = 0 \qquad (2.20)$$

without loss of generality.

The iteration procedure is divided into "major" and "minor" iterations.[6] A major iteration step starts with the input set $\{x_{\nu,i}\}$, $\{\alpha_{L\nu,1}\}$, and $\{\alpha_{R\nu,1}\}$. Using these, we calculate $y_{B\nu,ii}^{(0)}$ and $y_{C\mu,jm}^{(0)}$ in (2.13) and determine the output set $\{\hat{\alpha}\}$ by the minor iteration steps to be described below. When the output $\hat{\alpha}$'s are determined, the λ's are calculated by substituting (2.12) into the normalizations (2.1); then the information of $y^{(0)}$'s, λ's, and $\hat{\alpha}$'s leads to the output sets $\{\hat{y}_{B\nu,ii}\}$ and $\{\hat{y}_{C\mu,jm}\}$ from (2.12). The output set $\{\hat{x}_{\nu,i}\}$ is obtained from (2.9) using $\hat{y}$'s. Thus, one major iteration cycle is completed, and $\{\hat{x}_{\nu,i}\}$, $\{\hat{\alpha}_{L\nu,i}\}$, and $\{\hat{\alpha}_{R\nu,i}\}$ are used as the input set for the next major iteration cycle.

The minor iteration step is as follows. The input for the minor iteration are the sets $\{y^{(0)}\}$ and $\{\alpha\}$. Using these values, we calculate the S's in (2.15) and further A's in (2.19) and then obtain the output values $\alpha_{R\nu,1}$ and $\alpha_{L\nu,1}$ of one minor iteration cycle from (2.18) and (2.20). This output set α's is then used as the input on the right-hand side of (2.15) for the S's in the next minor iteration cycle.

We can prove the convergence of the major iteration by showing that the free energy function Φ in (2.11) always decreases at each major iteration step. The expression Φ is a function of the variables x's, y's, and α's. When these variables take the output values, we write $\hat{\Phi}$ with a caret, and we let Φ denote the function of the input values. Then using a technique similar to the one used in Ref. 5, and assuming that the constraints (2.9) are satisfied, we can derive

$$\Phi - \hat{\Phi} = 2\sum_{\nu,i,i}[y_{B\nu,ii}\ln(y_{B\nu,ii}/\hat{y}_{B\nu,ii}) + \hat{y}_{B\nu,ii} - y_{B\nu,ii}]$$

$$+ 2\sum_{\mu,j,m}[y_{C\mu,jm}\ln(y_{C\mu,jm}/\hat{y}_{C\mu,jm}) + \hat{y}_{C\mu,jm} - y_{C\mu,jm}]$$

$$+ 7\sum_{\nu,i}[\hat{x}_{\nu,i}\ln(\hat{x}_{\nu,i}/x_{\nu,i}) + x_{\nu,i} - \hat{x}_{\nu,i}] . \qquad (2.21)$$

Each term in the square brackets is nonnegative due to Gibbs' lemma,[10] and hence Φ always decreases at each major iteration step as long as the minor iterations have converged and the continuity relations (2.9) are satisfied by both the input and the output y's.

We have not attempted the analytic proof of the convergence of minor iterations. In numerical computations they do converge, however, and the reason for this convergence is interpreted as due to the averaging nature of (2.15)–(2.18).

We want to point out that the iteration processes of this section are almost exactly the same as the iteration method described by Weeks and Gilmer.[1] The only difference is that they do not treat the major and minor iterations as rigidly separated as in this section. In the method proposed in this section the output set $\{\hat{\alpha}\}$ makes the continuity requirements of (2.9) satisfied for the given $\{\hat{y}^{(0)}\}$, while in WG's method the output $\{\hat{\alpha}\}$ of one minor iteration cycle is regarded as the output of the major iteration cycle also. The fact that their iterations converge indicates that we do not need to be so strict about minor iterations, although the convergence of the latter is used in our proof of $\Phi > \hat{\Phi}$ in (2.21).

We can derive equations in the Kikuchi–Cahn paper from (2.12) and (2.13) by eliminating the λ's and α's:

$$\frac{y_{B\nu,11}}{y_{B\nu,22}}\frac{y_{C\mu,11}y_{C(\mu-1),21}}{y_{C(\mu-1),22}y_{C\mu,21}} = \left(\frac{x_{\nu,1}}{x_{\nu,2}}\right)^{7/2} ,$$

$$e^{4\beta\epsilon} = y_{C\mu,11}y_{C\mu,22}/y_{C\mu,12}y_{C\mu,21} ,$$

$$e^{4\beta\epsilon} = y_{B\nu,11}y_{B\nu,22}/y_{B\nu,12}^{2} . \qquad (2.22)$$

These are exactly Eqs. (2.8)–(2.10) of Ref. 3 for the case $\omega = 4$ and $\omega_t = \omega_i = 2$ in their notation. Although this set of equations is equivalent to the mathematical problem we treated in this paper using the NI method, when written in the form of (2.22) the NI technique is of no help. The Kikuchi–Cahn paper solved it successively starting from one end.

It may also be worth pointing out that the present method which is based on the cluster-variation formulation allows us to calculate the free energy of the system in (2.14) in terms of the Lagrange multiplier λ's for the normalizations. This is in contrast to the WG formulation which is based on the original Bethe treatment and does not lead to the free energy value in easy steps.

The formulation in this section was used in calculating the boundary structure for the interstitial-center case and the atomic-center case. The results agree with those of Kikuchi–Cahn,[3] and are compared with those of other methods in Sec. IV.3.

III. TETRAHEDRON TREATMENT OF BOUNDARY FREE ENERGY USING THE SCALAR-PRODUCT FORMULA

The iterative calculation of the boundary profile proposed by Weeks and Gilmer[1] and reinterpreted in the previous section in terms of the NI calculation suggests that a similar technique can be used with a larger clus-

ter than the pair. This is done in Sec. IV using a tetra-hedron as the basic cluster for the bcc $\langle 110 \rangle$ boundary.

As preparation for the formulation in Sec. IV, we solve the bulk properties of the bcc Ising lattice using the tetrahedron approximation in Sec. III. The bulk calculation is reported here as an introduction to the more involved formulation for the boundary in Sec. IV, and also because it leads to the scalar-product (SP) evaluation of the excess boundary free energy σ. The SP formulation is in Sec. III.2 and the results are compared with those of Sec. IV in Sec. IV.3.

The tetrahedron approximation for the bulk reported here has been used before, some results were published,[11,12] and the method was briefly sketched previously.[13] There are also three papers published by a Russian group using the same cluster.[14]

1. Bulk phase using tetrahedron

The tetrahedron we use in this calculation is $i-j-k-l$ in Fig. 1, which is not a regular tetrahedron but is made of four nearest-neighbor bonds $i-k$, $i-l$, $j-k$, $j-l$ and two second-neighbor bonds $i-j$ and $k-l$. The distribution variable for a lattice point is written as x_i and that for a nearest-neighbor pair is written as y_{il}, as can be understood from Table I. Besides x and y, we need three other kinds of distribution variables: z_{ij} for a second-neighbor pair (like $i-j$ in Fig. 1), u_{ijl} for a triangle of the shape $i-j-l$ in Fig. 1, and w_{ijkl} for a tetrahedron $i-j-k-l$ in Fig. 1.

The entropy of the system is written as

$$S = k \ln \Omega \ , \tag{3.1}$$

where Ω is the number of ways in which a system can be constructed for specified set of distribution variables $\{w_{ijkl}\}$ and is written for a system of N lattice points as

$$\Omega = \{\text{Triangle } u_{ijl}\}_N^{12} \{\text{Point } x_i\}_N \{\text{Tetrahedron } w_{ijkl}\}_N^{-6}$$
$$\times \{\text{Second-neighbor pair } z_{ij}\}_N^{-3}$$
$$\times \{\text{Nearest-neighbor pair } y_{il}\}_N^{-4} \ . \tag{3.2}$$

The meaning of the curly bracket notation is explained in any of the cluster-variation publications previously referred to.[8,9]

When the expression for Ω is given as in (3.2), it is a simple procedure to write the free energy of the system in terms of the distribution variables and then minimize it to obtain the equilibrium state. In the NI procedure we treat the w_{ijkl}'s as independent and all other variables as dependent. Following steps similar to those presented in Sec. III of Ref. 5 to keep the symmetry of the formulation explicit, we arrive at the "superposition" expression

$$w_{ijkl} = e^{\beta \lambda / 6} w_{ijkl}^{(0)} \ , \tag{3.3a}$$

where

$$w_{ijkl}^{(0)} = \exp(-\beta \epsilon_{ijkl})(u_{ijl} u_{ijk} u_{kli} u_{klj})^{1/2} (x_i x_j x_k x_l)^{1/24}$$
$$\times (z_{ij} z_{kl})^{-1/4} (y_{il} y_{jl} y_{ki} y_{kj})^{-1/6} \ . \tag{3.3b}$$

The energy parameter ϵ_{ijkl} is defined as the energy per

tetrahedron and is written in terms of the nearest-neighbor energy parameters ϵ_{ij} of (2.5) as

$$\epsilon_{ijkl} = (\epsilon_{ii} + \epsilon_{jl} + \epsilon_{ki} + \epsilon_{kj})/6 \ . \tag{3.4}$$

The definition of ϵ_{ijkl} in this paper is different from that in Eq. (9) of Ref. 13; in the latter, ϵ_{ijkl} is defined as the energy contained in a tetrahedron and the factor of 6 results because a nearest-neighbor bond is shared by six tetrahedra. The present definition is preferred in anticipation of the formulation[12] in which the second-neighbor interaction energy is to be taken into account.

The Lagrange multiplier λ in (3.3a) is for the normalization condition

$$\sum_{i,j,k,l} w_{ijkl} = 1 \tag{3.5}$$

and as is usually the case,[5] is equal to the free energy of the system, per lattice point:

$$F/N = \lambda \ , \tag{3.6}$$

when the free energy is a minimum.

Because of the symmetry of the bulk phase which is contained in the w_{ijkl} expression in (3.3), we do not need additional symmetry constraints nor the Lagrange multiplier α's as are used in Sec. II and in Ref. 6. The Natural Iteration procedure works when we combine (3.3) with the geometrical reduction relations:

$$u_{ijk} = \sum_l w_{ijkl}, \quad z_{ij} = \sum_k u_{ijk},$$
$$y_{ik} = \sum_j u_{ijk}, \quad x_i = \sum_k y_{ik} \ . \tag{3.7}$$

For the measure of convergence of the NI procedure, we take

$$\Delta^{(n)} = \sum_{ijkl} |\ln w_{ijkl}^{(n-1)} - \ln w_{ijkl}^{(n)}| \ , \tag{3.8}$$

where the superscript (n) denotes the nth iteration step. This test value $\Delta^{(n)}$ decreases below 10^{-6} when n is about 400 iterations for almost any temperature in the ordered phase in this particular problem. The difference of logarithms in the measure of the test as in (3.8) is preferred to the straight difference of w's, because the former yields same number of digits accuracy for all w's, which is the accuracy we need in the scalar-product evaluation of the boundary free energy as was discussed in Ref. 6.

2. Scalar-product evaluation of σ

The excess free energy σ of the $\langle 110 \rangle$ boundary can be calculated using the bulk phase results of Sec. III.1 and the SP expression. A $\langle 110 \rangle$ plane of the bcc lattice is drawn in Fig. 2. The lattice constant a is indicated.

The SP expression for the boundary excess free energy has previously been derived and proved.[15,16] Applied to the present problem, we write

$$\exp(-n \sigma_{\langle 110 \rangle} \beta a^2 / \sqrt{2}) = \sum_{\{u_{ijk}\}} \Omega \{u_{ijk}\} [p_I \{u_{ijk}\} p_{II} \{u_{ijk}\}]^{1/2}, \tag{3.9}$$

where $a^2/\sqrt{2}$ is the area per atom in the "parallel"

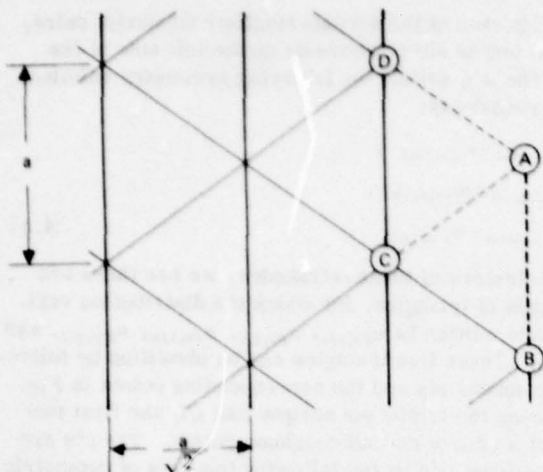FIG. 2. $A \langle 110 \rangle$ plane of the bcc lattice. The nearest-neighbor bond and the second-neighbor bond are drawn with a thin line and a thick line, respectively.

plane, n is the total number of lattice points in the plane, and $\sigma_{\langle 110 \rangle}$ is the excess boundary free energy per unit area. On the right-hand side, $p_1\{u_{ijk}\}$ is the probability that a $\langle 110 \rangle$ plane specified by the set of variables $\{u_{ijk}\}$ is realized in phase I, and $\Omega\{u_{ijk}\}$ is the number of ways the plane can be constructed when the set $\{u_{ijk}\}$ is specified.

The weight factor $\Omega\{u_{ijk}\}$ can be calculated by slightly *modifying the scheme used in Sec. G of Ref. 8. We* can follow the steps of Eq. (G. 1) if we regard bonds AC and AD in Fig. 8 of Ref. 8 as the nearest-neighbor

bonds, and AB and CD as the second-neighbor bonds, as indicated in Fig. 2 of this paper. The result is

$$\Omega\{u_{ijk}\} = \{\text{Second-neighbor pair } z_{ij}\}_n$$
$$\times \{\text{Nearest-neighbor pair } y_{jk}\}_n^2$$
$$\times \{\text{Triangle } u_{ijk}\}_n^{-2}\{\text{Point } x_i\}_n^{-1} \ , \quad (3.10)$$

where the curly bracket notation has the same meaning as that in (3.2) or as in those in Refs. 8 and 9.

Our experiences in Refs. 7, 17, and 6 tell us that we can use the schematic information in Ω of (3.10) when we write the probability function $p_1\{u_{ijk}\}$ appearing in (3.9). It is written as

$$p_1\{u_{ijk}\} = (p_{1,u}^2 \, p_{1,x} \, p_{1,z}^{-1} \, p_{1,y}^{-2})^n \quad (3.11a)$$

where

$$p_{1,u} = \prod_{i,j,k} (u_{ijk}^{(1)}) ** u_{ijk} \ ,$$

$$p_{1,z} = \prod_{i,j} (z_{ij}^{(1)}) ** z_{ij} \ ,$$

$$p_{1,y} = \prod_{j,k} (y_{jk}^{(1)}) ** y_{jk} \ ,$$

$$p_{1,x} = \prod_{i} (x_i^{(1)}) ** x_i \ . \quad (3.11b)$$

The double asterisk is the Fortran notation for "raised to the power of," and is used here to avoid subscripts of a superscript in typesetting. The quantities with the superscript (I) in (3.11), such as $u_{ijk}^{(1)}$, are those for the bulk (I) phase. Note that the powers on the p's on the right-hand side of (3.11a) correspond to those in (3.10).

When we use (3.10) and (3.11) in (3.9), we derive

$$\sigma_{\langle 110 \rangle}\beta a^2/\sqrt{2} = 2\sum_{i,j,k} \mathcal{L}(u_{ijk}) - \sum_{i,j} \mathcal{L}(z_{ij}) - \sum_{i,k} \mathcal{L}(y_{ik}) - \sum_{j,k} \mathcal{L}(y_{jk}) + \frac{1}{3}\Big[\sum_i \mathcal{L}(x_i) + \sum_j \mathcal{L}(x_j) + \sum_k \mathcal{L}(x_k)\Big]$$
$$- 2\sum_{i,j,k} u_{ijk} \ln\hat{u}_{ijk} + \sum_{i,j} z_{ij} \ln\hat{z}_{ij} + \sum_{i,k} y_{ik} \ln\hat{y}_{ik} + \sum_{j,k} y_{jk} \ln\hat{y}_{jk}$$
$$- \frac{1}{3}\Big[\sum_i x_i \ln\hat{x}_i + \sum_j x_j \ln\hat{x}_j + \sum_k x_k \ln\hat{x}_k\Big] + \beta\lambda\Big(1 - \sum_{i,j,k} u_{ijk}\Big) + 2\sum_{i,j,k} (\alpha_{ik} + \alpha_{jk} - \alpha_{ki} - \alpha_{kj})u_{ijk} \ . \quad (3.12)$$

The $\mathcal{L}$ operator is defined in (2.7). The quantity with a caret is defined as the geometric average of the corresponding bulk-phase quantities for phases I and II as

$$\hat{u}_{ijk} = (u_{ijk}^{(1)} u_{ijk}^{(11)})^{1/2} \ ,$$
$$\hat{z}_{ij} = (z_{ij}^{(1)} z_{ij}^{(11)})^{1/2} \ , \quad \text{etc.} \quad (3.13)$$

The Lagrange multipliers α_{jk} are introduced to take care of the symmetry of y_{jk}:

$$y_{jk} = \sum_i u_{ijk} = \sum_i u_{ikj} \ . \quad (3.14)$$

In minimizing σ in (3.12), we use the geometric relations

$$z_{ij} = \sum_k u_{ijk} \ , \quad x_i = \sum_{j,k} u_{ijk} \quad (3.15)$$

together with (3.14). The minimization leads to

$$u_{ijk} = u_{ijk}^{(0)} \exp(\tfrac{1}{2}\beta\lambda + \alpha_{ik} + \alpha_{jk} - \alpha_{ki} - \alpha_{kj}) \ , \quad (3.16a)$$

where

$$u_{ijk}^{(0)} = \hat{u}_{ijk} \frac{(\hat{x}_i \hat{x}_j \hat{x}_k)^{1/6}}{(\hat{z}_{ij}\hat{y}_{ik}\hat{y}_{jk})^{1/2}} \frac{(z_{ij} y_{ik} y_{jk})^{1/2}}{(x_i x_j x_k)^{1/6}} \ . \quad (3.16b)$$

When (3.16) holds and σ in (3.12) is a minimum, we can show that

$$\lambda = \sigma_{\langle 110 \rangle}a^2/\sqrt{2} \ , \quad (3.17)$$

which is the excess boundary free energy per lattice point in the plane. It is easy to see that $\lambda = 0$ when the bulk phase is in the disordered state so that $u_{ijk}^{(1)} = u_{ijk}^{(11)} = \hat{u}_{ijk} = u_{ijk}$.

The Lagrange multipliers, the α_{ik}'s, are determined from the constraints in (3.14). After transformations similar to those in (2.15)–(2.19), we arrive at

$$\exp(2\delta_{12}) = \frac{u_{121}^{(0)} + u_{221}^{(0)}\exp(-\delta_{12})}{u_{212}^{(0)} + u_{112}^{(0)}\exp(\delta_{12})} \quad , \tag{3.18}$$

where

$$\delta_{jk} = \alpha_{jk} - \alpha_{kj}$$

and

$$\delta_{11} = \delta_{22} = 0, \quad \delta_{12} = -\delta_{21} . \tag{3.19}$$

We can solve the set of simultaneous equations by the Natural Iteration technique. We need the major and minor iterations as was the case in Sec. II. However, since the constraint equation in (3.18) in a fourth order algebraic equation for $\exp(\delta_{12})$, the minor iterations can be done by the Newton–Raphson iteration method without trouble.

3. Phase transition within the boundary

As was reported in Ref. 17, the scalar-product treatment of the excess boundary free energy $\sigma_{(110)}$ using the pair approximation leads to a second-order phase change in $\sigma_{(110)}$. We may call this transition temperature T_o. We expect a similar phase change in the tetrahedron (bulk)-triangle (boundary) treatment of Sec. III.2.

In the triangle formulation of Sec. III.2, we see that there are two long-range order parameters:

$$\xi_1 \equiv x_1 - x_2, \quad \xi_2 \equiv u_{111} - u_{222} . \tag{3.20}$$

The transition point T_o can be determined as the point at which the following 2×2 determinant vanishes in the disordered phase:

$$\det\|\partial^2\sigma_{(110)}/\partial\xi_i\partial\xi_j\| = 0 . \tag{3.21}$$

The determinant can be worked out explicitly and the equation takes the form

$$\left(1 - \frac{1}{y_{11}} - \frac{1}{2z_{11}}\right) + \left(\frac{2}{u_{121}} + \frac{1}{u_{221}}\right)\left[1 + u_{111}\left(1 - \frac{1}{y_{11}} - \frac{1}{2z_{11}}\right)\right] = 0 . \tag{3.22}$$

It may be commented that in the disordered phase δ_{12} in (3.19) vanishes and we do not need the minor iteration of (3.18). When we solve the disordered phase in Sec. III.2 and evaluate Eq. (3.22), we do arrive at the second-order transition point T_o, qualitatively confirming the previous conclusions of the pair approximation.[17] The results are discussed in Sec. IV.3.

IV. TETRAHEDRON TREATMENT OF BOUNDARY FREE ENERGY USING THE SUM METHOD

1. Free energy and its minimization

We are now in a position to continue from Sec. II and extend the pair treatment of the boundary sum into the tetrahedron treatment. From Fig. 1, we see that there are three kinds of tetrahedra in an inhomogeneous system: one pointing towards the left $(i-j-k-l)$, one pointing towards the right $(i-j-l-m)$, and a third one $(i-n-l-m)$. We write the distribution variables corresponding to these three as $w_{Lv,ijkl}$, $w_{Rv,ijlm}$, and $w_{Cu,inlm}$, respectively, where ν and μ indicate the position as seen in Fig. 1. Of the four subscripts such as $ijkl$, the first two and the last two connect the second-neighbor lattice

points. In each of the second-neighbor subscript pairs, the first one is either above or on the left side of the pair. The w's satisfy the following symmetry relations among subscripts:

$$w_{Lv,ijkl} = w_{Lv,jikl} \quad ,$$

$$w_{Rv,ijlm} = w_{Rv,jilm} \quad ,$$

$$w_{Cu,inlm} = w_{Cu,lmin} \quad . \tag{4.1}$$

As subclusters of these tetrahedra, we see there are five kinds of triangles, for which the distribution variables are written as $u_{Bv,ijl}$, $u_{Mv,ijk}$, $u_{Pv,ijm}$, $u_{Ru,inl}$, and $u_{Lu,inm}$. These five triangles can be identified by following the subscripts and the corresponding points in Fig. 1. Among the triplet subscripts like ijl, the first two connect a pair of second-neighbor points. The u's are reduced from w's by the following two sets of geometric relations:

$$u_{Mv,ijk} = \sum_l w_{Lv,ijkl}, \quad u_{Pv,ijm} = \sum_l w_{Rv,ijlm} \tag{4.2}$$

and

$$u_{Bv,ijl} = \sum_k w_{Lv,ijkl} = \sum_m w_{Rv,ijlm} \quad ,$$

$$u_{Ru,inl} = \sum_n w_{Cu,inlm} = \sum_j w_{Rv,ijlm} \quad ,$$

$$u_{Lu,inm} = \sum_l w_{Cu,inlm} = \sum_j w_{L(v+1),jmin} \quad . \tag{4.3}$$

The symmetry relations among the w's in (4.1) are inherited by u's through the geometric relations (4.2) and (4.3). The equations among w's in (4.3) necessitate Lagrange multipliers, as shown below.

Two kinds of distribution variables for a second-neighbor pair are written as $z_{Bv,ij}$ (which is within the νth plane) and $z_{Cu,lm}$, which connects l of the νth plane and m on the $(\nu+1)$th plane. Together with w, u, and z we also use x and y defined in Table I.

Since we use w's as the independent variables, the energy of the system in (2.4) is rewritten in terms of w's as

$$E = 2n\sum_{i,j,k,l} \epsilon_{ijkl}\left[\sum_{v=2}^{\nu_g} w_{Lv,ijkl} + \sum_{v=1}^{\nu_g-1} w_{Rv,ijkl} + \sum_{\mu=1}^{\mu_g} w_{Cu,ijkl}\right] , \tag{4.4}$$

where ϵ_{ijkl}, the energy per tetrahedron, is the same as the expression (3.4) for the bulk phase. The multiplicative factor n in (4.4) is the number of lattice points within a plane parallel to the boundary; it should not be confused with the name of a lattice point n on the $(\nu+1)$th plane in Fig. 1.

The Ω expression for this case is derived by modifying Ω in (3.2). For example, the 12 triangles appearing in (3.2) are not all the same in the present case. By counting the frequencies of occurrence, we make the following replacement:

$$\{u_{ijl}\}_N^{12} \to \{u_{Bv,ijl}\}_n^2\{u_{Mv,ijk}\}_n\{u_{Pv,ijm}\}_n$$

$$\times \{u_{Ru,inl}\}_n^4\{u_{Lu,inm}\}_n^4 . \tag{4.5}$$

Applying similar replacements to other factors, we arrive at

$$\Omega = \prod_{\nu \text{ or } \mu} [\{u_{B\nu,ijl}\}_n^2 \{u_{M\mu,ijk}\}_n \{u_{P\nu,ijm}\}_n \{u_{R\mu,ink}\}_n^4$$
$$\times \{u_{L\mu,inm}\}_n^4 \{x_{\nu,i}\}_n][\{w_{L\nu,ijkl}\}_n^2 \{w_{R\nu,ijlm}\}_n^2 \{w_{C\mu,inim}\}_n^2$$
$$\times \{z_{B\nu,ij}\}_n \{z_{C\mu,in}\}_n \{z_{C\mu,im}\}_n \{y_{B\nu,il}\}_n^2 \{y_{C\mu,im}\}_n^2]^{-1} .$$

$$(4.6)$$

The free energy of the entire system can be derived using (4.4), (4.6), and $S = k \ln \Omega$ as in (3.1). We will skip writing the free energy expression to save space, and go directly to the relations obtained by minimizing the free energy with respect to $w_{L\nu,ijkl}$, $w_{R\nu,ijlm}$, and $w_{C\mu,inlm}$:

$$w_{L\nu,ijkl} = w_{L\nu,ijkl}^{(0)} \exp[\tfrac{1}{2}\beta\lambda_{L\nu} + \alpha_{B\nu,ijl} - \alpha_{L(\mu-1),klj}$$
$$- \alpha_{L(\mu-1),kli}] ,$$
$$w_{R\nu,ijlm} = w_{R\nu,ijlm}^{(0)} \exp[\tfrac{1}{2}\beta\lambda_{R\nu} + \alpha_{R\mu,iml} + \alpha_{R\mu,imj} - \alpha_{B\nu,ijl}],$$
$$w_{C\mu,inlm} = w_{C\mu,inlm}^{(0)} \exp[\tfrac{1}{2}\beta\lambda_{C\mu} + \alpha_{L\mu,inm} + \alpha_{L\mu,imn} - \alpha_{R\mu,iml}$$
$$- \alpha_{R\mu,inl}] ,$$

$$(4.7)$$

where

$$w_{L\nu,ijkl}^{(0)} = \exp(-\beta\epsilon_{ijkl})(u_{B\nu,ijl} u_{M\nu,ijk} u_{L(\mu-1),kli} u_{L(\mu-1),klj})^{1/2}$$
$$\times (x_{\nu,i} x_{\nu,j} x_{\nu,l} x_{\nu-1,k})^{1/24} (z_{B\nu,ij} z_{C(\mu-1),kl})^{-1/4}$$
$$\times (y_{B\nu,il} y_{B\nu,jl} y_{C(\mu-1),kl} y_{C(\mu-1),kj})^{-1/6} ,$$

$$w_{R\nu,ijlm}^{(0)} = \exp(-\beta\epsilon_{ijlm})(u_{B\nu,ijl} u_{P\nu,ijm} u_{R\mu,iml} u_{R\mu,imj})^{1/2}$$
$$\times (x_{\nu,i} x_{\nu,j} x_{\nu,l} x_{\nu+1,m})^{1/24} (z_{B\nu,ij} z_{C\mu,lm})^{-1/4}$$
$$\times (y_{B\nu,il} y_{B\nu,jl} y_{C\mu,im} y_{C\mu,jm})^{-1/6} ,$$

$$w_{C\mu,inlm}^{(0)} = \exp(-\beta\epsilon_{inlm})(u_{R\mu,inl} u_{R\mu,iml} u_{L\mu,inm} u_{L\mu,imn})^{1/2}$$
$$\times (x_{\nu,i} x_{\nu,l} x_{\nu+1,n} x_{\nu+1,m})^{1/24} (z_{C\mu,in} z_{C\mu,lm})^{-1/4}$$
$$\times (y_{B\nu,il} y_{B(\nu+1),mn} y_{C\mu,im} y_{C\mu,ln})^{-1/6} .$$

$$(4.8)$$

It can be seen that the three $w^{(0)}$'s in (4.8) reduce to $w^{(0)}$ for the bulk phase in (3.3b) when the system is homogeneous.

The Lagrange multipliers $\lambda_{L\nu}$, $\lambda_{R\nu}$, and $\lambda_{C\mu}$ in (4.7) take care of the normalizations:

$$\sum_{i,j,k,l} w_{L\nu,ijkl} = \sum_{i,j,l,m} w_{R\nu,ijlm} = \sum_{i,n,l,m} w_{C\mu,inlm} = 1 .$$

$$(4.9)$$

Similar to (2.11) and (2.14) for pair treatment, in the present case the free energy of the entire system including the boundary is written as the sum

$$\frac{F}{n} = \sum_{\nu=2}^{\nu_g} \lambda_{L\nu} + \sum_{\nu=1}^{\nu_g-1} \lambda_{R\nu} + \sum_{\mu=1}^{\mu_g} \lambda_{C\mu} .$$

$$(4.10)$$

When we compare this equation to (3.6) for the bulk, we see that each $\lambda_{L\nu}$, $\lambda_{R\nu}$, and $\lambda_{C\mu}$ reduces to $\lambda/3$ when the boundary is removed. That is the reason why the $\beta\lambda_{L\nu}$ term in (4.7) is divided by 2 in contrast to the factor $\tfrac{1}{6}$ in (3.3a).

The Lagrange multipliers α's in (4.7) are determined by the three continuity relations in (4.3). It is convenient to define

$$S_{BL\nu,ijl} \equiv \sum_k w_{L\nu,ijkl}^{(0)} \exp[-\alpha_{L(\mu-1),klj} - \alpha_{L(\mu-1),kli}] ,$$

$$S_{BR\nu,ijl} \equiv \sum_m w_{R\nu,ijlm}^{(0)} \exp[\alpha_{R\mu,iml} + \alpha_{R\mu,imj}] ,$$

$$S_{RR\nu,iml} \equiv \sum_j w_{R\nu,ijlm}^{(0)} \exp[\alpha_{R\mu,imj} - \alpha_{B\nu,ijl}] ,$$

$$S_{RC\mu,iml} \equiv \sum_n w_{C\mu,inlm}^{(0)} \exp[\alpha_{L\mu,inm} + \alpha_{L\mu,imn} - \alpha_{R\mu,inl}] ,$$

$$S_{LC\mu,inm} \equiv \sum_l w_{C\mu,inlm}^{(0)} \exp[\alpha_{L\mu,imn} - \alpha_{R\mu,iml} - \alpha_{R\mu,inl}] ,$$

$$S_{LL(\nu+1),inm} \equiv \sum_j w_{L(\nu+1),jmin}^{(0)} \exp[\alpha_{B(\nu+1),jmn} - \alpha_{L\mu,inj}] .$$

$$(4.11)$$

Then we can write the first equation in (4.3) as

$$u_{B\nu,ijl} = \exp(\tfrac{1}{2}\beta\lambda_{L\nu} + \alpha_{B\nu,ijl}) S_{BL\nu,ijl}$$
$$= \exp(\tfrac{1}{2}\beta\lambda_{R\nu} - \alpha_{B\nu,ijl}) S_{BR\nu,ijl} .$$

$$(4.12)$$

In treating this set of equations, we can follow Weeks and Gilmer's idea[1] and eliminate λ's by forming ratios, as was done in Sec. II. Further we note that, since the w's satisfy the normalization relations, one of the eight equations (since each of i, j, and l takes two values 1 and 2) in (4.12) is redundant. This redundancy also occurs in the rest of the equations in (4.3). Thus, we can choose without loss of generality, for example,

$$\alpha_{B\nu,222} = \alpha_{R\mu,222} = \alpha_{L\mu,222} = 0 .$$

$$(4.13)$$

By forming ratios from (4.12) and using (4.13), we obtain the following set of equations to determine the α's:

$$\alpha_{B\nu,ijl} = \tfrac{1}{2} \ln(S_{BR\nu,ijl} S_{BL\nu,222} / S_{BR\nu,222} S_{BL\nu,ijl}) ,$$
$$\alpha_{R\mu,iml} = \tfrac{1}{2} \ln(S_{RC\mu,iml} S_{RR\nu,222} / S_{RC\mu,222} S_{RR\nu,iml}) ,$$
$$\alpha_{L\mu,inm} = \tfrac{1}{2} \ln(S_{LL(\nu+1),inm} S_{LC\mu,222} / S_{LL(\nu+1),222} S_{LC\mu,inm}) .$$

$$(4.14)$$

From (4.11), we see that $S_{BL\nu,ijl}$ and $S_{BR\nu,ijl}$ are invariant under the exchange of i and j, and thus $\alpha_{B\nu,ijl}$ in (4.14) retains this symmetry. Because of this symmetry in $\alpha_{B\nu,ijl}$, when the input w's satisfy the symmetry properties in (4.1), the symmetry is guaranteed to be inherited by the output w's.

2. The natural iteration computations

We solve the simultaneous equations in Sec. IV.1 using the Natural Iteration method. As was mentioned following (2.20) in Sec. II, the iterations are divided into the major and the minor ones. A major iteration starts with the input data set $\{u_{B\nu}, u_{M\nu}, u_{P\nu}, u_{R\mu}, u_{L\mu}\}$ and $\{\alpha_{B\nu}, \alpha_{R\mu}, \alpha_{L\mu}\}$. We calculate $\{w_{L\nu}^{(0)}, w_{R\nu}^{(0)}, w_{C\mu}^{(0)}\}$ from (4.8). Then we do the minor iterations to satisfy the subsidiary conditions (4.14). After the minor iterations converge, the output is written as $\{\hat{\alpha}_{B\nu}, \hat{\alpha}_{R\mu}, \hat{\alpha}_{L\mu}\}$. We use these together with the $w^{(0)}$'s in (4.8), which have already been calculated, in (4.7) to derive the output set $\{\hat{w}_{L\nu}, \hat{w}_{R\nu}, \hat{w}_{C\mu}\}$ together with the set $\{\hat{\lambda}_{L\nu}, \hat{\lambda}_{R\nu}, \hat{\lambda}_{C\mu}\}$. The output $\hat{w}$'s lead to the next input set $\{\hat{u}_{B\nu}, \ldots, \hat{u}_{L\mu}\}$ thus closing one major iteration cycle.

In Cahn–Kikuchi's work[3,4] it was discovered that two

cases should be distinguished; one is the interstitial-center (IC) boundary in which the center of the boundary is between two parallel planes, and the other is the atomic-center (AC) boundary in which the center of the boundary is on one of the parallel planes. We did calculations for these two cases. In the IC case we took the number of parallel planes $\nu_z = 20$ (the center being between $\nu = 10$ and 11), and in the AC case we took $\nu_z = 19$ (the center at $\nu = 10$).

In both cases the initial condition for the iteration was chosen such that the left-hand side of the boundary center is in the bulk I phase and the right-hand side in the bulk II phase. When some variable is right at the center, we used the averaged value between the two bulk phase values. The initial values of α's are chosen as zero all through the system.

In carrying out this iteration calculation, several comments are in order. These comments are important when a system is as large as the present one, in which the total number of independent w's and α's is about 700. (Actually a system much larger than the present one has been successfully calculated by Sanchez at UCLA[18] using the Natural Iteration technique.) The first comment concerns the minor iteration procedure. Equation (4.14) corresponds to the minor iteration equation (2.18) in the pair case and to Eq. (2.20a) in Ref. 6. In Sec. II, Eqs. (2.17)–(2.19) work and converge nicely without trouble. In the present case, however, when we start from the initial set $\alpha = 0$, the output $\hat{\alpha}$ of the iterations from (4.14) diverges. This was not completely unexpected because the convergence of the minor iteration is not guaranteed, although the convergence of the major iteration can be analytically proved as in Sec. II. In the present case the convergence was achieved by the following trick. Instead of using the output $\hat{\alpha}$ from (4.14)
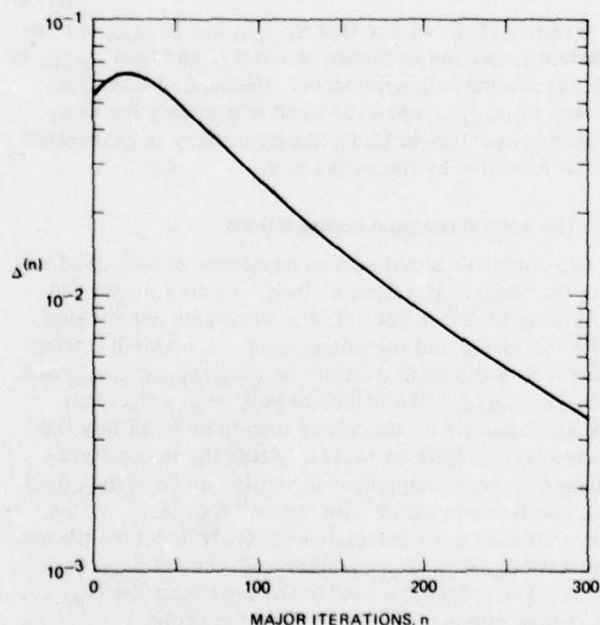

FIG. 3. The test measure $\Delta^{(n)}$ in (4.16) of the NI calculation of the bcc (110) boundary sum method plotted against the major iteration n in a semilog scale.
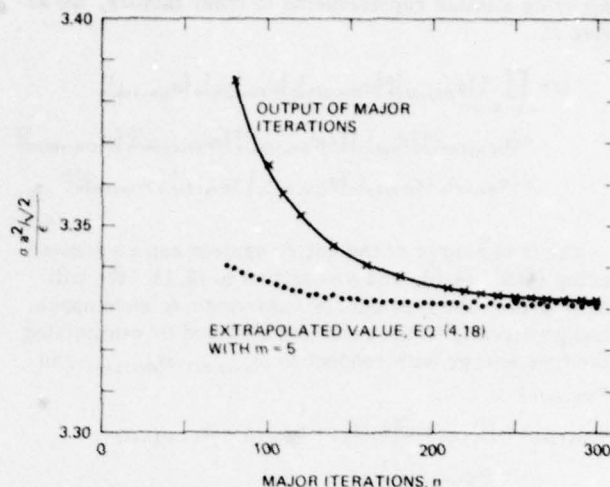

FIG. 4. The excess free energy and the extrapolated value using (4.18) calculated using the NI method.

directly as the input to the next minor iteration cycle, we use the average as the next input:

$$\alpha_{\text{next input}} = \tfrac{1}{2}(\alpha_{\text{input}} + \hat{\alpha}_{\text{output}}) . \qquad (4.15)$$

This brings the next input closer to the previous input than using $\hat{\alpha}_{\text{output}}$, and it works. Depending on the circumstances, we can conceive of many modifications of the scheme in (4.15). In the work reported in this paper, the number of minor iterations at each major iteration step was about 60.

The next important consideration we can make use of is the extrapolation of the major iteration steps. For the measure of convergence of the major iteration we used the following quantity:

$$\Delta^{(n)} = \sum_{i,j,k,l} \sum_{\nu \text{ or } \mu} \{ | w_{L\nu,ijkl}^{(n-1)} - w_{L\nu,ijkl}^{(n)} | $$
$$ + | w_{R\nu,ijkl}^{(n-1)} - w_{R\nu,ijkl}^{(n)} | + | w_{Cu,ijkl}^{(n-1)} - w_{Cu,ijkl}^{(n)} | \} . $$
$$(4.16)$$

Different from (3.8), we did not take the logarithms of w's in (4.16), but it is adequate for our present purposes. This test value $\Delta^{(n)}$ decreases logarithmically as illustrated in Fig. 3 for $kT/\epsilon = 3.0$, and we can prove that $\Delta^{(n)}$ is linear in the semilog scale for large number n of the major iteration.

In the same sense, σ also approaches the converged value $\sigma^{(\infty)}$ exponentially as is seen in an example of $kT/\epsilon = 3.0$ in Fig. 4. Using this property, we can extrapolate σ starting with the assumption

$$\sigma^{(n)} = \sigma^{(\infty)} + a e^{-nb} , \qquad (4.17)$$

where $\sigma^{(n)}$ is the value of the boundary excess free energy at the nth major iteration. It is a simple matter to derive

$$\sigma^{(\infty)} = \sigma^{(n)} - (\Delta_m \sigma^{(n)})^2 / (\Delta_m \sigma^{(n-m)} - \Delta_m \sigma^{(n)}) ,$$

where

$$\Delta_m \sigma^{(n)} \equiv \sigma^{(n-m)} - \sigma^{(n)} . \qquad (4.18)$$

The extrapolated value $\sigma^{(\infty)}$ is a function of n and m since

the exponential decay relation (4.17) does not hold exactly unless n is very large. As we see in Fig. 3, $\Delta^{(n)}$ is still slightly curved in the semilog plot at $n = 300$. The extrapolated value $\sigma^{(\infty)}$ is also plotted in Fig. 4 as a function of n. It is almost flat. This plot is based on the choice of $m = 5$, but other values ($m = 10$ and 20) give practically the same extrapolated value for $\sigma^{(\infty)}$.

The same extrapolation idea was used in the estimate of the profile. Figure 5 shows how $x_{\nu,1}$ for $\nu = 11$ and 12 are extrapolated using the same scheme as (4.18).

Actually, a much more desirable scheme is to extrapolate the entire set $\{w_{L\nu,ijkl}, w_{R\nu,ijlm}, w_{C\mu,inlm}\}$ to $n \to \infty$ starting from a finite iteration step n using a formula similar to (4.18). Such an extrapolation has been tried and found successful in other applications of the Natural Iteration method, but for no apparent reason has not yet been applied to the present problem.

3. Comparison of results

Figure 6 compares the results of the excess free energy σ of this paper and previous ones.[3,17] Of the four curves of σ, the upper one indicated as PAIR S.-P. is the result of the scalar-product formula using the pair approximation in Ref. 17. It has the second-order phase transition at T_σ of Table II, as shown by a cross in Fig. 6.

The broken curve named PAIR SUM is the result of Sec. II of this paper and is the same as the result shown in the curve (2), Fig. 9 of Ref. 3. This curve is for the
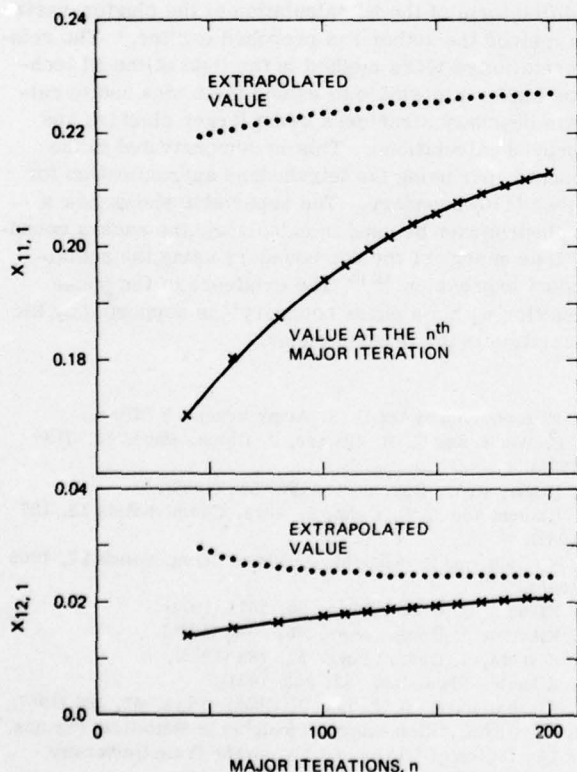

FIG. 6. The boundary excess free energy σ for the bcc $\langle 110 \rangle$ boundary calculated by four different methods. See the text.

IC boundary and is lower than the AC value. The difference of the two boundaries, σ_{AC-IC}, is plotted at the bottom of Fig. 6 in a broken curve.

The solid curve marked TRH S.-P. is the result of the scalar-product method in Secs. III.2 and III.3 of the present paper. The second-order phase transition point is again indicated by a cross at the value of T_σ of Table II.

The dot–dash curve which is the lowest and marked TRH SUM is the result of the method in Sec. IV of this paper, calculated for the IC boundary. The AC case was also calculated and the difference $\sigma_{AC} - \sigma_{IC}$ is again plotted by a dot–dash curve at the bottom.

The first general conclusion we can derive from the comparison of these four curves in Fig. 6 is that they agree well qualitatively and thus guarantee that our methods are sound. The second conclusion we derive is that the sum method of Secs. II and IV gives lower σ values than the corresponding approximation of the scalar-product results, in Ref. 17 and Sec. IV. The intrinsic reason for this is not known at this writing.

FIG. 5. The plus spin density at $\nu = 11$ and 12 planes and their extrapolated values.

TABLE II. Transition point data. The value with an asterisk was previously reported in Table I of Ref. 13.

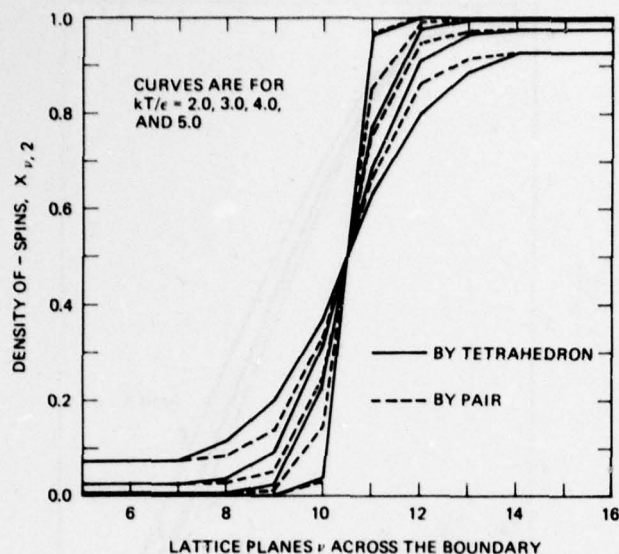| Method	Curie point in the bulk kT_c/ϵ	Transition point in σ kT_σ/ϵ	$\sigma(a^2/\sqrt{2})/\epsilon$ at T_σ
Pair, Ref. 17	6.9521	2.8854	3.5992
Tetrahedron, this paper	6.4907*	2.4918	3.7267

FIG. 7. Profiles of spin density for the bcc $\langle 110 \rangle$ boundary calculated by the pair method (dotted curve) and by the tetrahedron method (solid curve).

FIG. 8. Thickness L of the boundary defined by (4.19) for the bcc $\langle 110 \rangle$ boundary calculated by the two methods.

The profiles of the IC boundaries are plotted in Fig. 7. They are for temperatures $kT/\epsilon = 2.0$, 3.0, 4.0, and 5.0 from the sharpest to the most gradual in this order. The solid curves are the results of the tetrahedron treatment of Sec. IV and the dot curves of the pair treatment of Sec. II. The former is always more gradual than the latter for the same temperature.

For the rough measure of the "thickness" L of the boundary layer, we use the definition used by Weeks and Gilmer[1] in their Eq. (38):

$$L = (1 - 2x_{\nu=\infty,1}^{(II)})/(1 - 2x_{\nu=11,1}) \ . \tag{4.19}$$

Note that the center of the boundary is between $\nu = 10$ and 11. The quantity $x_{\nu=\infty,1}^{(II)}$ is the bulk value. This "thickness" L is plotted in Fig. 8. Reflecting the fact that the tetrahedron boundary is less sharp than the pair boundary, the L value for the former is larger than the latter.

The nature of the phase transitions within the boundary, marked by crosses in Fig. 6, is one of the prime interests of Weeks–Gilmer's paper[1] and of the present work as well. In Ref. 17 it was suggested that the unstable disordered phase below T_σ corresponds to the AC boundary and the stable ordered phase to the IC boundary. The $\sigma_{AC} - \sigma_{IC}$ plotted in Fig. 6 indicates that this identification almost holds but is not exact because the tail of $\sigma_{AC} - \sigma_{IC}$ extends into the temperature above T_σ. However, the prediction (C) in Sec. IV of Ref. 17 that $\sigma_{AC} - \sigma_{IC}$ becomes smaller as the approximation improves and would vanish in the limit of the exact treatment is supported without doubt by comparison of the two $\sigma_{AC} - \sigma_{IC}$ curves in Fig. 6.

The curves for "thickness" L were studied by Weeks and Gilmer[1] to obtain a clue for the nature of the transition point T_σ. The two curves in Fig. 8 do not give anything definite to answer the question.
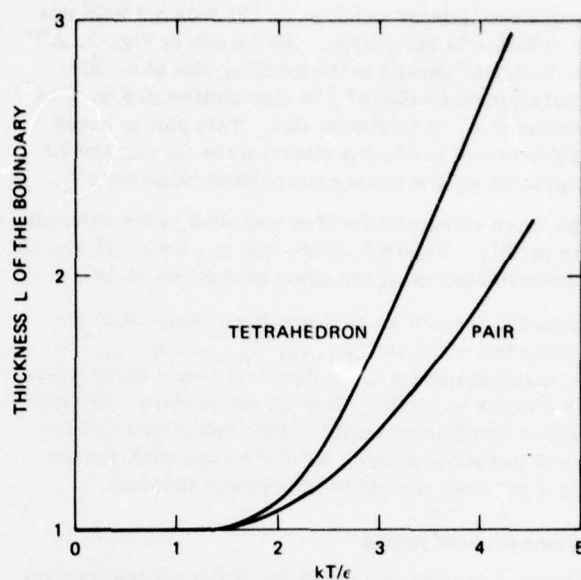
As was commented in Sec. IV(E) of Ref. 17, time-

dependent analysis of the boundary motion still remains a hopeful method of clarifying the nature of T_σ.

4. Summary

The present paper shows that the iterative calculation proposed by Weeks and Gilmer[1] can be interpreted as a modified form of the NI calculation of the cluster-variation method the author had proposed earlier.[5] The reinterpretation of WG's method in the light of the NI technique makes it possible to extend their idea and to calculate boundary structures using larger clusters and improved calculations. This is demonstrated in the present paper using the tetrahedron approximation for the bcc $\langle 110 \rangle$ boundary. The paper also shows how a tetrahedron can be used in calculating the excess boundary free energy of the bcc boundary using the scalar-product expression.[15,16] The existence of the phase transition within a phase boundary[17] is supported by the calculation in the present paper.

[1] J. D. Weeks and G. H. Gilmer, J. Chem. Phys. 63, 3136 (1975).
[2] H. Bethe, Proc. Roy. Soc. A150, 552 (1935).
[3] R. Kikuchi and J. W. Cahn, J. Phys. Chem. Solids 23, 137 (1962).
[4] J. W. Cahn and R. Kikuchi, J. Phys. Chem. Solids 27, 1305 (1966).
[5] R. Kikuchi, J. Chem. Phys. 60, 1071 (1974).
[6] R. Kikuchi, J. Chem. Phys. 65, 4545 (1976).
[7] R. Kikuchi, J. Chem. Phys. 57, 783 (1972).
[8] R. Kikuchi, Phys. Rev. 81, 988 (1951).
[9] R. Kikuchi and S. G. Brush, J. Chem. Phys. 47, 195 (1967).
[10] J. W. Gibbs, "Elementary Principles in Statistical Physics," in The Collected Works of J. W. Gibbs (Yale University, New Haven, CT, 1957), Vol. 2, Chap. 11.
[11] H. Sato and R. Kikuchi, AIP Conference Proceedings, No. 18, p. 605 (1974).

[12]R. Kikuchi and C. M. van Baal, Scripta Met. 8, 425 (1974).

[13]R. Kikuchi and H. Sato, Acta Met. 22, 1099 (1974).

[14]N. S. Golosov and A. M. Tolstik, J. Phys. Chem. Solids 36, 899, 903 (1975); N. S. Golosov, A. M. Tolstik, and L. Ya. Pudan, *ibid.* 37, 273 (1976).

[15]D. B. Clayton and G. W. Woodbury, Jr., J. Chem. Phys. 55, 3895 (1971).

[16]R. Kikuchi, J. Chem. Phys. 57, 777 (1972).

[17]R. Kikuchi, J. Chem. Phys. 57, 4633 (1972).

[18]J. M. Sanchez, private communication.

APPENDIX 3

(Reference [3])

THE SCALAR-PRODUCT EXPRESSION OF BOUNDARY
FREE ENERGY FOR LONG-RANGE INTERACTING
SYSTEMS

R. Kikuchi

J. Chem. Phys. 68, 119 (1978)

The scalar-product expression of boundary free energy for long-range interacting systems[a]

Ryoichi Kikuchi

Hughes Research Laboratories, Malibu, California 90265
(Received 5 July 1977)

The scalar-product formula of the excess free energy σ of a boundary between two phases (based on the lattice model) is proved for the case of interaction potential of the range longer than the nearest neighbor. The formula is $\exp(-A\sigma/kT) = \Sigma[p^{(I)}(\nu_1,\nu_2,...,\nu_k) \; p^{(II)}(\nu_1,\nu_2,...,\nu_k)]^{1/2} \exp[\alpha^{(I)}(\nu_1,\nu_2,...,\nu_k) - \alpha^{(II)}(\nu_1,\nu_2,...,\nu_k)]$, where A is the sectional area parallel to the boundary, ν_i is a configuration of an ith plane parallel to the boundary, $p^{(I)}(\nu_1,...,\nu_k)$ is the probability that k consecutive planes in the bulk I phase take configurations $\nu_1,...,\nu_k$, and the summation goes over all configurations $\nu_1,...,\nu_k$. The variable $\alpha^{(I)}(\nu_1,\nu_2,...,\nu_k)$ is a Lagrange multiplier to guarantee continuity of $p^{(I)}$: $\Sigma_\mu p^{(I)}(\mu,\nu_1,\nu_2,...,\nu_k) = \Sigma_\mu p^{(I)}(\nu_1,\nu_2,...,\nu_k,\mu)$. The expression is checked by two examples. The σ for the two-dimensional Ising model is calculated using a 3×2 cluster (i.e., a double square cluster made of six lattice points) with the "3"-side perpendicular to the boundary, and is compared with the previous σ calculated with a 2×3 cluster (with the "3"-side parallel to the boundary). The calculated σ's agree well when the α terms are included. As a second example, surface tension σ of a liquid of a two-dimensional lattice gas–liquid model (in which the first, second, and third neighbor pairs are excluded, and the fourth and fifth neighbor pairs attract) is calculated. It is then compared with σ calculated by a sum method (which calculates the equilibrium state of a sandwich system made of the gas and the liquid phases with the boundary between them). The agreement between the two calculations supports the correctness of the proposed σ expression.

I. INTRODUCTION

The purpose of this paper is to report how the scalar-product formula of the boundary free energy can be extended to cases of interactions of longer range than the nearest-neighbor distance.

The following formula of the boundary excess energy σ per unit area was first proposed by Clayton and Woodbury[1]:

$$e^{-\beta A\sigma} = \sum_\nu [p^{(I)}(\nu)p^{(II)}(\nu)]^{1/2} , \qquad (1.1)$$

where A is the sectional area of the system parallel to the boundary, and $\beta = 1/kT$. When we consider a crystalline plane parallel to the boundary (called a parallel plane, for short), ν in (1.1) denotes one of the configurations of the parallel plane. The probability that a parallel plane takes a configuration ν in the bulk phase I is written as $p^{(I)}(\nu)$, and the corresponding quantity for the bulk phase II is $p^{(II)}(\nu)$. When we regard the array of $p^{(I)}(\nu)^{1/2}$ for $\nu = 1, 2, ...$ as a vector, the expression (1.1) can be interpreted as a scalar product of the two bulk-phase vectors $\{p^{(I)}(\nu)^{1/2}\}$ and $\{p^{(II)}(\nu)^{1/2}\}$, and thus we may call (1.1) the scalar-product (SP) expression of the boundary free energy.

In the SP formula (1.1), ν is the configuration of an infinitely extended parallel plane of lattice points. Therefore, to use (1.1) for numerical computations, it is necessary to approximate it using configurations of a finite-sized cluster. This approximation[2,3] was done using the cluster-variation method, and the results were checked by comparing them with the exact results of Onsager[4] and of Fisher and Ferdinand[5] for the two-dimensional Ising model. The comparison supports the correctness of the SP expression. The SP formula

helped solve[6,7] the puzzle in the square gradient theory[8] of the boundary structure, and was also useful in predicting the existence of a phase transition within a boundary.[9] In spite of these successes, problems remain with regard to the SP formula. We consider these problems in this paper.

When Clayton and Woodbury[1] proposed the SP formula (1.1), the proof was not as complete as had been hoped for. Further study by the author[6,10] has supplemented the proof, but it still needs improvement. Another, somewhat related, problem is the case of interaction potential of longer range than the nearest-neighbor distance. The long-range interaction case was discussed in Ref. 6, Sec. V, but the reported expression was in error.

The corrected proof of the SP expression is presented in Secs. II and III in the present paper for the general case of a long-range interaction. An example of an Ising model is presented in Sec. IV and another example of a gas–liquid phase boundary in Sec. V.

II. PROOF OF THE SP EXPRESSION OF BOUNDARY FREE ENERGY

This section presents the corrected proof of the SP formula of the boundary free energy for interaction potentials of longer range than the nearest-neighbor distance. In the proof, we avoid using the inverse of the transfer matrix $\mathbf{P}$, which was used in the proof reported in Ref. 10.

In the system being considered, there is one phase boundary between the left (I) and the right (II) phases. A lattice plane parallel to the boundary is simply called a parallel plane. The position of a parallel plane is designated by i. Each parallel plane contains N lattice points; a configuration of the plane is designated by a Greek letter (μ, ν, ξ, or η) that takes values from 1

through K^N, K being the number of species in the system. For simplicity, the formulation in this section is done for a system which does not need superlattices.

In demonstrating the long-range interaction formulation, we use the probability function $p_i(\mu, \nu, \xi)$, which encompasses three consecutive parallel planes with the ith plane at the center. The three-plane formulation is sufficient to induce the general case from it. In writing the free energy F in terms of $p_i(\mu, \nu, \xi)$, we use the cluster-variation (CV) approach[11] and apply it to a cluster of three consecutive infinitely long lines. The method is exact (contrary to a widespread misconception that the CV method is always approximate) since the system is pseudo-one-dimensional. The method, which was explained in Ref. 6, Secs. II and V, leads to the following expression for the free energy of the entire inhomogeneous system:

$$F = \sum_i \sum_{\mu, \nu, \xi} \epsilon(\mu, \nu, \xi) p_i(\mu, \nu, \xi)$$

$$- kT \sum_i \left\{ \frac{1}{2} \sum_{\mu, \nu} \mathcal{L}[p_{i-1/2}(\mu, \nu)] + \frac{1}{2} \sum_{\nu, \xi} \mathcal{L}[p_{i+1/2}(\nu, \xi)] - \sum_{\mu, \nu, \xi} \mathcal{L}[p_i(\mu, \nu, \xi)] \right\}$$

$$+ kT \sum_i \sum_{\mu, \nu, \xi} \{\alpha_{i-1/2}(\mu, \nu) - \alpha_{i+1/2}(\nu, \xi)\} p_i(\mu, \nu, \xi) + \sum_i \lambda_i \left\{ 1 - \sum_{\mu, \nu, \xi} p_i(\mu, \nu, \xi) \right\} . \tag{2.1}$$

The notation differs slightly from that used in Ref. 6. In the first term, $\epsilon(\mu, \nu, \xi)$ is the energy per three-plane region; the $\mathcal{L}$ operator is defined as

$$\mathcal{L}[x] \equiv x \ln x - x ; \tag{2.2}$$

and $p_{i-1/2}(\mu, \nu)$ is the probability that the $(i-1)$th and the ith planes take configurations μ and ν, respectively. The Lagrange multiplier α's are used to satisfy the continuity requirements:

$$p_{i-1/2}(\mu, \nu) = \sum_\xi p_{i-1}(\xi, \mu, \nu) = \sum_\xi p_i(\mu, \nu, \xi) . \tag{2.3}$$

The sign of α in this section is reversed from that of Refs. 3 and 6. The last terms in (2.1) are for the normalization of p_i for every i,

$$\sum_{\mu, \nu, \xi} p_i(\mu, \nu, \xi) = 1 , \tag{2.4}$$

and λ_i are the Lagrange multipliers.

Minimizing F in (2.1) with respect to $p_i(\mu, \nu, \xi)$ yields

$$p_i(\mu, \nu, \xi) = \exp[\beta\lambda_i - \beta\epsilon(\mu, \nu, \xi)]$$
$$\times [p_{i-1/2}(\mu, \nu) p_{i+1/2}(\nu, \xi)]^{1/2}$$
$$\times \exp[\alpha_{i-1/2}(\mu, \nu) - \alpha_{i+1/2}(\nu, \xi)] . \tag{2.5}$$

When F is a minimum, we can derive

$$F = F - \sum_i \sum_{\mu, \nu, \xi} \frac{\partial F}{\partial p_i(\mu, \nu, \xi)} = \sum_i \lambda_i , \tag{2.6}$$

which shows that λ_i can be interpreted as the local free energy. For further transformations it is convenient to introduce

$$g_{i+1/2}(\nu, \xi) \equiv [p_{i+1/2}(\nu, \xi)]^{1/2} \exp[- \alpha_{i+1/2}(\nu, \xi)] ,$$
$$h_{i-1/2}(\mu, \nu) \equiv [p_{i-1/2}(\mu, \nu)]^{1/2} \exp[\alpha_{i-1/2}(\mu, \nu)] , \tag{2.7}$$
$$\Gamma(\mu, \nu, \xi) \equiv \exp[- \beta\epsilon(\mu, \nu, \xi)] ,$$

and write (2.5) as

$$p_i(\mu, \nu, \xi) = \exp(\beta\lambda_i) h_{i-1/2}(\mu, \nu)$$
$$\times \Gamma(\mu, \nu, \xi) g_{i+1/2}(\nu, \xi) . \tag{2.8}$$

It is important to note from (2.7) that

$$\sum_\mu \sum_\nu h_{i+1/2}(\mu, \nu) g_{i-1/2}(\mu, \nu) = 1 , \tag{2.9}$$

in which the normalization of $p_{i+1/2}(\mu, \nu)$ is used. By using the definitions of g and h in (2.7) and substituting (2.8) into the continuity relations in (2.3), the following two relations can be derived:

$$g_{i-1/2}(\mu, \nu) = \exp(\beta\lambda_i) \sum_\xi \Gamma(\mu, \nu, \xi) g_{i+1/2}(\nu, \xi) , \tag{2.10a}$$

$$h_{i+1/2}(\nu, \xi) = \exp(\beta\lambda_i) \sum_\mu \Gamma(\mu, \nu, \xi) h_{i-1/2}(\mu, \nu) . \tag{2.10b}$$

So far the transformations are similar to those in previous papers.[6,10] Now we formulate the new proof of the SP expression. We choose any two integers i and j with the requirement

$$i \leq j . \tag{2.11}$$

We first sum the following expression over ξ and use (2.10a); we then sum over μ and use (2.10b) to derive

$$\sum_\mu \sum_\nu \sum_\xi h_{i-1/2}(\mu, \nu) \Gamma(\mu, \nu, \xi) g_{j+1/2}(\nu, \xi)$$

$$= \sum_\mu \sum_\nu h_{i-1/2}(\mu, \nu) [\exp(- \beta\lambda_j) g_{j-1/2}(\mu, \nu)]$$

$$= \sum_\nu \sum_\xi [\exp(- \beta\lambda_i) h_{i+1/2}(\nu, \xi)] g_{j+1/2}(\nu, \xi) . \tag{2.12}$$

When $i = j$, use of (2.9) in the sums reduces (2.12) to $\exp(- \beta\lambda_i)$. In general, we can rewrite (2.12) and derive a general recurrence relation for shifting (i, j) into $(i+1, j+1)$:

$$\sum_\mu \sum_\nu h_{i-1/2}(\mu, \nu) g_{j-1/2}(\mu, \nu)$$

$$= \exp(- \beta\lambda_i + \beta\lambda_j) \sum_\mu \sum_\nu h_{i+1/2}(\mu, \nu) g_{j+1/2}(\mu, \nu) . \tag{2.13}$$

We start with $i = -m$ and $j = m+1$, and operate the recurrence relation (2.13) $M(\geq 2m)$ times to obtain

$$\sum_{\mu} \sum_{\nu} h_{-m-1/2}(\mu, \nu) g_{m+1/2}(\mu, \nu)$$

$$= \exp[-\beta(\lambda_{-m} + \lambda_{-m+1} + \cdots + \lambda_m) + \beta(\lambda_{-m+M} + \lambda_{-m+1+M} + \cdots + \lambda_{m+M})] \sum_{\mu} \sum_{\nu} h_{-m+M-1/2}(\mu, \nu) g_{m+M+1/2}(\mu, \nu) . \quad (2.14)$$

Note that $\lambda_{-m+1} + \cdots + \lambda_{-m+M-1}$ cancels between the $-\beta(\ )$ and the $+\beta(\ )$ sums. Since M in (2.14) can be arbitrarily large, we let it become infinite. Then $h_{-m+M-1/2}$ and $g_{m+M+1/2}$ can be replaced by the values for the bulk II phase so that

$$\lim_{M \to \infty} \sum_{\mu} \sum_{\nu} h_{-m+M-1/2}(\mu, \nu) g_{m+M+1/2}(\mu, \nu) = \sum_{\mu} \sum_{\nu} h^{(II)}(\mu, \nu) g^{(II)}(\mu, \nu) = 1 , \quad (2.15)$$

where we have used the normalization (2.9).

We choose that the geometry of the sum in (2.14) is such that the boundary lies between $-m$ and $+m$ when the m is made large. In the limit of $m \to \infty$, the λ-sum part leads to

$$-\beta \lim_{m \to \infty} \sum_{i=-m}^{+m} (\lambda_i - \lambda^{(0)}) \equiv -\beta A \sigma , \quad (2.16)$$

where $\lambda^{(0)}$ is the bulk value and σ is defined as the boundary excess free energy per unit area. In the limit as m becomes very large, $h_{-m-1/2}$ and $g_{m+1/2}$ in (2.14) approach the $h^{(I)}$ and $g^{(II)}$ functions for the respective bulk phases. Therefore, we obtain from (2.14) for the limit of $m \to \infty$

$$e^{-\beta A \sigma} = \sum_{\mu} \sum_{\nu} h^{(I)}(\mu, \nu) g^{(II)}(\mu, \nu) . \quad (2.17)$$

Writing this explicitly using (2.7), we obtain

$$e^{-\beta A \sigma} = \sum_{\mu} \sum_{\nu} [p^{(I)}(\mu, \nu) p^{(II)}(\mu, \nu)]^{1/2} \exp[\alpha^{(I)}(\mu, \nu) - \alpha^{(II)}(\mu, \nu)] , \quad (2.18)$$

where the superscripts I and II indicate the two phases.

The proof in this section can easily be generalized to the case where the probability functions $p(\lambda_1, \lambda_2, \ldots, \lambda_{k+1})$ of $k+1$ parallel planes are used in formulating the free energy. Then (2.18) is generalized to

$$e^{-\beta A \sigma} = \sum_{\nu_1} \sum_{\nu_2} \cdots \sum_{\nu_k} [p^{(I)}(\nu_1, \nu_2, \ldots, \nu_k) p^{(II)}(\nu_1, \nu_2, \ldots, \nu_k)]^{1/2} \exp[\alpha^{(I)}(\nu_1, \nu_2, \ldots, \nu_k) - \alpha^{(II)}(\nu_1, \nu_2, \ldots, \nu_k)] , \quad (2.19)$$

in which the α's are the Lagrange multipliers introduced in the bulk phase to satisfy

$$\sum_{\xi} p^{(I)}(\xi, \nu_1, \nu_2, \ldots, \nu_k)$$

$$= \sum_{\xi} p^{(I)}(\nu_1, \nu_2, \ldots, \nu_k, \xi) , \quad (2.20)$$

and can be shown to obey the antisymmetry relation

$$\alpha^{(I)}(\nu_1, \nu_2, \ldots, \nu_k) = -\alpha^{(I)}(\nu_k, \ldots, \nu_2, \nu_1) . \quad (2.21)$$

When the I and II phases are identical, the normalization of p makes σ in (2.19) vanish, as expected.

There is one remaining puzzle in the proof of this section. We required the condition $i \le j$ in writing (2.12). The choice $i = -m$ and $j = m+1$ in (2.14) satisfies this condition. However, the equalities in (2.12) and hence in (2.13) seem to hold even when $i > j$. If we allow $i > j$ in (2.13) and use it M times starting with the values $i = m+1$ and $j = -m$, this procedure is equivalent to reversing the signs in front of the λ's in (2.13) and (2.14). The sign reversal results in the expression $\exp(+\beta A \sigma)$ on the left-hand side of (2.17); this obviously is the wrong result. The interpretation of the wrong result and the reason why we need the condition $i \le j$ in (2.11) are discussed in the Appendix.

The proof of the SP expression in Sec. V of Ref. 6 for the long-range interaction case, which incorrectly omitted the α factor, is to be replaced by the correct proof in the present section.

III. APPLICATION OF THE FINITE-SIZE CLUSTER APPROXIMATION

In the general SP expression (2.19), ν_i represents one of the K^N configurations of a parallel plane (as was mentioned in Sec. II), and the number K^N is practically infinite as far as the computer calculation is concerned. Therefore, to make use of (2.19) in calculating σ, it is necessary to introduce a certain scheme which reduces (2.19) into a tractable form. The case of the one-plane probability function $p(\nu)$ was done in Refs. 2, 3, and 10 using the finite-size cluster (FSC) approximation of the cluster-variation (CV) technique.

In the general case of (2.19), however, the reduction scheme due to the FSC method faces a still-unsolved problem of reducing $\alpha^{(I)}(\nu_1, \nu_2, \ldots, \nu_k)$ into a tractable form. How to handle the α's is studied in this section by examining the homogeneous phase version of (2.5) as an example.

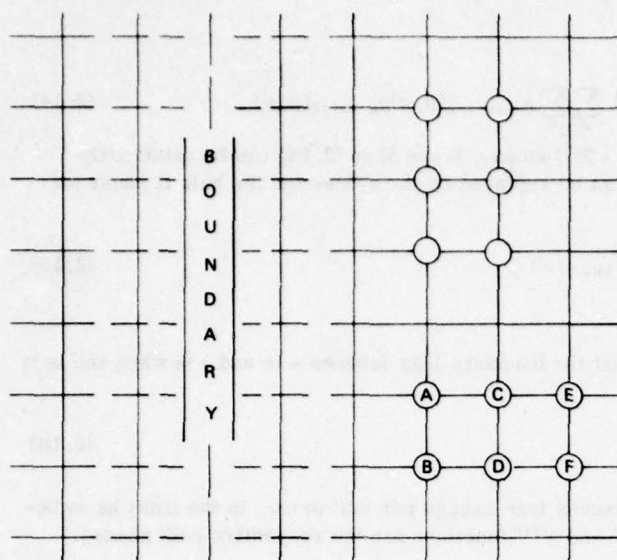To avoid cumbersome notation for a large-size three-

FIG. 1. A 2×3 and a 3×2 squares used in the formulation.

dimensional cluster, we present the discussion in this section based on a two-dimensional system. The parallel *plane* we considered in the previous section now becomes a parallel *line*.

In the homogeneous phase I, we can write (2.5) as

$$p^{(I)}(\mu, \nu, \xi) = \exp[\beta \lambda^{(I)} - \beta \epsilon(\mu, \nu, \xi)]$$
$$\times [p^{(I)}(\mu, \nu) p^{(I)}(\nu, \xi)]^{1/2}$$
$$\times \exp[\alpha^{(I)}(\mu, \nu) + \alpha^{(I)}(\xi, \nu)] , \qquad (3.1)$$

where μ, ν, or ξ represents one of K^N possible configurations of a parallel line made of N lattice points, and $p^{(I)}(\mu, \nu, \xi)$ is the probability that the three-line cluster takes the configuration specified by (μ, ν, ξ) in the bulk phase I. We have used in writing (3.1) the antisymmetry relation $\alpha^{(I)}(\nu, \xi) = -\alpha^{(I)}(\xi, \nu)$, which is a special case of (2.21).

In the actual computation of σ, we use an FSC. Our program is to rewrite $p^{(I)}(\mu, \nu, \xi)$ of (3.1) in terms of quantities of FSC and examine the α part of it. As an example, we take a two-dimensional square net for the system and a double square (DS), illustrated in the lower part of Fig. 1, as the FSC. The system does not include sublattices, but is otherwise general; it can be regarded as an Ising model system, a disordered phase of an alloy, or a lattice model of a gas–liquid system (the latter will be treated in the next section).

In Ref. 3, we used the upper cluster of Fig. 1, and used the simpler σ formula (1.1). To distinguish the two directions of the clusters in Fig. 1, we will call the upper one a 2×3 or a DS(‖) and the lower one a 3×2 or a DS($\perp$). Although the two cases look similar, the lower one needs the α's, which are of concern in the present paper.

The variables we use in treating the bulk homogeneous phase, (I) or (II), using the DS($\perp$) are listed in Table I. This table happens to be exactly the same as Ta-

ble II in Ref. 3. This is not surprising since the bulk phase does not depend on the direction in which the basic cluster is placed. The letter i in Table I(c) stands for the ith species (for example $i = 1$ for a plus spin and $i = 2$ for a minus spin).

The purpose of this section is to study the meaning of α in (3.1). To do this, we look into the "superposition" expressions in the bulk phase. When a DS is used in the CV method, the free energy minimization leads to the following expression [which was derived in (3.13) of Ref. 3]:

$$w_{ijklmn}^{(I)} = \hat{w}_{ijklmn}^{(I)} \exp(\lambda_0 \beta + \alpha_{ijkl}^{(I)} + \alpha_{mnkl}^{(I)} + \gamma_{ijkl}^{(I)} + \gamma_{mnkl}^{(I)}) , \qquad (3.2a)$$

where

$$\hat{w}_{ijklmn}^{(I)} = \exp(-\beta \epsilon_{ijklmn}) \frac{(v_{ijkl}^{(I)} v_{klmn}^{(I)} z_{ikm}^{(I)} z_{jln}^{(I)})^{1/2}}{(y_{ik}^{(I)} y_{km}^{(I)} y_{jl}^{(I)} y_{ln}^{(I)})^{1/4}} . \qquad (3.2b)$$

The notations are slightly different from those in Ref. 3. The superscript (I) indicates the bulk phase (I); ϵ_{ijklmn} is the energy per DS; and $\exp(\lambda_0 \beta)$ is the normalization factor, where λ_0 has the meaning of the free energy per lattice point [in contrast to (3.1), in which $\lambda^{(I)}$ is the free energy per N lattice points in one long line].

TABLE I. The double-square cluster.

Our aim is to write $p^{(I)}(\mu, \nu, \xi)$ of (3.1) using $w^{(I)}$ of (3.2) and then to find the quantity corresponding to $\alpha^{(I)}(\mu, \nu) + \alpha^{(I)}(\xi, \nu)$ of (3.1).

In (3.2a), α and γ are Lagrange multipliers, which are introduced to satisfy the continuity relations

$$v_{ijkl}^{(I)} = \sum_{m,n} w_{ijklmn}^{(I)} = \sum_{m,n} w_{mnijkl}^{(I)} \tag{3.3a}$$

for α, and the rotational symmetries

$$v_{ijkl}^{(I)} = v_{ikjl}^{(I)} \tag{3.3b}$$

for γ. The relations in (3.3a) for α are similar to the continuity requirement in (2.3), which introduces $\alpha_{i-1/2}(\mu, \nu)$. The rotational requirement did not appear in Sec. II and needs a special discussion at the end of this section.

When the system is a bulk homogeneous one, w satisfies the symmetry relations

$$w_{ijklmn}^{(I)} = w_{mnklij}^{(I)} \tag{3.4a}$$

and

$$w_{ijklmn}^{(I)} = w_{jilknm}^{(I)} . \tag{3.4b}$$

We can prove that these relations (3.4) in turn lead to the following symmetry relations for α and γ:

$$\alpha_{ijkl}^{(I)} = -\alpha_{klij}^{(I)} , \qquad \alpha_{ijkl}^{(I)} = \alpha_{jilk}^{(I)} , \tag{3.5a}$$

$$\gamma_{ijkl}^{(I)} = -\gamma_{ikjl}^{(I)} , \qquad \gamma_{ijkl}^{(I)} = \gamma_{jilk}^{(I)} . \tag{3.5b}$$

In Eqs. (3.2)–(3.5), the variables with the superscript (I) are those of the equilibrium state in the bulk phase I. Now we use these variables to write $p^{(I)}(\mu, \nu, \xi)$ in (3.1). The variables μ, ν, and ξ represent any, in general excited, state of the three consecutive lines in the bulk phase I. In designating such an excited state, we again

use the variables listed in Table I, but this time without the superscript (I). In other words, when we look at any 3×2 cluster portion of the three-line configuration (μ, ν, ξ), the probability of finding the configuration $i-j-k-l-m-n$ is written as w_{ijklmn}. Using this quantity, we can write $p^{(I)}(\mu, \nu, \xi)$ as

$$p^{(I)}(\mu, \nu, \xi) = \prod^{(6)} [w_{ijklmn}^{(I)}/z_{jln}^{(I)}] ** (Nw_{ijklmn}) , \tag{3.6}$$

where a double asterisk is a FORTRAN notation meaning "raised to the power of" and is used in this paper to avoid subscripts on a superscript. The number (6) above the product sign in (3.6) indicates that this is a sixfold product over i, j, k, l, m, and n. In (3.6) the factor in the square brackets is the conditional probability of finding $i-k-m$ next to $j-l-n$ when the latter is known. The logic of writing (3.6) is the same as that presented in Refs. 2, 3, and 10.

We now go back to (3.2) for the FSC and use it for $w_{ijklmn}^{(I)}$ in (3.6). The resulting expression can be simplified in several steps. Besides w_{ijklmn}, we use v's and z's as shown in Table I:

$$v_{ijkl} \equiv \sum_{m,n} w_{ijklmn} ,$$

$$z_{ikm} \equiv \sum_{j,l,n} w_{ijklmn} . \tag{3.7}$$

We note the following relations:

$$\prod^{(6)} (z_{ikm}^{(I)}/z_{jln}^{(I)}) ** (Nw_{ijklmn}) = 1 ,$$

$$\prod^{(6)} (y_{ik}^{(I)}/y_{jl}^{(I)}) ** (Nw_{ijklmn}) = 1 . \tag{3.8}$$

Using (3.8) and (3.2), we can transform $p^{(I)}(\mu, \nu, \xi)$ in (3.6) to

$$p^{(I)}(\mu, \nu, \xi) = \exp\left(\sum^{(6)} (\lambda_0 \beta - \beta\epsilon_{ijklmn}) N w_{ijklmn} \right) \prod^{(6)} \left(\frac{v_{ijkl}^{(I)} v_{klmn}^{(I)}}{y_{jl}^{(I)} y_{ln}^{(I)}} \right) ** \left(\frac{N}{2} w_{ijklmn} \right)$$

$$\times \exp\left(\sum^{(6)} (\alpha_{ijkl}^{(I)} + \alpha_{mnkl}^{(I)} + \gamma_{ijkl}^{(I)} + \gamma_{mnkl}^{(I)}) N w_{ijklmn} \right) . \tag{3.9}$$

Next we compare (3.9) with (3.1). Based on the normalization of w, we can identify

$$\lambda^{(I)} = \sum^{(6)} \lambda_0 N w_{ijklmn} \tag{3.10}$$

because $\lambda^{(I)}$ is the free energy per N lattice points and λ_0 is that per lattice point. For the energy, we can identify,

$$\epsilon(\mu, \nu, \xi) = \sum^{(6)} \epsilon_{ijklmn} N w_{ijklmn} . \tag{3.11}$$

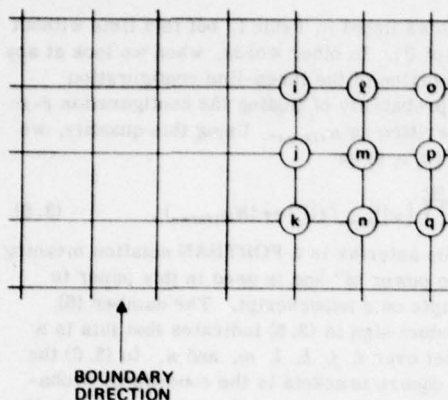Similar to (3.6), we can write

$$p^{(I)}(\mu, \nu) = \prod^{(4)} (v_{ijkl}^{(I)}/y_{jl}^{(I)}) ** (Nv_{ijkl}) , \tag{3.12a}$$

$$p^{(I)}(\nu, \xi) = \prod^{(4)} (v_{klmn}^{(I)}/y_{ln}^{(I)}) ** (Nv_{klmn}) . \tag{3.12b}$$

Because of the definition of v_{ijkl} in (3.7), v_{ijkl} in (3.12a) can be replaced by w_{ijklmn} and the product in (3.12) can be changed over six indices i, j, k, l, m, and n as in (3.9). Thus we can rewrite (3.9) in a form close to that of (3.1):

$$p^{(I)}(\mu, \nu, \xi) = \exp[\beta\lambda^{(I)} - \beta\epsilon(\mu, \nu, \xi)][p^{(I)}(\mu, \nu)p^{(I)}(\nu, \xi)]^{1/2}$$

$$\times \exp\left(\sum^{(4)} \alpha_{ijkl}^{(I)} N v_{ijkl} + \sum^{(4)} \alpha_{mnkl}^{(I)} N v_{klmn} + \sum^{(4)} \gamma_{ijkl}^{(I)} N v_{ijkl} + \sum^{(4)} \gamma_{mnkl}^{(I)} N v_{klmn} \right) . \tag{3.13}$$

BOUNDARY DIRECTION

FIG. 2. A 3×3 square used in the formulation.

When we compare (3.13) with (3.1), we are tempted to identify

$$\alpha^{(I)}(\mu, \nu) = N \sum_{i,j,k,l} (\alpha^{(I)}_{ijkl} + \gamma^{(I)}_{ijkl}) v^{(I)}_{ijkl} . \qquad (3.14)$$

This identification, however, cannot be justified, because $\alpha^{(I)}_{ijkl}$ satisfies, as in (3.5a), the same kind of the antisymmetry relation as $\alpha^{(I)}(\nu_1, \nu_2, \ldots, \nu_k)$ in (2.21), while the symmetry property of $\gamma^{(I)}_{ijkl}$ in (3.5b) is of a different kind.

When we think of the difference between the formulation in Sec. II based on the infinitely long line, and that of the present section based on the FSC, we note that the former does not need γ's because the rotational symmetry is automatically incorporated in the infinitely long cluster. This situation suggests that even for the FSC treatment the effect of γ's would be small; this is exactly the case that was explicitly pointed out in Sec. III of Ref. 3. In other words, even with $\gamma_{ijkl} = 0$, the anisotropy of the system is small and can be neglected. Based on this observation, in reducing Sec. II to a tractable FSC scheme of this section, we propose to tolerate a slight anisotropy of the system and make

$$\gamma^{(I)}_{ijkl} = 0 . \qquad (3.15)$$

Thus, instead of (3.14), we identify

$$\alpha^{(I)}(\mu, \nu) = N \sum_{i,j,k,l} \alpha^{(I)}_{ijkl} v^{(I)}_{ijkl} . \qquad (3.16)$$

The result (3.16) can be easily generalized to larger clusters. We show only one example. When we use a 3×3 FSC to calculate the bulk phase using the nine-point variables $w_{ijk,lmn,opq}$ based on Fig. 2, $\alpha^{(I)}(\mu, \nu)$ in (3.16) is to be identified as

$$\alpha^{(I)}(\mu, \nu) = N \sum^{(6)} \alpha^{(I)}_{ijk,lmn} v^{(I)}_{ijk,lmn} , \qquad (3.17)$$

where $\alpha^{(I)}_{ijk,lmn}$ is the Lagrange multiplier introduced for the translational symmetry condition:

$$v^{(I)}_{ijk,lmn} = \sum_{o,p,q} w^{(I)}_{ijk,lmn,opq} = \sum_{o,p,q} w^{(I)}_{opq,ijk,lmn} . \qquad (3.18)$$

The FSC expression of $\alpha^{(I)}(\mu, \nu)$ in (3.16) or (3.17) is the

one which is to be used in calculating $\exp(-\beta A\sigma)$ from (2.18).

IV. TWO-DIMENSIONAL ISING MODEL

As we did in our previous publications,[2,3] we go back to the two-dimensional Ising model to check if the new α terms in the SP expression are correct. We use the DS cluster of Sec. III, and the only difference between the present section and Sec. V of Ref. 3 is that we place the DS as perpendicular to the boundary, as in the lower part of Fig. 1, rather than the parallel position of Ref. 3 shown in the upper part of Fig. 1.

The expression for the excess boundary free energy σ is (2.18), combined with (3.16) for $\alpha^{(I)}$. Using FSC notation, we obtain

$$\exp(-N\sigma_{\langle 10 \rangle} a\beta) = \sum_{\{v_{ijkl}\}} \Omega\{v_{ijkl}\}$$

$$\times \frac{\Pi_{i,j,k,l}(v^{(I)}_{ijkl} v^{(II)}_{ijkl}) ** (\frac{1}{2} N v_{ijkl})}{\Pi_{i,k}(y^{(I)}_{ik} y^{(II)}_{ik}) ** (\frac{1}{2} N y_{ik})}$$

$$\times \exp\left[N \sum_{i,j,k,l} (\alpha^{(I)}_{ijkl} - \alpha^{(II)}_{ijkl}) v_{ijkl}\right] , \qquad (4.1)$$

where $\sigma_{\langle 10 \rangle}$ is the excess free energy per unit length, and a is the lattice constant. The variables with superscripts are those for the corresponding bulk phases, while v_{ijkl} and y_{ik} without superscript are the boundary variables to be determined. The definitions are in Table I. The Ω factor is the weight factor given as

$$\Omega\{v_{ijkl}\} = \frac{\Pi_{i,k}(Ny_{ik})!}{\Pi_{i,j,k,l}(Nv_{ijkl})!} \qquad (4.2)$$

for which we have the relations

$$y_{ik} = \sum_{j,l} v_{ijkl} . \qquad (4.3)$$

For the derivations of (4.1) and (4.2), Refs. 2 and 3 may be referred to. As we have been discussing so far, the new aspect in this paper is the last factor in (4.1) containing α.

To calculate $\sigma_{\langle 10 \rangle}$ from (4.1), it is convenient to find the maximum of the logarithm of the summand on the right-hand side, and in so doing use the natural iteration (NI) method.[3,10] The iteration converges with ease and the results are shown in Fig. 3 by the solid curve marked double square (1). It is satisfying to see that DS(1) is close to DS($\|$), which is the previous result reported in Fig. 3 of Ref. 3. It is particularly noteworthy that, when we deliberately put $\alpha^{(I)}_{ijkl} = \alpha^{(II)}_{ijkl} = 0$ in (4.1), the σ curve moves way up to the dotted position in Fig. 3; this fact shows the correctness of the α terms in (4.1) and hence in the general formula (2.19).

Because of the antisymmetry property of $\alpha^{(I)}_{ijkl}$ in (3.5a), we can replace the last exponential factor containing α in (4.1) by

$$\cosh\left[N \sum_{i,j,k,l} (\alpha^{(I)}_{ijkl} - \alpha^{(II)}_{ijkl}) v_{ijkl}\right] . \qquad (4.4)$$

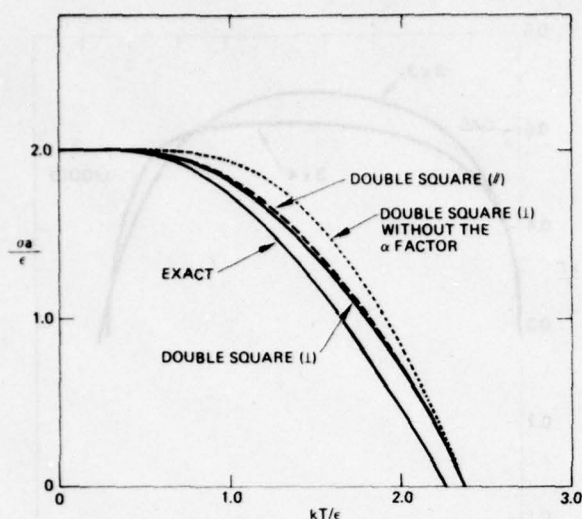Therefore the σ curve for which α is taken into account is always lower than the one for which α is left out. The

FIG. 3. Excess free energy σ at the boundary of square net Ising model.
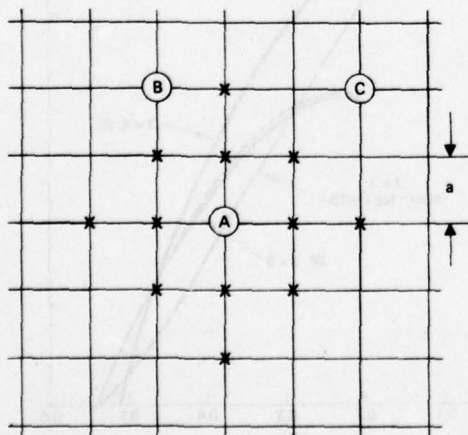

FIG. 5. Grand potential $\hat{G}$ versus chemical potential near the coexistence point for $kT/\epsilon = 0.50$.

DS($\perp$) curve and the dotted curve in Fig. 3 satisfy this general property.

V. LATTICE GAS–LIQUID SYSTEM

Although the Ising model example in the previous section is useful in supporting the validity of the α factor in (2.18) and of the expression (3.16), the quantity σ for the Ising model as shown in Fig. 3 can be calculated by always starting with a double-line cluster parallel to the boundary and applying the formula (1.1). In other words, when the interaction is of the nearest-neighbor type, we can do without the new formula (2.18) or (2.19). The new formula is needed only when the interaction becomes longer range. We show an example of the latter case in this section.

We calculate the surface tension of a two-dimensional gas–liquid phase boundary using a model proposed by

FIG. 4. Interacting pairs AB and AC.

Orban et al.[12] The model is illustrated in Fig. 4. When an atom sits at A, no atoms can come to the first, second, or third neighbor points (indicated by crosses). An atomic pair AB at the fourth neighbor distance attracts with the potential $-g\epsilon$ ($\epsilon > 0$), and a pair AC at the fifth neighbor attracts with $-\epsilon$. In their example, Orban et al. chose $g = 1.2$, and we will use the same number. They were interested in deriving three phases, gas, liquid, and solid, but in the present paper we will discuss the gas–liquid transition only. We will use a 3×3 cluster first to calculate homogeneous liquid and gas phases, and use the results to write (2.18) to evaluate σ.

Since the formulation of the bulk phase calculations follows the standard CV method, only some important points are discussed in this section. In working with gas and liquid phases, we fix the temperature and the chemical potential μ. The advantage of fixing μ rather than composition in the treatment of phase diagrams has been previously discussed.[13–15] When μ is fixed, the thermodynamic potential which is minimized is not the free energy $F = E - TS$ but the quantity

$$\hat{G} = F - \mu N_A \tag{5.1}$$

which we call the grand potential; N_A is the number of atoms in a system.

Keeping T and μ fixed, we minimize $\hat{G}$ with respect to the six cluster variables for a 3×3 cluster which specify the state of the system, using the natural interaction method.[16] The resulting $\hat{G}$, which is now a function of T and μ, is made of two branches, one for the gas phase and the other for the liquid phase as shown in Fig. 5. The point at which the two branches cross gives the $\mu_{c.e.}$
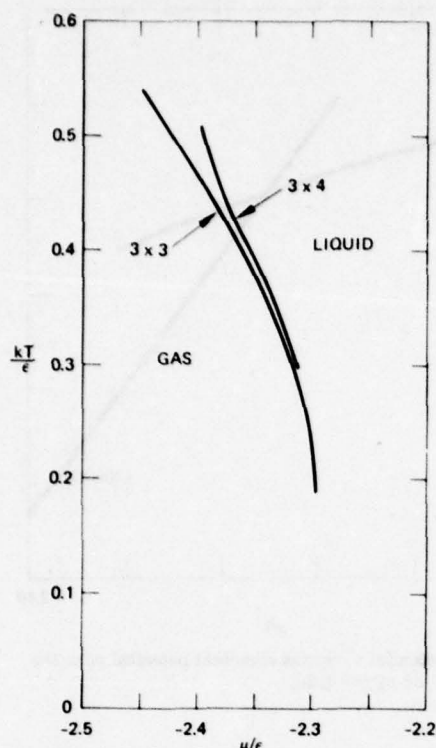
FIG. 6. T vs $\mu_{c.e.}$ at coexistence for the gas–liquid model.

for which two phases coexist. The curve marked by 3×3 in Fig. 6 shows the T vs $\mu_{c.e.}$ relations.

Since the chemical potential μ is the Gibbs potential per atom, thermodynamics tells us that $\hat{G}$ defined in (5.1) is equal to

$$\hat{G} = -pA ,   \tag{5.2}$$

where p is the pressure and A is the area of the system. (In a three-dimensional system, the corresponding equation is $\hat{G} = -pV$, V being the volume of the system.) The value of $\hat{G}$ corresponding to $\mu_{c.e.}$ gives the pressure of coexistence, $p_{c.e.}$. The $p_{c.e.}$ is plotted against T as the 3×3 curve in Fig. 7.

The crossing point (i.e., the coexisting point) in Fig.
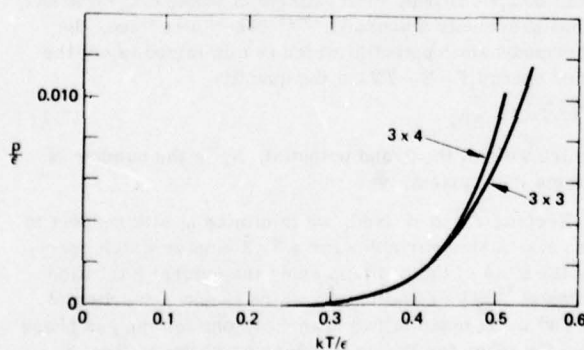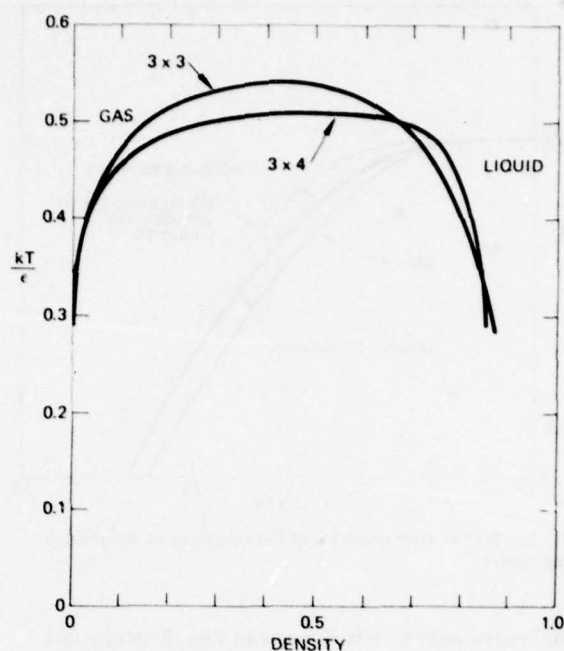

FIG. 7. T vs pressure $p_{c.e.}$ at coexistence for the gas–liquid model.

FIG. 8. Phase separation diagram of the gas and liquid phases.

5 also gives information about the densities of the coexisting gas and liquid phases. The curve marked 3×3 in Fig. 8 shows the result.

A comparison of Figs. 6, 7, and 8 with the results reported in Sec. IV of Ref. 12 shows them to be in good agreement except for the estimate of the critical point. Our Fig. 8 shows clearly that the maximum of the curve is at $kT/\epsilon = 0.54$, while Fig. 9 of Ref. 12 estimates that the critical value of kT/ϵ is somewhere beyond 0.7. Later we discuss an additional evidence which shows that the estimate of Ref. 12 is too large.
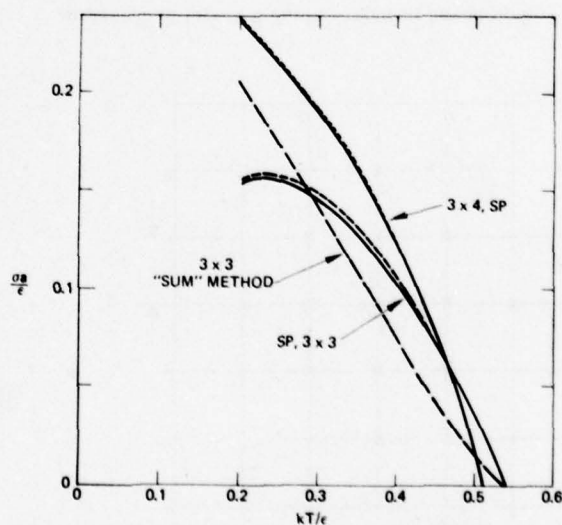
FIG. 9. Surface tension σ of the gas–liquid system calculated in Sec. V.

After the coexisting phases are thus determined, we use (2.18) to calculate the surface tension σ. Since (as we said at the outset of this section) the thermodynamic potential is $\hat{G}$ rather than F, the quantity σ is not the excess free energy but rather is the excess grand potential.[17,18] With this understanding, we call σ the surface tension. The result of the calculation is plotted by the solid curve marked SP, 3×3 in Fig. 9. The dotted curve accompanying it is the one for which α in (2.18) is deliberately put equal to zero. Different from the Fig. 3 case, the solid and dotted curves do not differ much, although the dotted curve ($\alpha = 0$) is higher than the solid curve ($\alpha \neq 0$), in agreement with the general requirement mentioned at the end of Sec. IV.

The reason why the effect of α is large in the Ising model (Fig. 3) and is practically nil in the gas–liquid surface tension (Fig. 9) can be traced in mathematics, but the physical reason is still to be determined.

For the two-dimensional Ising model, the result of σ calculated by the SP method can be compared with the exact calculation due to Onsager,[4] as we did in Fig. 3. Since in the gas–liquid model of this section there is no exact calculation to compare with, we calculate σ using two different methods to check the accuracy of the SP method. One of them is the "sum" method. We minimize the grand potential $\hat{G}$ of an inhomogeneous system that includes the gas–liquid boundary. We apply the CV method using a 3×3 square of Fig. 2 as the basic cluster. The technique is similar to the one used by Cahn and Kikuchi[17,18] and modified later,[10] taking into account the Weeks and Gilmer technique.[19] In calculation, we used 80 lattice lines and imposed the conditions that the left two end lines are in the gas phase and the right two end lines are in the liquid phase. In minimizing $\hat{G}$, the combination of T and μ are fixed, the latter being the value $\mu_{c.e.}$ for which the gas and liquid phases coexist at that temperature, as determined in Figs. 5 and 6.

The results of σ calculated by the sum method are plotted by the broken curve in Fig. 9. When we com-
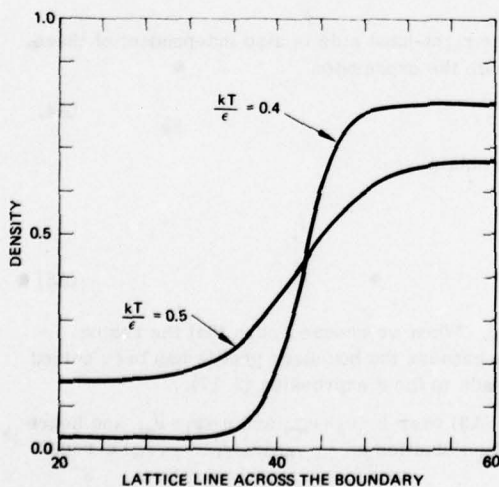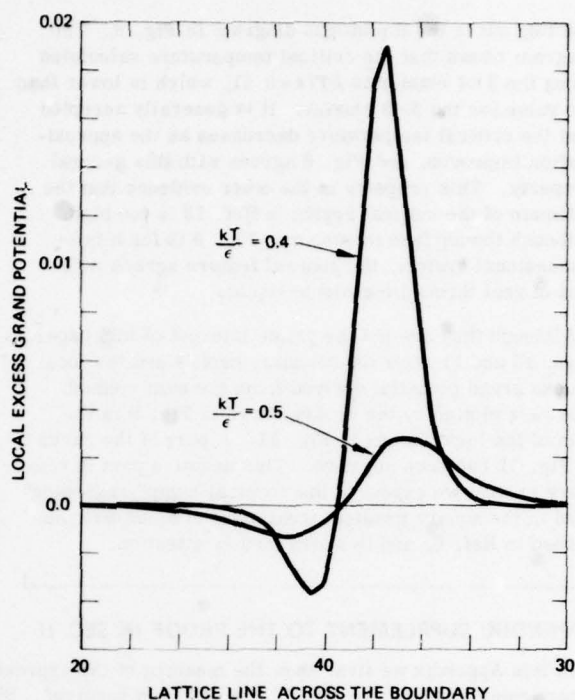

FIG. 11. Local excess grand potential across the boundary calculated by the sum method.

pare the SP (3×3) curve and the sum curve, the former is higher than the latter for the region of physical significance, $kT/\epsilon > 0.4$. (For the temperatures below about 0.4, the solid phase is more stable, as was shown in Ref. 12, and the curves in Fig. 9 lose their meaning.) This situation qualitatively agrees with the bcc $\langle 110 \rangle$ boundary results reported in Fig. 6 of Ref. 10; in the bcc case also, the SP curve is higher than corresponding sum curve.

We can then almost say that the SP expression (2.18) is supported by these calculations. There is, however, one bothersome feature of the SP (3×3) curves in Fig. 9: they bend over around $kT/\epsilon = 0.25$. We can disregard, if we want, this bending-over behavior, because it occurs in the (T, μ) region in which the gas and liquid phases are not stable, as we discussed above. (In this regard, we may quote Barker[20] who pointed out that the CV calculation can sometimes give unphysical results in the region where the phase being calculated is not the most stable one.) However, to further verify the SP method, we calculated σ using a 3×4 cluster. The results are plotted by the curves marked 3×4, SP in Figs. 6–9. The solid curve in Fig. 9 is the $\alpha \neq 0$ case and the dotted one is the $\alpha = 0$ case; the latter is higher, in agreement with the requirement at the end of Sec. IV. The 3×4, SP curve does not show the bending over that the 3×3 curve does, and behaves more normally; therefore, we do not need to be concerned about the somewhat bothersome shape of the 3×3 curve for low temperatures.

One other result of the 3×4 cluster calculation worth

FIG. 10. Density profile versus the boundary calculated by the sum method.

pointing out is the liquid–gas diagram in Fig. 8. The diagram shows that the critical temperature calculated using the 3×4 cluster is $kT/\epsilon = 0.51$, which is lower than the value for the 3×3 cluster. It is generally accepted that the critical temperature decreases as the approximation improves, and Fig. 8 agrees with this general property. This property is the other evidence that the estimate of the critical region in Ref. 12 is too high. Although the surface tension σ in Fig. 9 is for a two-dimensional system, the general feature agrees with that of real three-dimensional liquid.

Although they are not the prime interest of this paper, Figs. 10 and 11 show the boundary profile and the local excess grand potential derived from the sum method. The $\sigma a/\epsilon$ plotted by the broken curve in Fig. 9 is the sum of the local values in Fig. 11. A part of the curve in Fig. 11 becomes negative. This negative part is contrary to what we expect in the "central hump" reasoning used in the square gradient treatment[8] of σ, as was discussed in Ref. 6, and is worth further attention.

VI. SUMMARY

The scalar-product (SP) expression of the excess boundary free energy σ writes σ in terms of the properties of two bulk phases that meet at the boundary. Another method of calculating σ, called the sum method in this paper, evaluates σ as the difference between the free energy of an inhomogeneous system including a boundary and that of the homogeneous phase. Compared with the sum method, the SP method has the advantage that it can calculate σ more easily and can derive some of the properties of σ more accurately. In the papers published so far, the SP method has been applied only to cases of nearest-neighbor interaction. The present paper extends the SP method to cases of longer range interactions than the nearest neighbor. The extended SP formula is in (2.18) and more generally in (2.19). As examples, σ's are calculated for a two-dimensional Ising model (nearest-neighbor interaction) and for a two-dimensional gas–liquid model taking into account up to the fifth neighbors.

APPENDIX: SUPPLEMENT TO THE PROOF IN SEC. II

In this Appendix we first show the meaning of the expression $h_{i+1/2}(\mu, \nu)g_{j+1/2}(\mu, \nu)$ which appears in (2.14), with a particular emphasis on why $i \le j$ in (2.11) is required. Since the interaction potential in this formulation is defined to be extended to the second neighboring plane but not farther, the joint probability distribution of four plane configuration $p_{i+1/2}(\mu, \nu, \xi, \eta)$ centered at the position $i + 1/2$ is written without approximation as

$$p_{i+1/2}(\mu, \nu, \xi, \eta) = p_i(\mu, \nu, \xi)p_{i+1}(\nu, \xi, \eta)/p_{i+1/2}(\nu, \xi) . \tag{A1}$$

We use (2.8) for $p_i(\mu, \nu, \xi)$ and divide both sides of (A1) by $\Gamma(\mu, \nu, \xi)\Gamma(\nu, \xi, \eta)$ to obtain

$$\exp(\beta\lambda_i + \beta\lambda_{i+1})h_{i-1/2}(\mu, \nu)g_{i+3/2}(\xi, \eta) = p_{i+1/2}(\mu, \nu, \xi, \eta)\exp[\beta\epsilon(\mu, \nu, \xi) + \beta\epsilon(\nu, \xi, \eta)] . \tag{A2}$$

We can continue multiplying the conditional probabilities, as was done in (A1), m times to arrive at the probability distribution of $(m+1)$-plane configurations $\nu_0, \nu_1, \nu_2, \ldots, \nu_m$ on planes $i, i+1, \ldots, i+m$ as

$$\exp(\beta\lambda_{i+1} + \beta\lambda_{i+2} + \cdots + \beta\lambda_{i+m-1})h_{i+1/2}(\nu_0, \nu_1)g_{i+m-1/2}(\nu_{m-1}, \nu_m)$$

$$= p_{[i,\ldots,i+m]}(\nu_0, \nu_1, \ldots, \nu_m)\exp[\beta\epsilon(\nu_0, \nu_1, \nu_2) + \cdots + \beta\epsilon(\nu_{m-2}, \nu_{m-1}, \nu_m)] . \tag{A3}$$

This is the meaning of the factor $h_{i+1/2}(\mu, \nu)g_{j+1/2}(\mu, \nu)$. In order that the expression (A3) be meaningful, m must be larger than or equal to unity; this is the condition exactly equivalent to the condition $i \le j$ required in (2.11) to accompany (2.13).

Since the left-hand side of (A3) does not contain $\nu_2, \nu_3, \ldots, \nu_{m-2}$, the right-hand side is also independent of these configurations although they appear in the expression. Now we start with the expression

$$S \equiv \exp(\beta\lambda_{i+1} + \cdots + \beta\lambda_{i+m}) \sum_\mu \sum_\nu \sum_\xi h_{i+1/2}(\mu, \nu)\Gamma(\mu, \nu, \xi)g_{i+m+1/2}(\nu, \xi) , \tag{A4}$$

and sum this first over ξ and later over μ. With the use of (2.10), we obtain

$$S = \exp(\beta\lambda_{i+1} + \cdots + \beta\lambda_{i+m-1}) \sum_\mu \sum_\nu h_{i+1/2}(\mu, \nu)g_{i+m-1/2}(\mu, \nu)$$

$$= \exp(\beta\lambda_{i+2} + \cdots + \beta\lambda_{i+m}) \sum_\nu \sum_\xi h_{i+3/2}(\nu, \xi)g_{i+m+1/2}(\nu, \xi) . \tag{A5}$$

The equality in (A5) shows that this sum is independent of the location i. When we choose i such that the region from i to $i+m$ covers the boundary (this assignment is always possible because the boundary profile has been solved beforehand, and m is to be made very large), the invariance in (A5) leads to the σ expression (2.17).

Note that in this proof the expression S in (A5) is exactly the sum of (A3) over $\mu = \nu_0 = \nu_{m-1}$ and $\nu = \nu_1 = \nu_m$, and hence that the boundary free energy is closely tied to the multiplane distribution function $p_{[i,\ldots,i+m]}(\nu_0, \nu_1, \ldots, \nu_m)$ across the boundary.

Now we go to the puzzle mentioned at the end of Sec. II. The key to solve the puzzle is the fact that the probability expression for $m+1$ planes $p_{[i,\ldots,i+m]}(\nu_0, \nu_1, \ldots, \nu_m)$ in (A3) requires that the h function lies always on the left of

the g function. As a mathematical expression, however, we can interchange location $i+1/2$ and $i+m-1/2$ for h and g and can work with $g_{i+1/2}(\nu_0, \nu_1)h_{i+m-1/2}(\nu_{m-1}, \nu_m)$. We now examine the physical meaning of this expression. Our interpretation is that this new formulation corresponds to a different expression $\hat{p}_{[i,\ldots,i+m]}(\nu_0, \nu_1, \cdots, \nu_m)$ for a model of different interaction energies. We use a caret to indicate a function in the redefined system. The $\hat{h}$ and $\hat{g}$ functions are defined using the quantities in the old system as

$$\hat{h}_{i-1/2}(\mu, \nu) \equiv g_{i-1/2}(\mu, \nu) = [p_{i-1/2}(\mu, \nu)]^{1/2}\exp[-\alpha_{i-1/2}(\mu, \nu)] ,$$

$$\hat{g}_{i+1/2}(\nu, \xi) \equiv h_{i+1/2}(\nu, \xi) = [p_{i+1/2}(\nu, \xi)]^{1/2}\exp[+\alpha_{i+1/2}(\nu, \xi)] . \tag{A6}$$

The energy factor $\Gamma(\mu, \nu, \xi)$ in (2.7) are replaced by $\hat{\Gamma}$ which obeys

$$\sum_\mu \hat{\Gamma}(\mu, \nu, \xi)\Gamma(\mu, \nu, \eta) = \delta_{\xi, \eta} , \tag{A7a}$$

$$\hat{\Gamma}(\mu, \nu, \xi) = \hat{\Gamma}(\xi, \nu, \mu) . \tag{A7b}$$

Then $p_i(\mu, \nu, \xi)$ in (2.5) is replaced by

$$\hat{p}_i(\mu, \nu, \xi) = \exp(-\beta\lambda_i)\hat{h}_{i-1/2}(\mu, \nu)\hat{\Gamma}(\mu, \nu, \xi)\hat{g}_{i+1/2}(\nu, \xi) . \tag{A8}$$

Note that $\beta\lambda_i$ in (2.5) is replaced by $-\beta\lambda_i$ in the new expression (A8). The $(m+1)$-plane probability corresponding to (A3) is written as

$$\hat{p}_{[i,\ldots,i+m]}(\nu_0, \nu_1, \ldots, \nu_m)[\hat{\Gamma}(\nu_0, \nu_1, \nu_2)\hat{\Gamma}(\nu_1, \nu_2, \nu_3)\cdots\hat{\Gamma}(\nu_{m-2}, \nu_{m-1}, \nu_m)]^{-1}$$

$$= \exp(-\beta\lambda_{i+1} - \cdots - \beta\lambda_{i+m-1})\hat{h}_{i+1/2}(\nu_0, \nu_1)\hat{g}_{i+m-1/2}(\nu_{m-1}, \nu_m)$$

$$= \exp(-\beta\lambda_{i+1} - \cdots - \beta\lambda_{i+m-1})g_{i+1/2}(\nu_0, \nu_1)h_{i+m-1/2}(\nu_{m-1}, \nu_m) . \tag{A9}$$

Note that the h function appears on the right of g, although $\hat{h}$ appears on the left of $\hat{g}$ as required. From the invariance argument similar to (A5), we can prove that the boundary free energy $\hat{\sigma}$ for this new system is

$$A\hat{\sigma} = -\sum_i (\lambda_i - \lambda^{(0)}) < 0 \tag{A10}$$

as we said at the end of Sec. II. The negative $\hat{\sigma}$ means that the newly defined system does not sustain a stable phase boundary in it.

Note added in proof: As the answer to the comment at the end of Sec. V, Professor J. W. Cahn told the author that the negative part of the local excess grand potential in Fig. 11 can be understood from the square gradient theory by a partial integration.

[1]D. B. Clayton and G. W. Woodbury, Jr., J. Chem. Phys. **55**, 3895 (1971).

[2]R. Kikuchi, J. Chem. Phys. **57**, 783 (1972).

[3]R. Kikuchi, J. Chem. Phys. **65**, 4545 (1976).

[4]L. Onsager, Phys. Rev. **65**, 117 (1944).

[5]M. E. Fisher and A. E. Ferdinand, Phys. Rev. Lett. **19**, 169 (1967).

[6]R. Kikuchi, J. Chem. Phys. **57**, 777 (1972).

[7]R. Kikuchi, J. Chem. Phys. **57**, 787 (1972).

[8]J. W. Cahn and J. E. Hilliard, J. Chem. Phys. **28**, 258 (1958).

[9]R. Kikuchi, J. Chem. Phys. **57**, 4633 (1972).

[10]R. Kikuchi, J. Chem. Phys. **66**, 3352 (1977).

[11]R. Kikuchi, Phys. Rev. **81**, 988 (1951).

[12]J. Orban, J. van Graen, and A. Bellmans, J. Chem. Phys. **49**, 1778 (1968).

[13]R. Kikuchi, Acta Met. **25**, 195 (1977).

[14]R. Kikuchi, D. de Fontaine, M. Murakami, and T. Nakamura, Acta Met. **25**, 207 (1977).

[15]R. Kikuchi and D. de Fontaine, Scripta Met. **10**, 995 (1976).

[16]R. Kikuchi, J. Chem. Phys. **60**, 1071 (1974).

[17]R. Kikuchi and J. W. Cahn, J. Phys. Chem. Solids **23**, 137 (1962).

[18]J. W. Cahn and R. Kikuchi, J. Phys. Chem. Solids **27**, 1305 (1966).

[19]J. D. Weeks and G. H. Gilmer, J. Chem. Phys. **63**, 3136 (1975).

[20]J. A. Barker, Proc. R. Soc. London Ser. A **216**, 45 (1953).

APPENDIX 4

(Reference [4])

GROUND STATE OF F.C.C. ALLOYS WITH
MULTIATOM INTERACTIONS

J.W. Cahn and R. Kikuchi

Acta Metallurgica (in press)

APPENDIX 4

GROUND STATE OF FCC ALLOYS WITH MULTIATOM INTERACTIONS

John W. Cahn
National Bureau of Standards
Washington, DC 20234

and

Ryoichi Kikuchi[*]
Hughes Research Laboratories
Malibu, CA 90265

ABSTRACT

The ground state of a binary fcc alloy with nearest-neighbor interactions and tetrahedral multiatom interactions (characterized by two parameters α and β) is derived and presented in a chart which shows classification of phases in the space of α and β. Where non-stoichiometric phases can occur, the phase boundaries at T=0 are computed using the tetrahedron approximation of the cluster variation method. Duality of the composition and the chemical potential is emphasized, and results are presented and/or interpreted in the dual approaches.

1. Introduction

Statistical mechanical calculations of alloy problems usually assume a model with pair-wise interaction energies. Even the simplest model with near neighbor pair-wise interactions on an undistorted lattice poses a formidable problem which has not been solved in three dimensions.[1] The cluster variation method (CVM) has been a widely used tool for performing approximate but increasingly accurate calculations on such models.[2]

To make the models more realistic, several routes are open. Higher-neighbor interactions can be considered,[3] but in the CVM the complexity of the calculation increases with cluster size and the minimum cluster size is dictated by the largest interaction distance. An alternate possibility is to assume multiatom interactions such that the energies of clusters are given by numbers that cannot be obtained by summing pair-wise energies.*

These possibilities have been explored in fcc ordering reactions. With near neighbor pair-wise interactions the Bragg-Williams approximation gives a completely unrealistic phase diagram which is unaltered by considering higher neighbor pair-wise energy.[4] In the CVM the pair approximation is unrealistic for different reasons.[5] It is not until the tetrahedron approximation that a phase diagram which resembles a symmetric version of the Cu-Au diagram is obtained. With practically no

---

* It may be remarked that composition-dependent pair-wise energies is a multiatom interaction concept in which the energy of a pair depends on all the atoms in the volume element over which composition is measured.

increase in computational complexity, four-atom interaction parameters can be introduced in the CVM calculations that match the asymmetric Cu-Au phase diagram.[7]

There are ways of demonstrating that pair-wise interactions are inadequate to describe alloys.[8] Furthermore, there are quantum mechanical methods that lend themselves to the direct calculation of multiatomic cluster energies,[9] so that eventually these may become available as input for the statistical mechanical calculation.

Because of the use of multiatom forces in statistical mechanical phase diagram calculations in fcc, we undertook a calculation[10] of antiphase and interphase boundaries (APB and IPB) in such a system. As in previous calculations,[11-13] it became apparent that the ground state[14,15] was a clue to some of the low temperature behavior. We therefore undertook a study of the ground state reported in this paper. The IPB and APB are the subject of a companion paper.[10]

2. Ground State Energy

We use the linear programming method of Allen and Cahn.[15] The problem is to minimize the energy used by Kikuchi and deFontaine[7]

$$E/N = 3w(1 + \alpha) Z_1 + 4wZ_2 + 3w(1 + \beta) Z_3 \qquad (1)$$

where N is the total number of fcc lattice sites, Z_n is the fraction of four-atom tetrahedra containing exactly n B atoms and (4-n) A

atoms,† w is an interaction energy and α and β are dimensionless numbers
that express the strength of the four-body forces. If pair-wise near-
neighbor interactions suffice to describe the energy, $\alpha = \beta = 0$.
Equation (1) is subject to two constraints:

$$1 = Z_0 + Z_1 + Z_2 + Z_3 + Z_4 \qquad (2)$$

and the composition, given as a fraction x of atoms that are B,

$$4x = Z_1 + 2Z_2 + 3Z_3 + 4Z_4 \qquad (3)$$

Using the constraints (2) and (3) to eliminate two of the five Z_n's we
obtain a linear equation for E in terms of the remaining three which
then is subject only to the constraints that $0 \leq Z_n \leq 1$. If the
coefficients of these remaining Z's in these expressions are
positive, E is a minimum when these Z's are zero. By successively

───────────

† In the notation of Reference 7 and in a later section of this
paper various tetrahedral clusters that differ only by rotation
are distinguished, and A's are called 1 and B's are called 2.
Thus, z_{1112} and z_{1211} both represent the tetrahedron A_3B with
the B atom on different corners of the tetrahedron. The Z's
in the present section are given in terms of z's with four
subscripts by the following relations

$$Z_0 = z_{1111}$$
$$Z_1 = z_{2111} + z_{1211} + z_{1121} + z_{1112} \text{ , etc.}$$

Also, ε_{12} in Reference 7 eq. (4.2) is written as w in the present
paper.

eliminating all pairs of Z's the minima in E are explored. For instance, eq. (1) is already in the form of Z_0 and Z_4 eliminated. Therefore, if

$$w > 0, \quad 1+\alpha > 0, \quad 1+\beta > 0, \tag{4}$$

then the minimum in E occurs at

$$E = 0$$
$$Z_1 = Z_2 = Z_3 = 0,$$
$$Z_0 = 1 - 4x, \tag{5}$$
$$Z_4 = 4x.$$

From the constraint that the Z's lie between 0 and 1 it follows that $0 \leq x \leq 1/4$.

If instead we solve eqs. (2) and (3) for Z_1 and Z_2:

$$Z_1 = (2-4x) - 2Z_0 + Z_3 + 2Z_4$$
$$Z_2 = (4x-1) + Z_0 - 2Z_3 - 3Z_4$$

and use these to eliminate Z_1 and Z_2 from eq. (1), we obtain

$$E/N - 3w(1+\alpha)(2-4x) - 4w(4x-1)$$
$$= - 2w(1+3\alpha) Z_0 - w(2-3(\alpha+\beta)) Z_3 - 6w(1-\alpha) Z_4 \tag{6}$$

Thus, when

$$w(1+3\alpha) < 0$$
$$w(2-3(\alpha+\beta)) < 0 \tag{7}$$

and

$$w(1-\alpha) < 0$$

the minimum value for E is given by

$$p \quad (\mu, \nu, \zeta) - \exp(\mu x \quad - \mu \zeta(\mu, \nu, \zeta)) [p \quad (\mu, \nu)p \quad (\nu, \zeta)]$$

$$\times \exp\left(\sum^{(4)} \alpha^{(1)}_{ijkl} N\nu_{ijkl} + \sum^{(4)} \alpha^{(1)}_{mnkl} N\nu_{klmn} + \sum^{(4)} \gamma^{(1)}_{ijkl} N\nu_{ijkl} + \sum^{(4)} \gamma^{(1)}_{mnkl} N\nu_{klmn}\right). \tag{3.13}$$

$$E/N = 3w(1+\alpha)(2-4x) + 4w(4x-1) \tag{8a}$$

when

$$Z_0 = Z_3 = Z_4 = 0, \ Z_1 = 2-4x, \ Z_2 = 4x-1, \ 0.25 \leq x \leq 0.50. \tag{8b}$$

These equations and inequalities are more easily obtained by considering eqs. (1-3) as three simultaneous equations in six unknowns. Using Cramer's rule,[16,17] we obtain

$$|Enm| = \sum_k |knm| \ Z_k \tag{9a}$$

where $|Enm|$ and $|knm|$ are determinants formed by three columns from the matrix

$$\begin{bmatrix} 0 & 3w(1+\alpha) & 4w & 3w(1+\beta) & 0 & E/N \\ 1 & 1 & 1 & 1 & 1 & 1 \\ 0 & 1 & 2 & 3 & 4 & 4x \end{bmatrix} \tag{9b}$$

labelled E,n,m, and k,n,m respectively. The first five columns of the matrix, labelled 0 to 4 are the coefficients of Z_0 to Z_4 respectively in eqs. (1-3), and the last column labelled E is composed of the remaining terms. Because a determinant in which a column is repeated is zero, the terms involving Z_n and Z_m vanish in eq. (9a). Setting $|Enm|$ to zero gives the ground state energy when tetrahedra n and m are present, while the inequalities are given by requirements that $|knm|$ have the same sign as $(m-n)$. Thus, eq. (4) may be written in terms of determinants $|104|$, $|204|$, $|304|$, (5) in terms of $|E04|$, (7) in terms of $|012|$, $|312|$, $|412|$ and (8) in terms of $|E12|$, where each symbol represents a column in (9b).

The FSC expression of $\alpha^{(1)}(\mu, \nu)$ in (3.16) or (3.17) is the

Therefore the σ curve for which α is taken into account is always lower than the one for which α is left out. The

The results are summarized in Tables 1 and 2, and in figure 1. The conditions in Table 1 are constructed from the above rules, bearing in mind that permutation of two columns changes the sign of a determinant. Each line segment in figure 1 is a boundary where one of the determinants is zero and thus changes sign. Regions in which a particular intermediate phase will appear at the appropriate composition form polygons in figure 1.

3. Ground State Degeneracy

This linear programming method gives the combination of clusters that would give the lowest energy. At most, two types of clusters can be in the ground state. The presence of any others would raise the energy above the minimum. For example, eq. (6) indicates that Z_1 and Z_2 can be in the ground state, but the presence of any other clusters raise the energy above the minimum. Since each cluster type by itself gives a stoichiometric phase, a two-phase mixture of stoichiometric phases would have the ground state energy apart from any excess due to unwanted clusters at the interfaces between the stoichiometric phases.

In this model, however, the ground state can have many different configurations. There are three sources of degeneracy in the ground state. Each stoichiometric ordered phase can have one dimensional disorder without raising the energy. Parallel planes of certain anti-phase boundaries (APB) can be created without changing the cluster type. Both the $L1_2$ (Cu_3Au) structure and the DO_{22} (Ni_3V) structure are made up of only A_3B clusters. The DO_{22} structure can be thought of as $L1_2$ with evenly spaced (001) APB's, and vice versa. In fact, any distribution of parallel (001) APB has the ground state energy. The same holds true for APB's in $L1_0$ (CuAu) of the type that converts it into the CuAu II structure.[5]

method.[16] The resulting $\hat{G}$, which is now a function of T and μ, is made of two branches, one for the gas phase and the other for the liquid phase as shown in Fig. 5. The point at which the two branches cross gives the $\mu_{c.e.}$

When a system is exactly at a stoichiometric composition where only one cluster is present, the APB's discussed above are the only degeneracy. APB's with other orientations create clusters that raise the energy. In non-stoichiometric systems, when the pairs of clusters present are not adjacent in composition, $|m-n| \neq 1$, the ground state phases cannot deviate from stoichiometry for that would always create clusters adjacent in composition and raise the energy. All interphase boundaries (IPB) also raise the energy, as do APB's except the type discussed above. Thus, for non-adjacent clusters the only degeneracy is that due to one kind of parallel APB's.

For adjacent clusters, $|m-n| = 1$, in a non-stoichiometric system there are several more sources of degeneracy. Adjacent clusters can be mixed to give non-stoichiometric phases, nonuniform phases including mixtures of region with differing composition, "IPB's" where such regions meet, and APB's. Any such arrangement will have the ground state energy as long as only the two types of clusters are used. "Two-phase" dispersions on any scale down to the atomic is permitted.

As the composition varies from one stoichiometry to the next a symmetry change is occurring and there must be a phase transition. Thus, as B is added to pure A in a (0-1) case the ground state requires only that no two B's are neighbors. When x is small, this must look like a dilute almost-random solid solution, but as x approaches 0.25, it must tend toward an ordered alloy. The question of the nature of the ordering transition is examined in the next section.

The APB's involved in one-dimensional disorder have zero excess energy. So do APB's and IPB's when adjacent clusters are present in the ground state (e.g., cluster pairs 0-1 and 1-2). For all the other conditions these boundaries have finite energies at T=0. For the APB's

this situation is similar to the results of an investigation of the CsCl structure,[11] and will be used to understand the limiting behavior of calculations on IPB's and APB's in the companion paper.[10]

4. The Ordering Limits at T=0

In the ground state under conditions when w<0 and A_3B clusters exist [(0,1) in Table 1] there must be a phase transition from the fcc (disordered) to the A_3B structure as x increases from 0 to 0.25. The energy provides no clue since it is linear over the entire range, (fig. 2). The classical common tangent construction based on the energy does not provide definite compositions, for it is tangent along the entire composition range. For the same reason chemical potentials are also constant over this composition range (fig. 2). The terminal composition x=0 is not the phase limit for obviously a dilute mixture of B in A need not be a two-phase system. The answer is not to be found in the energy but in the entropy or the ground state degeneracy as it affects the entropy. In this section then we first undertake to calculate the free energy at finite temperature and examine the low-temperature limit under the condition where the (0,1) limit of Table 1 applies. Later in this section, we derive the combinatorial equations using the tetrahedron approximation for ground state degeneracy and examine the entropy for two-phase behavior. The two procedures give equivalent results.

The two species A and B are designated by i=1 and 2, respectively. In the tetrahedron approximation of CVM, the basic variable $z_{ijk\ell}$ is the probability of finding atomic species i, j, k and ℓ on the four vertices of a tetrahedron. We further require that the fourth subscript

bothersome shape of the 3×3 curve for low temperatures.

One other result of the 3×4 cluster calculation worth

ℓ is for the atom located on the sublattice which is preferentially occupied by B atoms in the ordered A_3B structure. For the sake of brevity we call this sublattice the B sublattice and the rest the A sublattices; the three A sublattices are equivalent.

Besides $z_{ijk\ell}$'s we use the pair variables y_{ij} and $v_{i\ell}$ together with the point variables x_i and u_ℓ. For y_{ij} both atoms are on the A sublattices while in $v_{i\ell}$ the first and second subscripts indicate the species on the A and B sublattices, respectively. For the point variables, x_i is the probability of finding an ith species on an A sublattice point, and u_ℓ is the corresponding quantity on the B sublattice. These variables are connected by the geometrical relations:

$$y_{ij} = \sum_{k,\ell} z_{ijk\ell} \tag{10}$$

$$v_{i\ell} = \sum_{j,k} z_{ijk\ell} \tag{11}$$

$$x_i = \sum_{j,k,\ell} z_{ijk\ell} \tag{12}$$

$$u_\ell = \sum_{i,j,k} z_{ijk\ell} \tag{13}$$

The normalization of z's is

$$1 = \sum_{i,j,k,\ell} z_{ijk\ell} \tag{14}$$

that the boundary free energy is closely tied to the multiplane distribution function $p_{[i,\ldots,i+m]}(\nu_0, \nu_1, \ldots, \nu_m)$ across the boundary.

Now we go to the puzzle mentioned at the end of Sec. II. The key to solve the puzzle is the fact that the probability expression for $m+1$ planes $p_{[i,\ldots,i+m]}(\nu_0, \nu_1, \ldots, \nu_m)$ in (A3) requires that the h function lies always on the left of

When the grand potential $\hat{G}$

$$\hat{G} = E - TS - \sum_i \mu_i N_i \tag{15}$$

is written in terms of $z_{ijk\ell}$'s and then is minimized with respect to z's, we obtain the following set of equations:

$$z_{ijk\ell} = \exp\left[\left(\frac{\lambda}{2} + w_{ijk\ell}\right)/kT\right] Y_{ijk\ell}^{1/2} X_{ijk\ell}^{-5/2} \tag{16}$$

where

$$w_{ijk\ell} \equiv -\varepsilon_{ijk\ell} + (\mu_i + \mu_j + \mu_k + \mu_\ell)/8 \tag{17}$$

$$Y_{ijk\ell} \equiv y_{ij} y_{ik} y_{jk} v_{i\ell} v_{j\ell} v_{k\ell} \tag{18}$$

$$X_{ijk\ell} \equiv x_i x_j x_k u_\ell \tag{19}$$

Although the order of subscripts are meaningful in $z_{ijk\ell}$, $Y_{ijk\ell}$ and $X_{ijk\ell}$, the order is immaterial in $w_{ijk\ell}$ since the energy parameter $\varepsilon_{ijk\ell}$ does not depend on the order of the subscripts. The quantity $\exp(\lambda/2kT)$ in (16) is the normalization factor and is determined from the normalization condition (14).

When the energy parameters $\varepsilon_{ijk\ell}$ and the chemical potentials μ_i together with the temperature T are given, the equilibrium state of the system is solved by finding $z_{ijk\ell}$'s which satisfy eqs. (10)

through (19) simultaneously. When these equations are solved, the parameter λ is identified as the grand potential $\hat{G}$ per lattice point:

$$\lambda = \hat{G}/N \qquad (20)$$

where N is the total number of lattice points in a system.

Because the system we are calculating has a fixed number of lattice points N, individual chemical potentials are not defined; only their difference is. We can arbitrarily choose

$$\mu_1 = -\mu_2 \equiv -\mu. \qquad (21)$$

At T=0, the entropy part does not contribute and we can write

$$\mu_2 - \mu_1 = \frac{\partial E/N}{\partial x}$$

$$= 2\mu \qquad (22)$$

The quantity 2μ is the diffusion potential of Larché and Cahn.[18] It is tabulated in Table 1 for the various ground states. From Table 1 and figure 2 we see that μ is a step function of composition. In the (0-1) range applying equation to the energy listed in Table 1 we obtain

$$\mu = 2E_1 = -6(1+\alpha)\,|w| \qquad (23)$$

Note that $w<0$. This must also be the value of μ for the two-phase equilibrium at T=0. At low temperature, we expand μ away from the value in (23) and write

$$\mu = - 6(1+\alpha) \, |w| + bkT + \ldots, \tag{24}$$

in which a is the expansion coefficient yet undetermined. In the quantities $w_{ijk\ell}$ in (17) we use the definition of the energy parameter $\varepsilon_{ijk\ell}$ in eq. (4.2) of Reference 7. The explicit form of $w_{ijk\ell}$'s are written in eq. (31) below in the following section. For the derivation of this section, we use the first two: w_{1111} and w_{1112}. Since the numerator of kT in eq. (16) should vanish at T=0 we expand λ also as

$$\lambda = - 6(1+\alpha) \, |w| + bkT + \ldots. \tag{25}$$

When we use the expansions (24) and (25), we see that w_{1111} and w_{1112} are different by a/4. Then the general formulas in (16-19) reduce to the following:

$$z_{1111} = \exp\left(\frac{b}{2} - \frac{a}{2}\right) \frac{\left(y_{11} \, v_{11}\right)^{3/2}}{\left(x_1^3 \, u_1\right)^{5/8}}$$

$$z_{1112} = \exp\left(\frac{b}{2} - \frac{a}{4}\right) \frac{\left(y_{11} \, v_{12}\right)^{3/2}}{\left(x_1^3 \, u_2\right)^{5/8}} \tag{26}$$

$$z_{1121} = z_{1211} = z_{2111} = \exp\left(\frac{b}{2} - \frac{a}{4}\right) \frac{\left(y_{11} \, y_{12}^2 \, v_{11}^2 \, v_{21}\right)^{1/2}}{\left(x_1^2 \, x_2 \, u_1\right)^{5/8}}$$

The rest of $z_{ijk\ell}$'s are negligible and are not needed. These are for the A_3B phase. The $z_{ijk\ell}$'s for the disordered phase can be obtained from (26) by imposing the disordering conditions: $y_{ij} = v_{ij}$ and $x_i = u_i$.

The formulation is now complete. We use the computer to solve the set of equations in (26) for different values of a. For the computation we used the values of $\alpha=0.01$ and $\beta=-0.08$ which can make the Cu_3Au phase diagram best fit with experiments as will be discussed in the accompanying paper.[10] The quantity b is determined as a function of the quantity a from the normalization of z's:

$$1 = z_{1111} + z_{1112} + 3z_{1121} \tag{27}$$

Note that the rest of $z_{ijk\ell}$'s are negligibly small. The solid curve in figure 4 shows the result. We repeat the solution for the disordered phase, and obtain the dashed curve in figure 4.

Since λ is the grand potential as was mentioned in (20), the point at which the two curves cross in figure 4 represent the coexistance of the two phases. The value of a at the intersection is a=0.8109 and is the right value of the gradient of the kT vs. μ curve at T=0 in figure 5.

The disorder-Cu_3Au phase boundary points at T=0 in figure 6 were calculated in this way. Since the exponential factors in (26) do not depend on T, the phase boundary curves in this figure are vertical near T=0. It is believed that this vertical property is a general result.

Another general property we can deduce from (26) is the fact that the equations are independent of the parameters α and β within the limits imposed by (0-1) in Table I. Because of this, the positions of the phase boundaries at $T \to 0$ are independent of α and β. This is readily understood since this problem involves only different ways of arranging the same ground state clusters.

Similar calculations were done for the Cu_3Au-$CuAu$ boundary at $T \rightarrow 0$ and the results are plotted in figure 6.

As was mentioned in the introductory paragraph of this section, to start from eq. (16) is not the only way of deriving the $T=0$ phase boundary. An alternative method is to work with the entropy. For the (0-1) cluster pair, the ground state energy is linear in the composition x as is shown in the first row of Table 1, and thus does not contribute to the phase separation. Therefore, the phase boundaries at $T=0$ between the disordered fcc phase and the A_3B phase are to be calculated by the common tangent construction based on the two entropy curves as shown schematically in figure 7.

We now show that to draw S_D and S_O as functions of the composition x and then determine the phase boundaries x_D and x_O from the common tangent is equivalent to the method presented in this section.

For this purpose, we introduce a parameter a and define functions $\Phi_D(a)$ and $\Phi_0(a)$ as

$$\Phi_D(a) \equiv \underset{x}{\text{Max}} \left[S_D(x) - ax \right]$$

$$\Phi_0(a) \equiv \underset{x}{\text{Max}} \left[S_0(x) - ax \right]$$

(28)

When we plot the two functions $\Phi_D(a)$ and $\Phi_0(a)$ against the parameter a, they cross as in figure 8. The point P at which the two curves cross corresponds to the common tangent situation in figure 7. The proof is the following:

At P, we have

$$\Phi_D(a_0) = S_D(x_D) - a_0 x_D = S_0(x_0) - a_0 x_0 = \Phi_0(a_0) \qquad (29a)$$

and since the Φ's are maxima

$$\frac{dS_D(x_D)}{dx_D} = a_0 = \frac{d S_0(x_0)}{dx_0} \qquad (29b)$$

Thus, we obtain

$$\frac{S_0(x_0) - S_D(x_D)}{x_0 - x_D} = a_0 = \frac{d S_D(x_D)}{dx_D} = \frac{d S_0(x_0)}{dx_0} \qquad (30)$$

This shows that the two curves $S_D(x_D)$ and $S_0(x_0)$ posses a common tangent. Therefore, x_D and x_0 are the boundaries of the two phases.

When we formulate the entropy using the tetrahedron approximation of the CVM, and proceed formulating the functions Φ_D and Φ_0, we arrive exactly at the eqs. in (26).

One conclusion which is clearly derived from the illustration in figures 7 and 8 is that the phase boundaries are determined by the entropy formula only, and thus depend on the approximation used in the CVM.

The singularity at T=0 is illustrated in figures 5 and 6. Each of the six lines numbered 1 through 6 in the two figures are two representations of an approach to T=0. For any x in the range in the range $0 < x < 1/4$, μ approaches the same limit, each x in figure 6 corresponding to a fixed limiting slope in figure 5.

5. Alternative Derivation of Figure 1

Combinations of figures 5 and 6 and of figures 7 and 8 indicate the dual properties between the μ and composition space analysis. In the present section we briefly show an alternative derivation of figure 1 based on the μ space analysis.

We go back to eq. (16) for $z_{ijk\ell}$. In this expression the Y and X parts come from the entropy expression and hence we can disregard in our derivation of figure 1. The energy and the chemical potential information is contained in the quantity $w_{ijk\ell}$. Because of the permutation symmetry among the subscripts, there are five $w_{ijk\ell}$'s, which are written explicitly here:

$$w_{1111} = -\frac{1}{2}\mu$$
$$w_{1112} = -\frac{3}{2}(1+\alpha)w - \frac{1}{4}\mu$$
$$w_{1122} = -2w \qquad\qquad (31)$$
$$w_{1222} = -\frac{3}{2}(1+\beta)w + \frac{1}{4}\mu$$
$$w_{2222} = \frac{1}{2}\mu$$

Each of the five $w_{ijk\ell}$'s in (31) is a line in the $w_{ijk\ell}$ vs. μ space. Of these, w_{1111}, w_{1122}, and w_{2222} are independent of α and β and are drawn by thick lines in figure 9. For the purpose of illustration, figure 9 is drawn for the case $w<0$.

In figure 9 for the region $\mu<-4|w|$, w_{1111} is larger than w_{1122}. This means that in this region of μ, the cluster 1111 is more stable than the cluster 1122 in T=0 because $w_{ijk\ell}$ is divided by T. By draw-

ing five $w_{ijk\ell}$'s of (31) on this diagram and comparing which is the largest, we see which cluster is present in the system for a given value of μ. When two $w_{ijk\ell}$ lines cross, it means the two clusters can coexist.

The w_{1112} in (31) depends on α and is drawn by a chain line of negative slope in figure 9. The w_{1222}, which depends on β, is drawn by a chain line of positive slope.

When $\beta<-1/3$, w_{1222} is always suppressed, as indicated by the w_{1222} line marked by β_1. This corresponds to the fact that AB_3 does not appear in the region $\beta<-1/3$ in figure 1(a).

At the point P in figure 9, three lines meet: $w_{1112}(\alpha_2)$, w_{1122} and $w_{1222}(\beta_2)$. For $\beta=\beta_2$ when α is in the range $-1/3<\alpha<\alpha_2$, all five clusters can be stable at some value of μ. The combination $\beta=\beta_2$ and $\alpha=\alpha_2$ is a boundary such that either $\alpha_2<\alpha$ or $\beta_2<\beta$ makes the w_{1122} phase suppressed. At P, the equations

$$w_{1112} = w_{1122} = w_{1222} \tag{32}$$

hold and use of (31) leads to the relation

$$\alpha+\beta = \frac{2}{3} \tag{33}$$

which is the line marked (P) in figure 1(a).

At Q in figure 9, three lines meet: $w_{1112}(\alpha_2')$, $w_{1222}(\beta_2)$ and w_{2222}. Proceeding in the similar way, as in the preceding paragraph, we arrive at

$$\alpha-3\beta=2 \tag{34}$$

which is the line marked (Q) in figure 1(a). The line marked (R) in figure 1(a) corresponds to the point R in figure 9.

6. Summary and Concluding Remarks

Multiatom forces (characterized by two parameters α and β), rather than the composition-dependent energy parameters, were used recently successfully in deriving the asymmetry of Cu_3Au phase diagram.[6,7] This formulation forms the basis of the accompanying paper on phase boundaries.[10] As a study to back up the use of the parameters α and β, their effect on the stability of phases at T=0 is worked out in the first part of the present paper. The results are shown in figure 1.

In figure 1, as well as in previous studies[14,15] of possible phases at T=0, only the energy expression of the system comes into play. In the second part of the paper, we derive the position of phase boundaries at T→0. This is done using the entropy expression, and hence the position of the boundary depends on the approximation used in the entropy expression. Figures 4, 5 and 6 show the results. A general conclusion is that in the temperature T vs. composition x plot, a phase boundary near T=0 is always parallel to the T axis and comes straight down to the x axis.

The dual nature between the composition and the chemical potential μ is one theme repeated in the paper. The fact that μ takes the same constant value for a range of x in the single phase regions is illustrated in figures 5 and 6.

References

(1) C. Domb, p. 357 in "Phase Transitions and Critical Phenomena," Vol. 3 (ed. C. Domb and M. S. Green) Academic Press, N.Y. 1974.

(2) R. Kikuchi, "The Cluster Variation Method," J. de Phys. $\underline{38}$, C7-307 (1977).

(3) S. C. Moss and P. C. Clapp, Phys. Rev. $\underline{171}$, 764 (1968).

(4) W. Shockley, J. Chem. Phys. $\underline{6}$, 130 (1938).

(5) R. Kikuchi and H. Sato, Acta Met. $\underline{22}$, 1099 (1974).

(6) C. M. van Baal, Physica $\underline{64}$, 571 (1973); N. S. Golosov, L. E. Popov and L. Ya Pudan, J. Phys. Chem. Solids $\underline{34}$, 1149 and 1157 (1973); R. Kikuchi, J. Chem. Phys. $\underline{60}$, 1071 (1974).

(7) R. Kikuchi and D. deFontaine, "Applications of Phase Diagrams in Metallurgy and Ceramics," Vol. 2, NBS Special Publication 496, p. 967 (1978).

(8) P. C. Clapp, Acta Met. $\underline{22}$, 563 (1974).

(9) K. H. Johnson in "Advances in Quantum Chemistry" Vol. 6, p. 1, Academic Press, N.Y. (1972).

(10) R. Kikuchi and J. W. Cahn, Acta Met. (subsequent paper).

(11) J. W. Cahn and R. Kikuchi, J. Phys. Chem. Solids $\underline{20}$, 94 (1961).

(12) R. Kikuchi and J. W. Cahn, J. Phys. Chem. Solids $\underline{23}$, 137 (1962).

(13) J. W. Cahn and R. Kikuchi, J. Phys. Chem. Solids $\underline{27}$, 1305 (1966).

(14) M. J. Richards and J. W. Cahn, Acta Met. $\underline{19}$, 1263 (1971); J. Kanamori and Y. Kakehashi, J. de Phys. $\underline{38}$, C7-274 (1977).

(15) S. M. Allen and J. W. Cahn, Acta Met. $\underline{20}$, 423 (1972).

(16) A. C. Aitken "Determinants" Interscience, N.Y. (1949).

(17) J. W. Cahn, "Thermodynamics of Solids and Fluid Surfaces" 1977 ASM
Symposium on Segregation. Appendix II. To be published.

(18) F. L. Larché and J. W. Cahn, Acta Met., 26 (1978).

Table 1

Clusters present (n,m)	Range in x	Energy (see Table 2)	Chem. Pot. (μ)	Conditions (see Table 2)		
0,1	0-1/4	$4xE_1$	$2E_1$	$\|012\|>0$	$\|013\|>0$	$\|014\|>0$
0,2	0-1/2	$2xE_2$	E_1	$\|012\|<0$	$\|023\|>0$	$\|024\|>0$
0.3	0-3/4	$\frac{4}{3}xE_3$	$\frac{2}{3}E_3$	$\|013\|<0$	$\|023\|<0$	$\|034\|>0$
0,4	0-1	0	0	$\|014\|<0$	$\|024\|<0$	$\|034\|<0$
1,2	1/4-1/2	$(2-4x)E_1+(4x-1)E_2$	$2(E_2-E_1)$	$\|012\|>0$	$\|123\|>0$	$\|124\|>0$
1,3	1/4-3/4	$(\frac{3}{2}-2x)E_1+(2x-\frac{1}{2})E_3$	(E_3-E_1)	$\|013\|>0$	$\|123\|<0$	$\|134\|>0$
1,4	1/4-1	$\frac{4}{3}(1-x)E_1$	$-\frac{2}{3}E_1$	$\|014\|>0$	$\|124\|<0$	$\|134\|<0$
2,3	1/2-3/4	$(3-4x)E_2+(4x-2)E_3$	$2(E_3-E_2)$	$\|023\|>0$	$\|123\|>0$	$\|234\|>0$
2,4	1/2-1	$2(1-x)E_2$	$-E_2$	$\|024\|>0$	$\|124\|>0$	$\|234\|<0$
3,4	3/4-1	$4(1-x)E_3$	$-2E_3$	$\|034\|>0$	$\|134\|>0$	$\|234\|>0$

Table 2

Determinants

$$\frac{1}{2}|012| = -(1+3\alpha)w \qquad\qquad \frac{1}{12}|034| = -(1+\beta)w$$

$$\frac{1}{3}|013| = -(2+3\alpha-\beta)w \qquad\qquad \frac{1}{2}|123| = -(2-3(\alpha+\beta))w$$

$$\frac{1}{12}|014| = -(1+\alpha)w \qquad\qquad \frac{1}{6}|124| = -(1-\alpha)w$$

$$\frac{1}{8}|023| = -(1-\beta)w \qquad\qquad \frac{1}{3}|134| = -(2-\alpha+3\beta)w$$

$$\frac{1}{16}|024| = -w \qquad\qquad \frac{1}{2}|234| = -(1+3\beta)w$$

Energies

$$E_1 = 3w(1+\alpha) \qquad\qquad E_2 = 4w \qquad\qquad E_3 = 3w(1+\beta)$$

Figure Captions

Fig. 1. Classification of stable phases in the α and β space. (a) is for $w<0$ and (b) is for $w>0$.

Fig. 2. An example of the ground state energy-composition diagram. This is for the case where A_3B and AB are the only intermediate phases. In the range $0<x<1/2$ solid solutions are possible. The question of two phase regions shown dashed is examined in Section 4. Where there is a missing intermediate phase in the range $1/2<x<1$ no solid solutions are possible in the ground state.

Fig. 3. The chemical potential corresponding to the situation in fig. 2. Note that this is a step function. The chemical potentials at two-phase equilibrium are fixed in this construction, although the coexisting compositions are not.

Fig. 4. Plots of b vs. a from computer calculations. Note that the disorder and the A_3B phases cross at $a = 0.8109$. The tetrahedral multiatomic interaction parameters chosen are $\alpha=0.01$ and $\beta=-0.08$.

Fig. 5. The chemical potential μ and temperature diagram calculated for $w<0$, $\alpha=0.01$ and $\beta=-0.08$. Note that $\mu=-(6+\alpha)w$ at T=0. The lines indicated by 1 through 6 all radiate from this point.

Fig. 6. The composition and temperature phase diagram corresponding to figure 5. The short numbered lines correspond to the lines with the same number in figure 5.

Fig. 7. Schematic diagram of entropy curves, S_D for the disordered phase and S_0 for the ordered A_3B phase. The common tangent determines the phase x_D and x_0.

Fig. 8. Schematic plot of the functions $\Phi_D(a)$ and $\Phi_0(a)$ in eq. (28). The point P at which the two curves cross correspond to the coexistence of two phases.

Fig. 9. Working diagram which is used to lead to fig. 1(a) from the alternative treatment of Section 5. Points P, Q and R corresponds to the lines (P), (Q) and (R) in fig. 1.
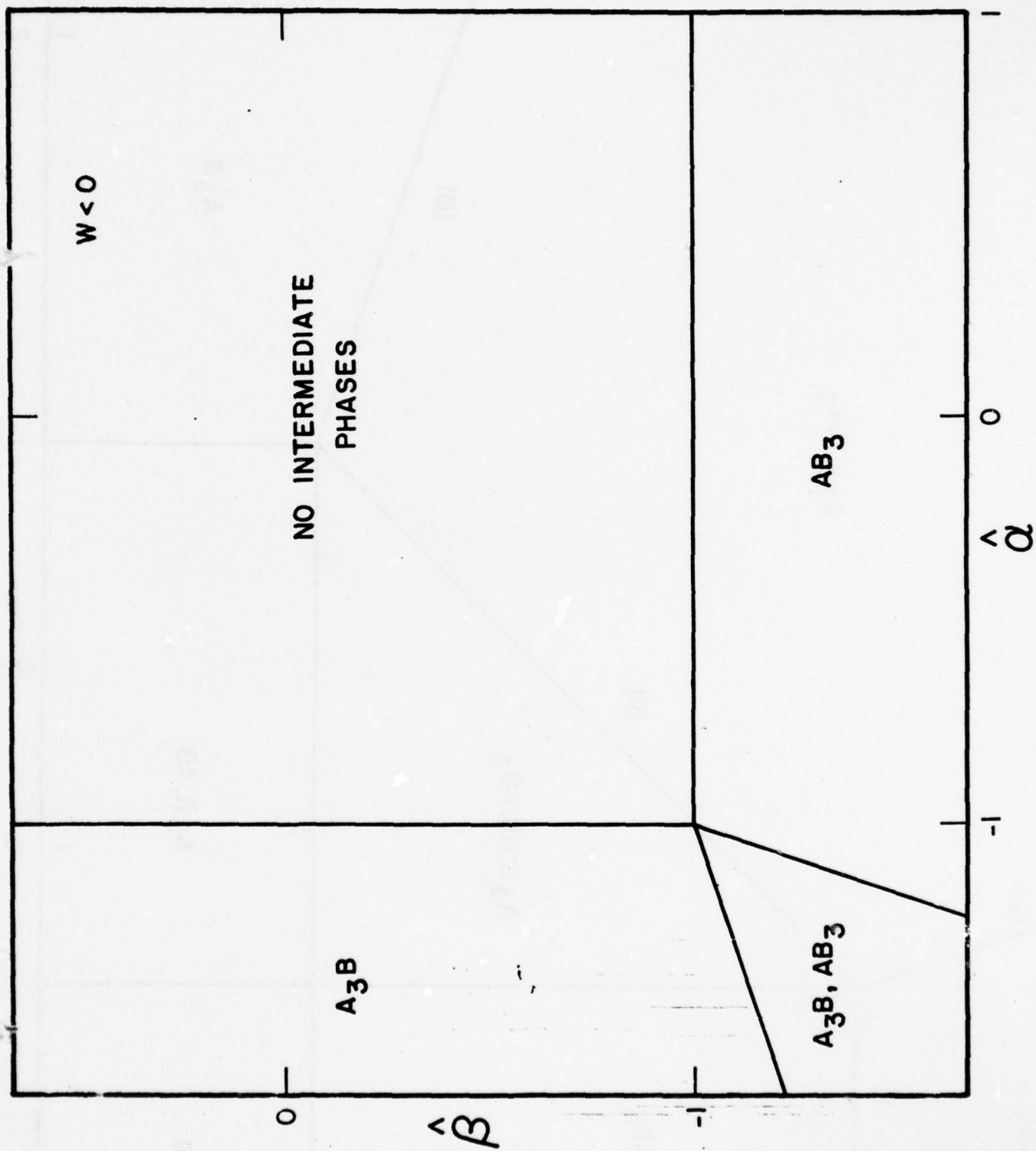
Figure 1.

Figure 2.
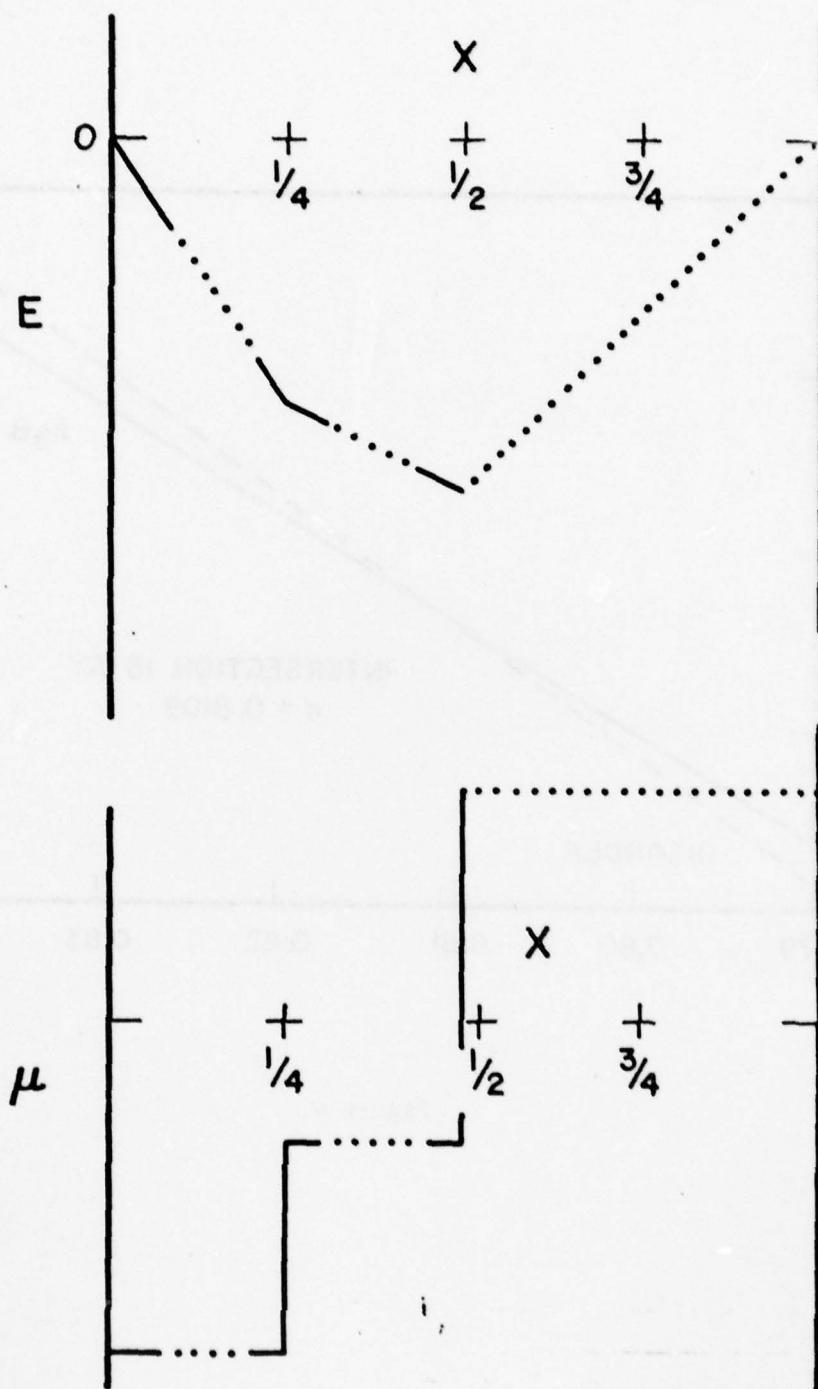
Figure 3.
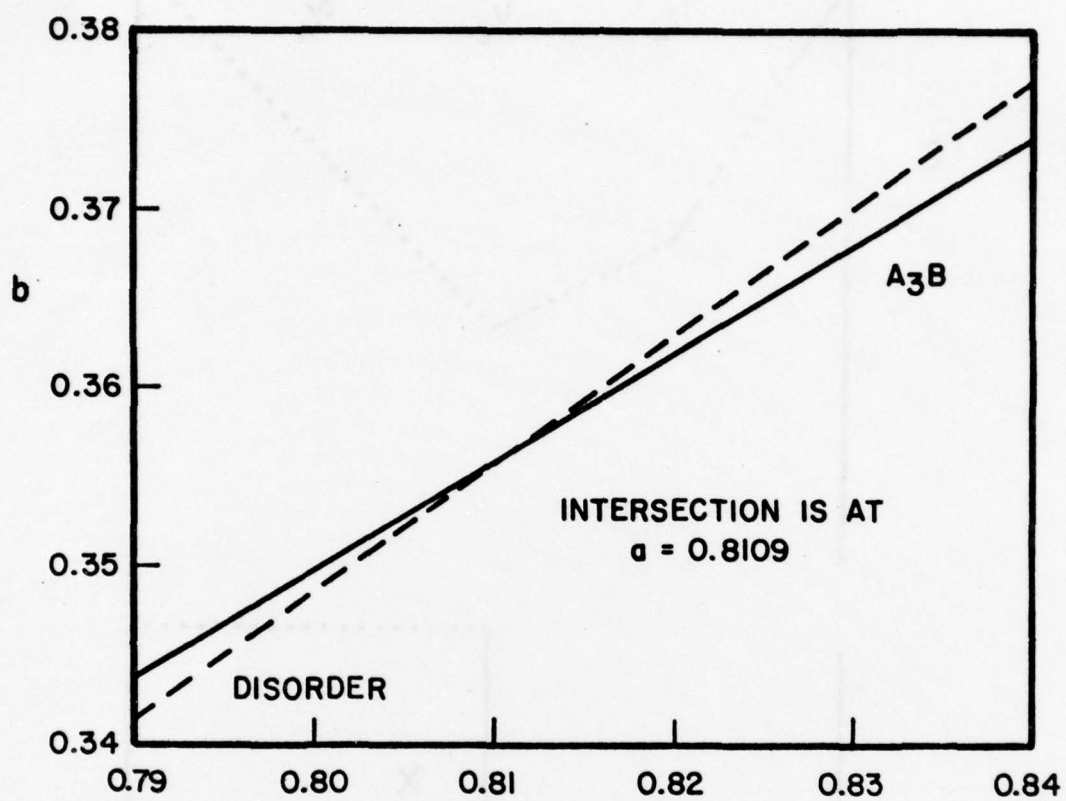
Figure 4.
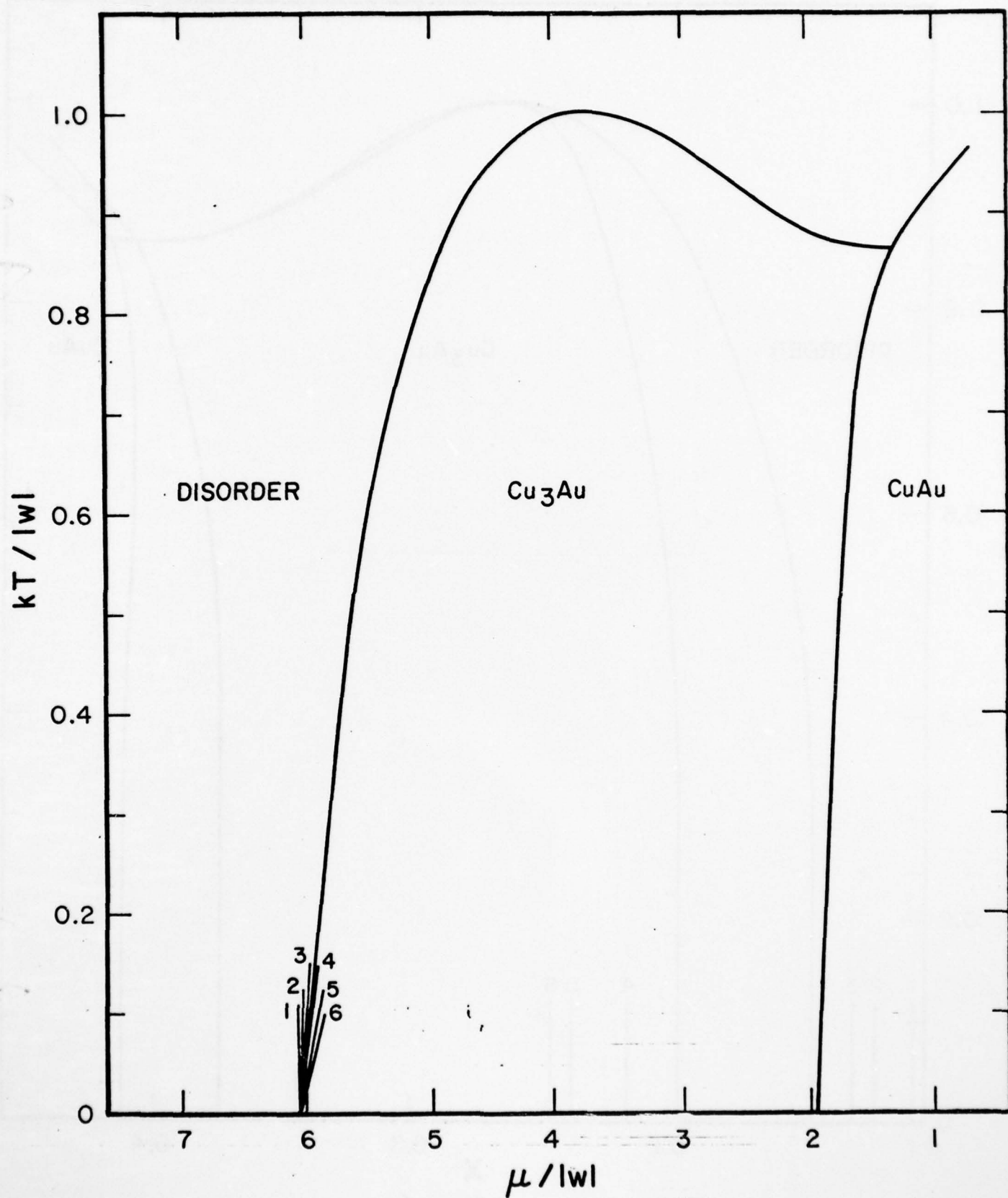
Figure 5.
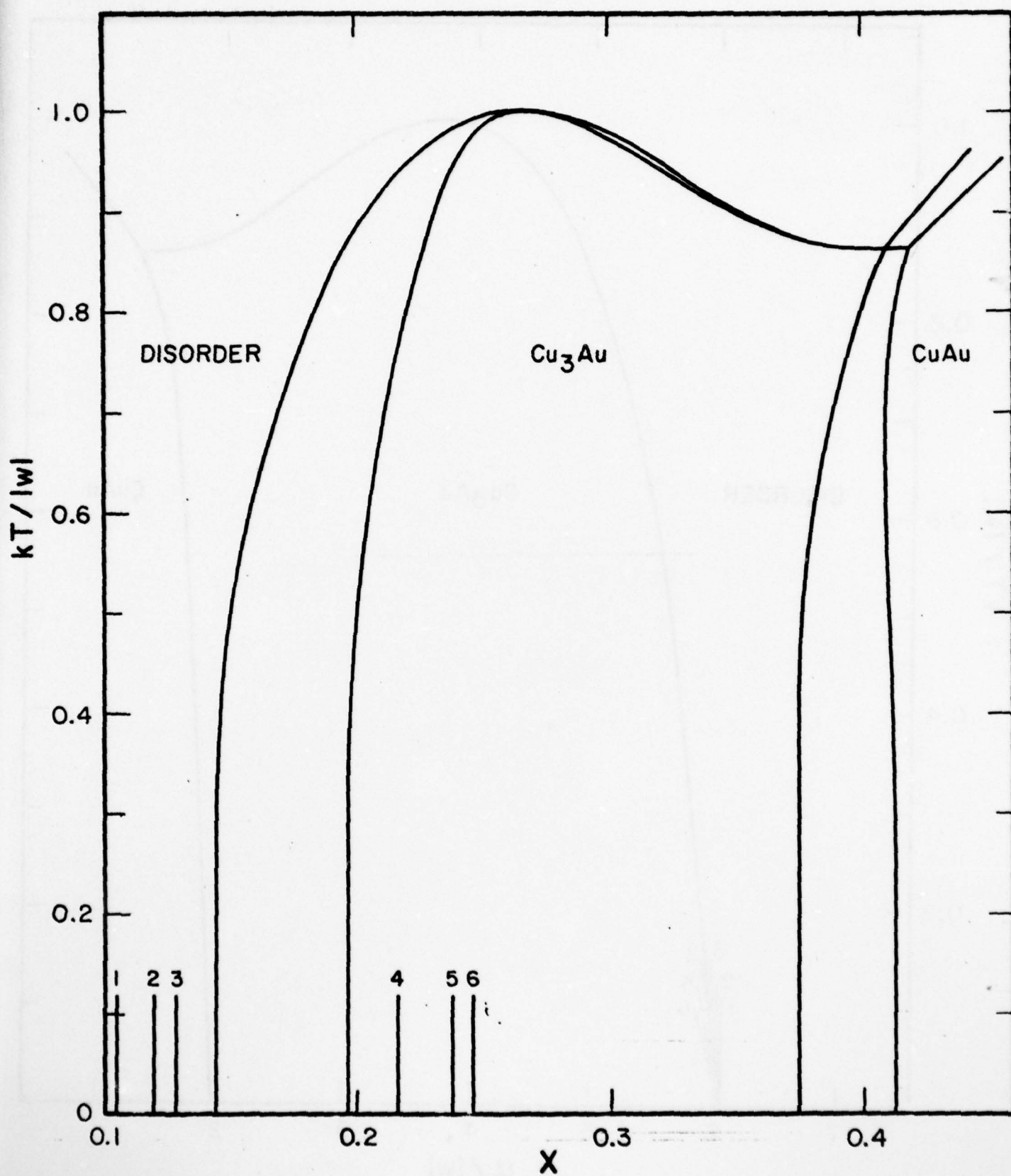
Figure 6.
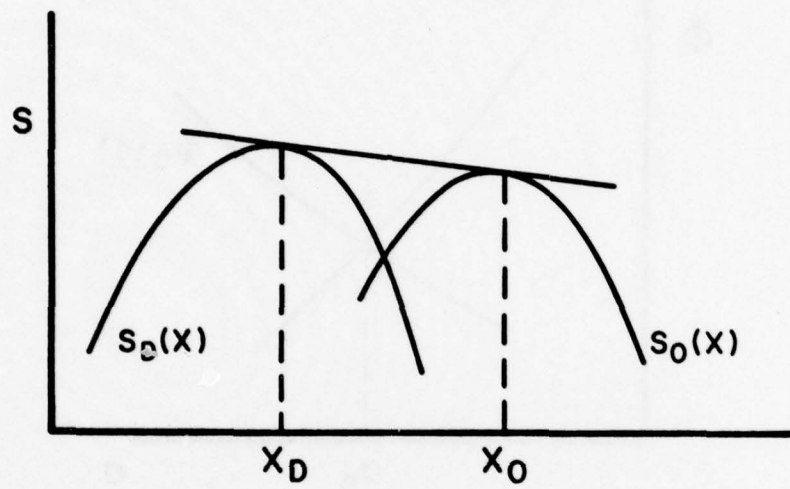
Figure 7.
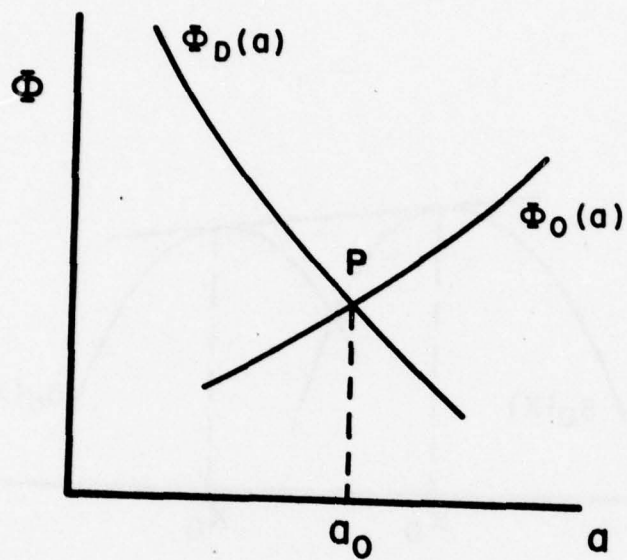
Figure 8.
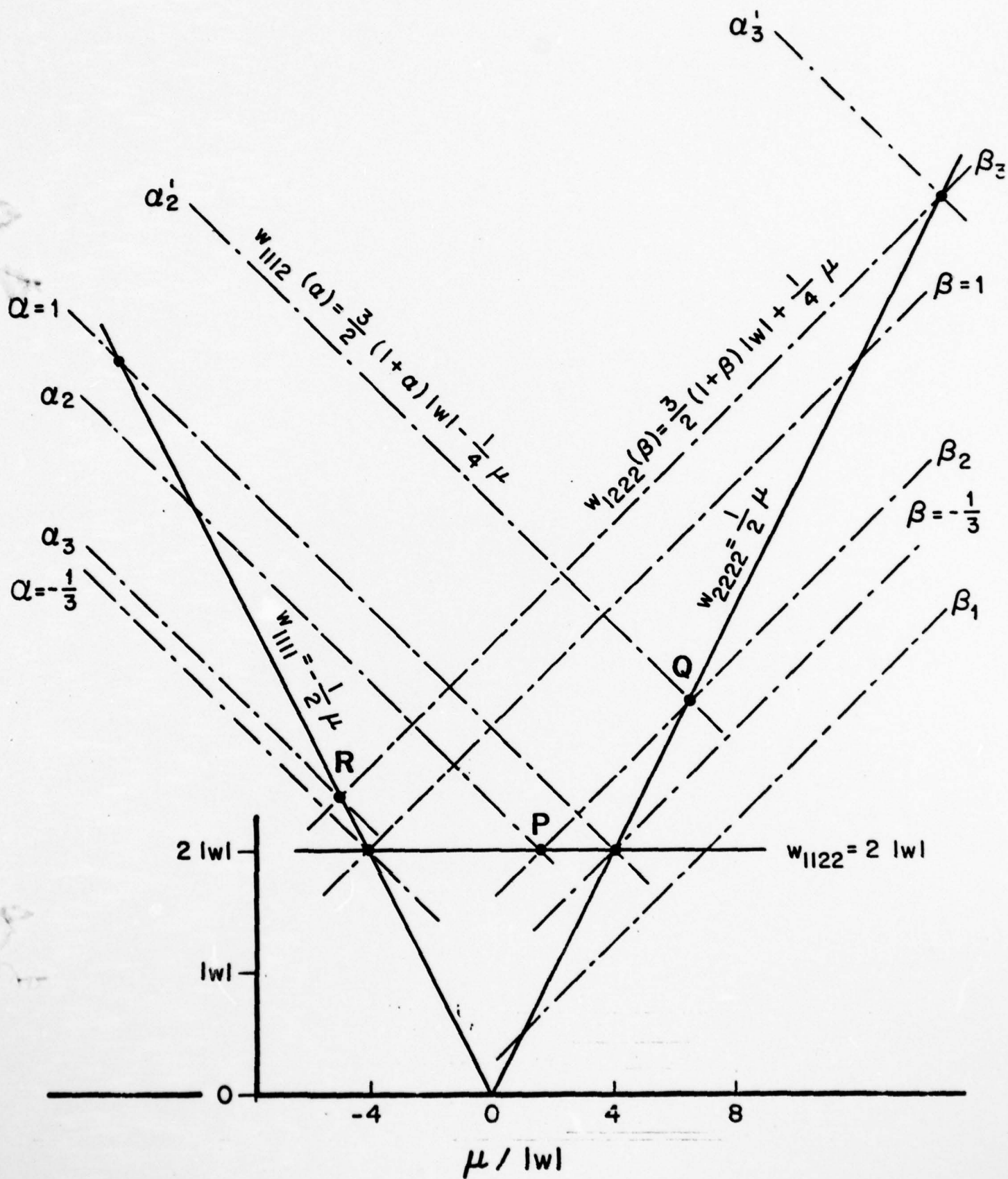
Figure 9.

APPENDIX 5

(Reference [5])

THEORY OF INTERPHASE AND ANTIPHASE BOUNDERIES
IN F.C.C. ALLOYS

R. Kikuchi and J.W. Cahn

Acta Metallurgica (in press)

Theory of Interphase and Antiphase Boundaries
in Face Centered Cubic Alloys

Ryoichi Kikuchi*
Hughes Research Laboratories
Malibu, CA 90265

and

John W. Cahn
National Bureau of Standards
Washington, D.C. 20234

Abstract

Equilibrium antiphase (APB) and interphase (IPB) boundaries in the Cu-Au system are examined theoretically using the cluster variation method with multi-atom interactions whose magnitudes were previously obtained from a fit of the phase diagram. The IPB energy between equilibrium disordered fcc and ordered Cu_3Au phases is strongly temperature (and hence composition) dependent, being much higher for the copper-rich side of the congruent point T_c and having a maximum on that side at about $0.95 T_c$. The IPB energies are only slightly anisotropic. The APB energies at constant chemical potential decrease monotonically with increasing temperature; at constant nonstoichiometric composition they increase at low temperature to a maximum well below the disordering temperature. Near the congruent point, the APB undergoes one or more second order surface phase transition in which an interfacial layer resembling inhomogeneous Cu-Au (Ll_o) phase develops within the boundary. The APB with (hk0) orientation (in our notation) should be perfectly wet by the disordered phase at the disordering temperature for that particular composition.

I. Introduction

In ordering systems there occur two kinds of particularly simple
coherent interfaces, antiphase domain boundaries (APB) and coherent
interphase boundaries (IPB). If we ignored the difference in the
identity of the atomic species, the two domains or phases meeting at
coherent interface would be part of the same single crystal as is
illustrated in Fig. 1. An APB separates two domains of the same ordered
phase. An IPB separates two different phases. IPB's can occur between
disordered phases differing in composition, between an ordered and a
disordered phase, or between two ordered phases.

APB's can exist in all ordered phases. They result from the symmetry
breaking during ordering processes which can start in different ways in
various locations in a disordered lattice. The APB's form wherever two
such regions contact. APB's result also from the presence (or motion)
of dislocations whose Burger's vector are not translation vectors of
the superlattice. The mechanical properties of superlattices are strongly
affected by the fact that motion of such dislocations changes the area
of APB's. Often deformation can only occur by groups of dislocations
whose Burger's vectors sum to a superlattice translation vector, and
whose motion as a group resotres long-range order in the structure [1,2].

The IPB's are important in alloys which order by first-order transition.
The free energy of an IPB is a factor in determining the rate of
nucleation [3] of the ordered phase on cooling or the disordered phase
on heating. For multiphase alloys it also affects the shape and dispersion
of particles and is the main driving force in the long-time coarsening
of such a dispersion [4].

Phase transitions within such interfaces have been predicted [5], but the order of the transition is very high, so that all properties that are related to low derivatives of the surface free energy will be continuous through this transition. There would be important implication of a change in character of these interfaces on properties of such alloys, if the order of the surface transition were lower.

Whether the ordering transition itself is first order or higher order is an important factor in discussing such interfaces. At the critical temperature of a higher-order transition the disordered and the various domains of the ordered phase all become identical to each other. Consequently APB's disappear as the critical temperature is approached and their energy vanishes [6-10]. Because there is no coexistence of ordered and disordered phases (except trivially at the critical temperature) there are no equilibrium IPB's between phases related by higher-order transitions.

For first-order transitions two-phase equilibrium occurs over a range of temperatures and the two phases are never identical. The ordered phase retains a finite amount of order up to the transition temperature. Consequently both APB's and IPB's exist right up to the transition temperature and there is no reason to assume that their energy would vanish there.

Several ordering transitions are first order. In this paper we shall examine IPB's and APB's in an fcc (Cu-Au type) system which undergoes an ordering transition to form a phase with the Cu_3Au structure (Ll_2). In addition to the Cu-Au system these interfaces also occur in a number of important nickel-base systems, notably in the Ni-Al system which is the basis of superalloys. These alloys are treated to form a fine scale dispersion of coherent Ni_3Al in a disordered nickel solid solution.

They are useful because their strength increases with increasing temperatures to approximately 800°C, and then declines at higher temperatures [11,12]. .Increases of strength with increasing temperature seems to be quite commonly observed in ordered alloys [13-18].

APB's have been studied theoretically for the CsCl (or CuZn) structure derived from the ordering of bcc [8-10]. In the model chosen, (near-neighbor pair-wise interaction energies) this is a second-order transition. The corresponding model for fcc gave completely unrealistic phase-diagrams [19] until it was recently shown that these resulted from the Bragg-Williams and pair approximation [18-21] rather than the model itself. A cluster-variation method (CVM) in the tetrahedron approximation can give a phase diagram in which there are three ordered phases, A_3B, AB and AB_3, which disorder by first-order transitions [20-21]. A close match to the phase diagram found for the Cu-Au system is obtained if four-body interactions are introduced [22]. The phase diagram calculation made it feasible to undertake a theoretical study of APB's and IPB's in such a model system.

A previous study of IPB's in ordering systems [23] suffers from several assumptions and possibly some computational errors that have limited its applicability. In this study IPB's were created theoretically between phases of arbitrary composition and order, not necessarily ones that would ever be in equilibrium with each other, by cutting and joining and computing the energy from the changes in the bond count. No rearrangement of atoms near the boundary was permitted. Such "weld" interfaces can have negative energies as well as positive and the energy can almost always be reduced further. Under some conditions rearrangement might tend even to complete homogenization by rearrangement. We note that for many of the ground state cases we obtain rigorous results that differ

1.0

1.1

1.25 1.4 1.6

2.8 2.5
3.2 2.2
3.6
4.0 2.0

1.8

MICROCOPY RESOLUTION TEST CHART
NATIONAL BUREAU OF STANDARDS-1963-A
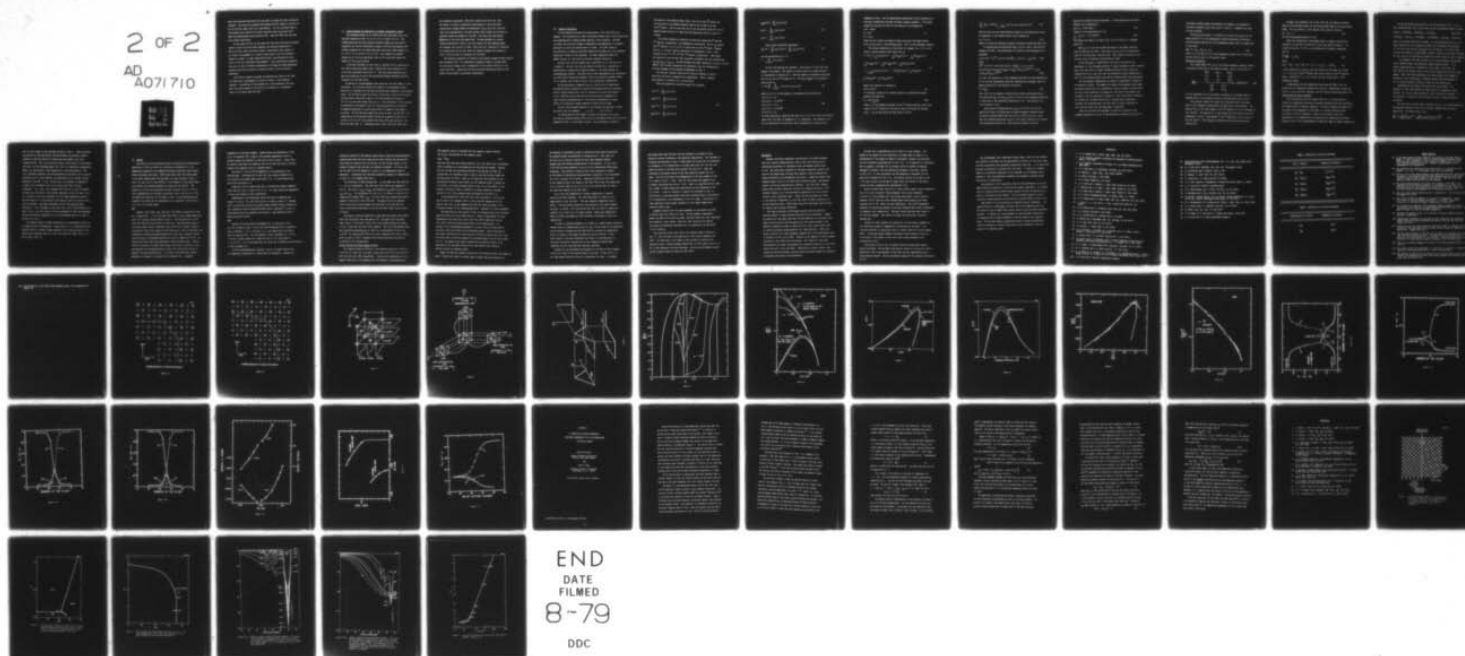
from those obtained previously [23] even when we assume the same interaction energies. The study also examined APB energies without regard to whether or not the initial phase could be in equilibrium. For the Ll_2 phase negative APB energies were reported [23] under condition where DO_{22} should have been the stable ground state structure [24]. Here the "APB" was the first step towards equilibrium.

In this paper we will use the model with four-body interaction energies chosen to match the Cu-Au phase diagram, and calculate properties of APB's and IPB's which have been allowed to equilibrate with respect to all atomic rearrangement in a crystal constrained to have two different domains or phases. At high temperatures and/or slow deformation rates there is time for diffusional rearrangement. Such equilibrated boundaries obey all the laws of surface thermodynamics including the Gibbs adsorption equation which can be used for a sensitive check on the calculation procedures.

If an APB is created so rapidly by shearing that there is not time for diffusional rearrangement of atoms, we obtain a very different boundary. Calculations of the properties of such boundaries have been made for various models [7,25] and will be examined in a subsequent paper for the model used here [26].

II. Crystallography and Definition of Surface Orientation Indices

The disordered phase is fcc (Fm3m) with four equivalent sites with
m3m point symmetry at 000, 1/2 1/2 0, 1/2 0 1/2 and 0 1/2 1/2. The
ordered phase has the Cu_3Au crystal structure (Pm3m) with one kind of
occupation for the site arbitrarily chosen at 000 with m3m symmetry and
another occupation at the three equivalent sites with 4/mmm symmetry at
1/2 1/2 0, 1/2 0 1/2 and 0 1/2 1/2 [27]. Four domains are possible
because any of the four equivalent sites in fcc could have become the
origin for the Cu_3Au structure.

It has been customary in this field to describe the fcc structure by
four inter-penetrating simple cubic "sublattices" each centered on one
of the four equivalent sites (Fig. 2). The Cu_3Au type ordering occurs
when the occupation of one of the sublattices becomes different from the
occupation on the other three.

We define our crystallographic axes along the cube axes common to both
structures. For the IPB we choose the origin of the coordinate system
such that it coincides with the atom having m3m point symmetry in the ordered
phase. For the APB we place the origin at this point in one of the domains
and arbitrarily choose the z-axis so that the m3m position occurs at
1/2 1/2 0 in the other domain (See Fig. 3). The orientation of the boundary
is specified by its normal $\hat{n}$, but all such properties must be invariant
to symmetry operations of a point group which is common to both domains
or phases. For the IPB this common point group is m3m. For the APB it is
4/mmm because the translation which carries the occupation from the site
at 000 to the 1/2 1/2 0 site destroys the three-fold axes and two of the
four-fold axes (Fig. 3). Accordingly while (100), (010) and (001) IPB's

are completely equivalent, (001) APB's differ from (010) and (100).
The former is called a conservative APB because it could have been
created from a single domain by conservative slip; while the (100) and
(010) are nonconservative, and with perfect order either two enriched or
depleted layers are adjacent at the APB. They have also been called
boundaries of the first and second kind. We may represent all scalar
surface properties by plots on the unit sphere, but the symmetry makes
the triangle with corners at (001), (101) and (111) sufficient to describe
all orientations for the IPB, while the larger triangle with corners at
(001), (100) and (110) is necessary for the APB's.

The symmetry properties of bicrystals with planar boundaries have recently
been developed [28]. The formulation is general enough to include APB's
(no orientation change, just a translation of one crystal relative to the
other) and IPB's. Application of this new group-theoretical method to the
present system leads to equivalent descriptions.

III. General Formulation

In this section we develop the formulations of the (100) APB as an

example. The formulation for other orientations differ only in the interactions

and configurations of atomic planes parallel to the interface. The APB

can exist over the entire range of temperature and composition (or chemical

potential) in which the ordered phase is stable. For IPB's there is

the limitation on chemical potential imposed by the phase rule that different

phases must coexist at the interface. For each temperature where the

phases coexist, an IPB occurs at discrete chemical potentials.

We shall call the four simple cubic sublattices I, II, III and IV as

in Figure 2. We shall call the A_3B domains in which the I sublattice is

preferentially occupied by B atoms the domain I; the other domains are

correspondingly defined. The [001] axis is then determined by our convention.

The (100) APB is formed when domains I and II are placed on opposite sides

of the boundary and allowed to relax to the equilibrium configuration.

By the definition of domains I and II, the III and IV sublattices

are preferentially occupied by A atoms in both phases while the occupancy

pattern changes between the I and II sublattices as we go from domain I

to II. Therefore we see that the entire system can be regarded as a

layer structure perpendicular to the boundary consisting of P layers

mostly of A atoms and Q layers composed of mixed A and B atoms.

We call lattice planes parallel to the boundary as "parallel" planes,

for short; they are numbered . . ., n, n+1, . . ., as in Fig. 2.

In formulating the free energy including the boundary layer using

the cluster variation method (CVM), we take a tetrahedron like the I-II-III-IV

connected in Fig. 2 as the basic cluster. Each tetrahedron is made of

two points on one parallel plane (like I and III on the nth plane) and of two points on an adjacent parallel plane (like II and IV on the $(n+1)^{th}$ plane). Also we note that one of the two points (like III) on one parallel plane lies on a P layer and the other point (like I) lies on a Q layer.

In a binary system an A atom and a B atom are called the 1st and the 2nd species, respectively, for mathematical convenience. We let i_{Pn} denote the ith species, (i=1 or 2) on a P layer point on the nth plane. Suppose the III, I, IV and II points connected as a tetrahedron in Fig. 2 are occupied by the ith, j^{th}, k^{th} and l^{th} species, respectively. Then using our notation we can say that this connected tetrahedron has the configuration $i_{Pn} j_{Qn} k_{P(n+1)} l_{Q(n+1)}$. We now introduce the basic variable zn (i,j,k,ℓ) of the theory; this variable designates the probability that the configuration (i,j,k,ℓ) appears in the connected tetrahedron of Fig. 2.

For the pair variable there are five kinds as defined in Table 1. Note that the order of arguments has significance. Table 2 defines the probability variables for a lattice point.

There are geometrical relations among the variables:

$$y_n(i,j) = \sum_{k,\ell} z_n(i,j,k,\ell)$$

$$v_{PPn}(i,k) = \sum_{j,\ell} z_n(i,j,k,\ell)$$

$$v_{PQn}(i,\ell) = \sum_{j,k} z_n(i,j,k,\ell)$$

$$v_{QPn}(j,k) = \sum_{i,\ell} z_n(i,j,k,\ell)$$

(1)

$$v_{QQn}(j,\ell) = \sum_{i,k} z_n(i,j,k,\ell)$$

$$x_n(i) = \sum_{j,k,\ell} z_n(i,j,k,\ell) \tag{2}$$

$$u_n(j) = \sum_{i,k,\ell} z_n(i,j,k,\ell)$$

Also we have continuity constraints

$$y_n(i,j) = \sum_{k,\ell} z_n(i,j,k,\ell) = \sum_{k,\ell} z_{n-1}(k,\ell,i,j) \tag{3}$$

and the normalization of z is

$$1 = \sum_{i,j,k,\ell} z_n(i,j,k,\ell) \tag{4}$$

We have thus defined the variables. Now we go on to write the free energy of the system. The number of lattice points in a plane parallel to the boundary is written as N. Then the number of tetrahedra connecting the nth and the $(n+1)^{th}$ planes is 2N. The total energy of the system is then written as

$$E = 2N \sum_n \sum_{i,j,k,\ell} \epsilon(i,j,k,\ell)\, z_n(i,j,k,\ell) \tag{5}$$

where $\epsilon(i,j,k,\ell)$ is the energy per tetrahedron and is written as

$$\epsilon(1,1,1,1) = 0.0$$
$$\epsilon(1,1,1,2) = 1.5\, w(1+\hat{\alpha})$$
$$\epsilon(1,1,2,2) = 2.0\, w \tag{6}$$
$$\epsilon(1,2,2,2) = 1.5\, w(1+\hat{\beta})$$
$$\epsilon(2,2,2,2) = 0.0$$

In these expressions, which are the same as Eq. (4.2) in Kikuchi-de Fontaine's paper [22], the order of arguments in ϵ is immaterial. The parameter w is for an interaction of an A-B pair, and its magnitude is related to the

temperature scale. The two dimentionless parameters $\hat{\alpha}$ and $\hat{\beta}$ represent the four-body interactions and make the phase diagram asymmetric. The values chosen for the best fit [29] for the observed Cu-Au diagram are

$$w/k = -663°K$$

$$\hat{\alpha} = 0.01 \tag{7}$$

$$\hat{\beta} = -0.08$$

which lie well within the range of values that give the proper ground state as was shown in the preceding paper. The k is the Boltzmann constant.

The entropy expression is taken from, for example, Eq. (3.5) of the Natural Iteration Method (NIM) paper [30] as

$$S = kN \sum_n \{[\sum_{i,j} \mathcal{L}(y_n(i,j)) + \sum_{i,k} \mathcal{L}(v_{PPn}(i,k)) + \sum_{i,\ell} \mathcal{L}(v_{PQn}(i,\ell)) +$$

$$\sum_{i,k} \mathcal{L}(v_{QPn}(j,k)) + \sum_{j,\ell} \mathcal{L}(v_{QQn}(j,\ell)) \div \sum_{k,\ell} \mathcal{L}(y_{n+1}(k,\ell))]$$

$$\tag{8}$$

$$- 2 \sum_{i,j,k,\ell} \mathcal{L}(z_n(i,j,k,\ell)) - 1 - \frac{5}{4} [\sum_i \mathcal{L}(x_n(i)) + \sum_j \mathcal{L}(u_n(j)) +$$

$$\sum_k \mathcal{L}(x_{n+1}(k)) + \sum_\ell \mathcal{L}(u_{n+1}(\ell))]\}$$

where the $\mathcal{L}$ operator is defined as

$$\mathcal{L}(x) \equiv x\ln x - x \tag{9}$$

In treating a system of our present interest we formulate the grand potential $\hat{G}$ defined by

$$\hat{G} = E - TS - \sum_{i=1}^{2} \mu_i \hat{N}_i \tag{10}$$

where μ_i is the chemical potential of the ith species and $\hat{N}_i$ is the total number of the ith species in the entire system including the boundary region. We can also write the last term of (10) as

$$-\sum_{i=1}^{2} \mu_i N_i = -(N/4) \sum_{n} \sum_{i,j,k,\ell} (\mu_i + \mu_j + \mu_k + \mu_\ell) z_n(i,j,k,\ell) \qquad (11)$$

Since we have only two substitutional species in the system and we have no vacancies, we can choose without loss of generality

$$-\mu_1 = \mu_2 \equiv \mu \qquad (12)$$

where μ is twice the diffusion potential defined by Larché and Cahn [31].

In calculating the equilibrium state, we fix T and μ, and find the minimum of $\hat{G}$ [30]. The minimization of $\hat{G}$ leads to the following set of equations:

$$z_n(i,j,k,\ell) = z_n^{(0)}(i,j,k,\ell) \exp\left[\frac{\beta}{2}\lambda_n + \alpha_n(i,j) - \alpha_{n+1}(k,\ell)\right] \qquad (13a)$$

where

$$z_n^{(0)}(i,j,k,\ell) = \exp\left[-\beta\epsilon(i,j,k,\ell) + \frac{1}{8}\beta(\mu_i + \mu_j + \mu_k + \mu_\ell)\right] \times$$
$$[y_n(i,j)v_{PPn}(i,k)v_{PQn}(i,\ell)v_{QPn}(j,k)v_{QQn}(j,\ell)y_{n+1}(k,\ell)]^{1/2} \times [x_n(i)$$
$$u_n(j)x_{n+1}(k)u_{n+1}(\ell)]^{-5/8} \qquad (13b)$$

In (13a), the quantity λ_n is the Lagrange multiplier for the normalization in (4) and has the meaning, after the iteration has converged, that the grand potential $\hat{G}$ of the system is written as

$$\hat{G} = N \sum_n \lambda_n. \qquad (14)$$

Note that N is the number of lattice points within one parallel plane. The quantities $\alpha_n(i,j)$ and $\alpha_{n+1}(k,\ell)$ in (13a) are the Lagrange multipliers to take care of the continuity constraints in (3). The quantity β in (13) is equal to 1/kT.

The process of solving the set $\{z_n(i,j,k,\ell)\}$ from (13) for the equilibrium state is divided into the major and minor iteration steps. One major iteration starts with the values of $z_n^{(0)}(i,j,k,\ell)$ in (13b). Then the Lagrange multipliers $\{\alpha_n(i,j)\}$ are solved iteratively to satisfy the continuing relations (3). The iterative process of solving

$\{\alpha_n(i,j)\}$ is called the minor iteration. In this process we can choose, without loss of generality,

$$\alpha_n(1,1) = 0 \text{ for every } n \tag{15}$$

because of the normalization on y's:

$$\sum_{i,j} y_n(i,j) = 1 \text{ for every } n \tag{16}$$

The details are similar to those in Eq. (4.14) of the b.c.c. boundary paper [5].

When $\alpha_n(i,j)$'s are thus solved the output of one major iteration step is obtained from (13a). This output $\{z_n(i,j,k,\ell)\}$ is used as the input for the next major iteration step. This iterative solution of z's has been called the Natural Iteration Method (NIM).

As was discussed in length before [22,29,30], the NIM has the advantages (i) that the grand potential $\hat{G}$ always decreases at each iteration step, (ii) hence that it always converges whatever initial values the iteration may start, and (iii) that the formulation avoids subtraction so that all the variables always stay positive however small the value may be.

For the boundary computations, we choose a system made of either 60 or 80 parallel planes. The number N of atoms in one parallel plane drops out when we assume that N is sufficiently large and neglect the end effect. For the initial conditions, we choose the left half of the system to be in domain I and the right half in domain II. With this initial condition, the interaction converges after about a thousand major iterations, sometimes less sometimes more, and the number of minor iterations is less than ten except near the beginning of iterations.

When the iteration has converged, we know the structure of the boundary expressed by the set of the probability variables $\{z_n(i,j,k,\ell)\}$.

The density profile across the boundary, for example, is expressed by the point variables $\{x_n(i)\}$ and $\{u_n(j)\}$ of Table 2. Examples are shown in later sections.

The excess free energy σ is defined [5,10,32] as the excess of the grand potential $\hat{G}$ in the inhomogeneous system containing the boundary over the grand potential $\hat{G}_h$ in the homogeneous phase, and σ is normalized to unit area:

$$\hat{a}\sigma = \hat{G} - \hat{G}_h = N \sum_n (\lambda_n - \lambda_\infty) \tag{17}$$

where λ_∞ is the value of λ_n in the homogeneous system, and $\hat{a}$ is the area per fcc lattice point in the parallel plane.

Derivative Quantities

In a recent paper [32], one of the authors prepared a general formula to estimate derivatives of the IPB free energy. One of the formulas is

$$\left(\frac{\partial\sigma}{\partial T}\right)_P = - \frac{\begin{vmatrix} [S] & [N_1] & [N_2] \\ S' & N_1' & N_2' \\ S'' & N_1'' & N_2'' \end{vmatrix}}{\begin{vmatrix} N_1' & N_2' \\ N_1'' & N_2'' \end{vmatrix}} \equiv -[S/N_1 N_2] \tag{18}$$

In this expression, [S] is the entropy contained in a cylinder which is perpendicular to the boundary and whose cross-sectional area is unity.

This cylinder extends far enough into each phase that it encloses some of each homogeneous phase beyond the influence of the boundary. The quantity $[N_i]$ is the total number of the ith species (i=1 or 2) contained in this cylinder. The quantity S' is the entropy per unit volume of the bulk homogeneous, and N_i' is the number of the ith species in a unit volume of the bulk phase I. The $[S/N_1 N_2]$ is identified with the surface excess entropy [32].

We apply the expression (18) to the (100) IPB, for which the primed phase is the disordered phase and the double-primed phase is the A_3B ordered phase. For this problem, we can simplify (18) using the relation

$$N_1' + N_2' = 1 \tag{19}$$

and the corresponding equation for N_i''.

Since the formulation in the present paper is based on the lattice structure, we can write [S] and [N_i] as sums over parallel planes n. By using the relations in (19), we can reformulate the general expression (18) as

$$\frac{a^2}{2} \left(\frac{\partial \sigma}{\partial T}\right) = - \sum_n [S]_n \tag{20}$$

where

$$[S]_n \equiv -(N_2' - N_2'')^{-1} [N_2' S'' - N_2'' S' + N_{2,n}(S' - S'')] + S_n \tag{21}$$

In this expression S_n and $N_{2,n}$ are the entropy and the number of B atoms (i.e., the atom of the 2nd species) per lattice point on the nth parallel plane. Quantities S', S'', N_2', and N_2'' are per lattice point of the homogeneous phases.

A modification of this formulation can be used for APB's [32], but because the two homogeneous domains have identical thermodynamic properties there is little difficulty defining invariant surface excess quantities [10].

Ground State for IPB's and APB's

As in the previous work on β-brass APB's [8], it is instructive to examine low temperature variation of boundary properties with the orientation and compositional or chemical potential. To this we examine the ground state and ground state degeneracy in this model of a system containing APB's and IPB's of various orientation. While no real system could reach equilibrium at low temperatures, the calculated low temperature equilibria display a clue to the understanding of trends that begin at higher temperatures.

We use the methods and notation of the preceding paper [33]. For the case considered here, $w<0$, $\hat{\alpha}$ and $\hat{\beta}$ small we have for nonstoichiometric alloys:

$$E-4xE_1 = -2(1+3\hat{\alpha})wZ_2 - (2+3\hat{\alpha}-\hat{\beta})wZ_3 - 12(1+\hat{\alpha})wZ_4 \qquad \text{when } 0<x<\tfrac{1}{4} \qquad (21)$$

$$E-(2-4x)E_1 - (4x-1)E_2 = -2(1+3\hat{\alpha})wZ_0 - (2-3\hat{\alpha}-3\hat{\beta})wZ_3 - 6(1-\hat{\alpha})wZ_4 \quad \text{when } \tfrac{1}{4}<x<\tfrac{1}{2}$$

where x is the mole fraction of B atoms. For the ground state the r.h.s. of these equations is zero, because the atoms can be arranged with $Z_2=Z_3=Z_4=0$ for the first case and with $Z_0=Z_3=Z_4=0$ for the second. If an IPB or APB requires the presence of these higher energency clusters the increase in energy per unit area is the limiting low temperature surface energy for such a boundary.

It is apparent that IPB's between fcc and A_3B and between A_3B and AB can be created without introducing any higher energy clusters. It is readily demonstrated by a construction such as Fig. 1 that (100) and (001) APB can be created entirely from allowed clusters and thus with zero energy. APB's with other orientation can always achieve zero energy by facetting to cube orientations. Therefore ground state APB energies at T=0 for nonstoichiometric crystal are zero for all orientations.

Stoichiometric A_3B alloys can contain only A_3B clusters. The formation of (001) APB requires no energy because it requires no other clusters, but for all other orientations other clusters are required. It is convenient to formulate the stoichiometric case in terms of chemical potentials.

The result for the (100) APB is sketched in Fig. 4 as a three-dimensional stereographic drawing of the (σ,μ,x) relation together with its three projections. The lines in Fig. 4 are

$$\frac{\sigma_a{}^2}{|w|} = \begin{cases} -2(1-3\hat{\alpha}) - \mu/|w| & \text{when } -4 < \mu/|w| < -2(1-3\hat{\alpha}) \\ \mu/|w|- 6(1+\hat{\alpha}) & \text{when } -6(1+\hat{\alpha}) \le \mu/|\bar{w}| \le -4 \end{cases} \qquad (22)$$

and a is the length of the cube edge as shown in Fig. 2. These relations are derived by counting bonds of the APB between two perfectly ordered domains; we skip the details of derivations and present only their interpretations. The (μ,x) projection shows a step function in accordance with Fig. 3 of the preceding paper [33], the (σ,x) projection consequently shows σ as a δ-function of the composition at the stoichiometry. The (σ,μ) projection reflects that the adsorption by this APB is ±1 B atom per sectional area a^2, since $(\partial\sigma/\partial\mu)_T$ is proportional to the excess B atoms adsorbed on the APB. On the $\mu\leq-4|w|$ side, the boundary is composed of a layer of A_4 tetrahedra, and on the $-4|w|\leq\mu$ side there are A_2B_2 tetrahedra. At $\mu=-4|w|$, σ is a maximum and either A_4 or A_2B_2 tetrahedral clusters give the same σ. The constant adsorption on the two legs of the (σ,μ) projection are thus consistent with the Gibbs adsorption equation. The two values of μ at the bottom of the legs are resp. the values at T=0 for the disorder - A_3B phase coexistence and for the $A_3B-A_2B_2$ phase coexistence. The σ converges to the point (T=0, x=1/4) non-uniformly as is seen in Fig. 5, and the nature of the non-uniformity is that the converged values are different depending on μ as is illustrated near T=0 in Fig. 6, as well as in Fig. 4.

The energy of APB's of other orientation in a stoichiometric alloy is a strong function of orientation. A polar plot of σ vs. orientation can be described [8] as a rasberry figure composed of the outer envelope of four spheres with diameters equal to σ (100) and centers at $(\frac{\pm1}{2}\sigma$ (100), 0, 0) and $(0, \frac{\pm1}{2}\sigma$ (100), 0)

IV. Results

The results of the calculations yield the profiles and thermodynamic properties of IPB's and APB's as a function of orientation $\hat{n}$ in the temperature-composition (or temperature-chemical potential) region where these interfaces could exist. APB's could exist over the closed region on the phase diagram where the A_3B phase is stable as shown in Fig. 5; IPB's can exist only at that portion of the boundary of this region where both ordered and disordered phases are stable and can coexist. The properties of APB's are determined by three variables $(\hat{n}, T, x)$ or $(\hat{n}, T, \mu)$ since $\mu = \mu(T, x)$. Along the two-phase coexistence curve μ and the x's of the two phases are functions of T as shown in Fig. 5 of the preceding paper; therefore IPB properties are determined by two variables; $\hat{n}$ and either μ, T, or the x's of either phase.

IPB

Figures 7 and 8 show σ for (100) and (110) IPB as a function of T and of μ, respectively. It is to be noted that there is only slight anisotropy with (110) surfaces having slightly higher σ. The anisotropy falls well below the range that would result in facetting. The equilibrium shape of an ordered domain within a disordered matrix would be a "sphere" slightly flattened (by about 10%) along the (100) directions. This is consistent with transmission electron microscope observations that small coherent ordered Cu_3Au and Ni_3Al in disordered matrixes are close to spherical [34-36]. As the particles grow they tend increasingly towards rounded cubes. Several factors in addition to surface free energy, particularly coherency strain are important in determining particle shape, but surface free energy is dominant for small particles [4]. It is also to be noted that neither a minimum nor a maximum in σ occurs at the congruent (i.e. maximum)

temperature of the phase diagram. Indeed because the denominator of the r.h.s. of equation (18) is zero at this maximum temperature, $d\sigma/dT$ is infinite unless the numerator is also zero at such a point. Unless there are special conditions the numerator will not be zero and such an infinite slope at the congruent point is a general result.

The value of σ for an IPB is important in the nucleation of the ordered phase. One prediction is that the Cu_3Au alloys enriched in Au will nucleate the ordered phase more easily, i.e., at less undercooling than alloys enriched in Cu.

Consistent with our model which has no interactions between neighbors other than the first, σ tends to 0 at 0 °K. In a real system low temperature σ values must depend on other interactions.

Thermodynamic self-consistency within the model is demonstrated by Figure 9 in which σ for (100) IPB is given at several values of T together with a slope given by minus the surface excess entropy $[S/N_1N_2]$ obtained at that temperature from the same IPB profile used to calculate σ in Fig. 6. This demonstration that equation (18) holds is a very sensitive test of self-consistency [10,37].

APB

Because of the non-uniform convergence of μ at the point $(T,x) = (0, 1/4)$, we give in Fig. 6 σ vs T for (100) boundaries both at constant x and at constant μ. At $x = 1/4$ and $T = 0$, μ can range within the limits given in equation (22). All the constant μ curves converge to $x = 1/4$ at 0 °K and to finite values of σ, while all the $x \neq 1/4$ curves lead to $\sigma = 0$ at 0 °K. It is to be noted that the curves for a constant nonstoichiometric x show a maximum in σ.

For the nonstoichiometric constant x curves, the major term in the low temperature dependence of σ comes from the adsorption. Because the

reversible creation of APB removes excess species from the nonstoichiometric ordered phase where they have high partial molar entropy and concentrates them along the boundary with low entropy, the net entropy change for the system is negative when APB area is reversibly increased. As in the case for bcc APB's [10] the maximum in σ occurs in the temperature range of desorption. Consistency with the Gibbs adsorption equation is demonstrated in Fig. 10, to be compared with Fig. 6.

The anisotropy of APB is pronounced. In this model the (001) APB has $\sigma = 0$ at all temperatures. The (100) and (110) results are compared in Fig. 6. The ratio of σ_{110} to σ_{100}, and therefore σ_{110} does not facet into σ_{100} and σ_{010}. Our calculation for (101) led to a value of σ which at all temperatures exceeded $\sqrt{1/2}\ \sigma_{100}$. The (101) APB could always reduce their energy by facetting to (001) and (100). Although we have not computed other orientations we would expect the anisotropy to be such that all (h,k,ℓ) orientation would facet to $(h,k,0)$ and (001), while $(h,k,0)$ would be stable.

The domain structures observed for Cu$_3$Au show both facets and rounded APB's that are mostly near cube planes [37]. We expect that the sharp edges connect a (100) with a (001), while the rounded portions lie along $(h,k,0)$, connecting (100) with (010) segments. The (111) APB energies have been determined experimentally at 350°C in a stoichiometric alloy to be 25 mJ/m^2. We calculate $\sigma a^2/|w|=0.4$ for this temperature for $(h,k,0)$ APB's, which is given 23 mJ/m^2. Because of the strong anisotropy we calculate 18 mJ/m^2 for (111) orientations.

Perfect Wetting and Phase Changes in APB's

Our computed values of $\sigma a^2/|w|$ at the congruent point are 0.1469 and 0.1541 for the (100) and (110) APB's respectively and 0.0722 and 0.0767 for the (100) and (110) IPB's respectively. Taking into consideration of the special limitation in the capability of the computer in calculating the

APB congruent point, we conclude that the computer results indicate for (h,k,0) orientations at the congruent point

$$\sigma_{APB} = 2\sigma_{IPB} \tag{23}$$

Thus the (100) APB could either consist of two (100) IPB's with a disordered layer in between or it coincidentally has the same free energy. Figures 11a and 11b show the calculated profiles of the APB and the IPB, and confirm that the disordered layer is part of the APB and that indeed the APB has become two IPB's. There is no reason why the thickness of the equilibrium disordered layer exactly at the congruent point T_c should not be infinite; the finite thickness shown in Fig. 11a is the result of the computer calculation which is difficult to attain perfectly converged solution in the finite computer space allocated for the APB at T_c.

We determined σ for (100) and (110) IPB's from $kT/|w| = 0.50$ on the low Au side of the congruent point to the eutectoid temperature on the high Au side (Fig. 5) and compared this with the limiting values at the two-phase boundary of the corresponding APB's. Equation (23) held everywhere.

The implication of this result is that in two-phase alloys the disordered phase will coat all (h,k,0) APB's near T_c. Since at equilibrium all other orientations will facet into (h,k,0) and (001) APB's there will be only (001) APB's within equilibrated particles of the ordered phase. By analogy to the corresponding phenomenon in fluids, this is called perfect wetting of the (h,k,0) APB's by the disordered phase. Perfect wetting has been shown theoretically to occur near all tricritical points [39] and it has been found that in the Fe-Al system the disordered phase coats all Fe-Al APB's [40,41]. The general proof which applies near tricritical points is not applicable to the A_3B APB's and we do not know whether the finding of perfect wetting is a general result.

Figure 11 shows the internal structure of (100) APB and IPB at the congruent point. Within each there is a thick layer in which each plane parallel to

the boundary is disordered (a pair of sublattices have equal occupations) but adjacent planes are modulated in occupation by B. This layer has the CuAu (Ll_0) structure in which the CuAu order parameter gradual changes sign with distance perpendicular to the boundary. At the center of the APB the order parameter is zero, all four sublattices having equal occupation. The notation of Shockley [19] lists structures of phases by the number of sublattices having identical occupation; (4) is disordered fcc, (3,1) is Cu_3Au, (2,2) is CuAu. Using this notation we find that at the congruent point, the layers of the (001) IPB in Fig. 11b change from (3,1) on the far right to (2,1,1) to (2,2) to on the far left (4) while the (100) APB consists of two such IPB's.

As we lower the temperature at constant composition or chemical potential the APB's diminish. The (100) APB profile is shown for two temperatures in Fig. 12a and b. From the congruent temperature down to $KT/|w| = 0.90$ the profile narrows but the sequence of the layers remains the same. At $KT/|w| = 0.87$ the APB has lost the (2,2) and (4) layers and contains (2,1,1) and (1,1,1.1) layers instead. Below this temperature, there is further narrowing, but this structure is retained to quite low temperatures.

In order to ascertain whether or not there is a surface phase transition between these two temperatures we give in Fig. 13 the values of the adsorption and the excess in entropy for the (100) APB as a function of temperature. There is a break in the slopes of these two curves at $KT/|w| = 0.882$. Such a break in the curves indicates that there is a discontinuity in the second derivative of σ and that we have computed a second order transition for the (100) APB with classical exponents.

Another way of describing the transition is in terms of the thickness of the (2,2) layer in the central region of the APB. In Fig. 12a it is two atom planes thick and is really a disordered (4) layer. It becomes

six planes thick when $KT/|w|$ is 0.99 and continues to increase to what should be infinite thickness at the consolute temperatures. The increases in thickness are monitored in Fig. 14 which shows two curves for the difference in occupation of two sublattices on a single atom plane for n=28 and n=30 (when the center of the APB occurs between n=30 and n=31). When the difference in occupation drops to zero that plane has joined the (2,2) layer. The n=30 curve shows the disappearance of the last remnant of the (2,2) layer at $KT/|w|$ = 0.882. The n=28 curve shows what appears to be an abrupt thickening near $KT/|w|$ = 0.99. There is a possibility that there are a number of phase transitions associated with the thickening of the (2,2) layer. It was not possible to improve the precision of Fig. 13 sufficiently to ascertain whether there were discontinuities in derivatives of σ corresponding to the thickening of the (2,2) layer. The question of these additional surface phase transition at the higher temperatures requires further study.

Symmetry requires that the order parameter at the center of an APB in the bcc with CsCl order go to zero. No such symmetry requirement exists for APB's in fcc with Ll_2 order, and APB's below the 0.882 transition were ordered at their center. Above the .882 transition the central two planes are disordered consistent with the symmetry of an APB within a (2,2) structure.

The structure of the (110) IPB at the congruent point is shown in Fig. 15. The (110) APB is not shown but it very closely resembles two IPB's. If there were a (2,2) layer in this boundary it would not be apparent in Fig. 15 which averages compositions on (110) planes that cut at 45° to the layering in the CuAu structure. We did not investigate whether or not a phase transition occurs in (110) APB's.

Discussion

Because statistical mechanical calculations of fcc phase diagrams
have only recently become possible, this is the first calculation of
equilibrium properties of interfaces within and between phases based
on fcc. The first-order character of the phase transitions implies that
none of the higher-order critical point behavior could be expected for
these interfaces at the disordering transitions. Indeed the surface free
energies remain finite at the first-order transition point. Nonetheless
several interesting phenomena were uncovered. The (100) APB's undergo
second order surface transitions in which the internal structure of the
boundary changes, and at the disordering temperature the $(h,k,0)$ APB's
contain a thick disordered layer. Indeed the APB has become two IPB's
at the congruent temperature T_c, and near there the APB is perfectly wet
by the disordered phase. Modern high resolution microscopy should be able
to resolve these internal structures.

The large anisotropy in IPB energy expected from the cubically
distorted sphere of large coherent particles was not calculated. Indeed
the observation that small particles are more spherical is consistent with
these calculations and with the expectation that surface energy is the
dominant determiner of shape in small particle, while other factors such
as elastic anisotropy become important for large particles. APB's were
shown in Section II to have tetragonal symmetry and to be surprisingly close
to isotropic in the zone of (001). Because of our neglect of second neighbor
interaction, (001) APB's have zero energy. This leads to a very high
anisotropy for all other orientations and a prediction that all (h,k,ℓ) APB's
would facet into $(h,k,0)$ and (001). Observations on APB's indicate both
runded and facetted portions, and such domain structures should be reexamined
to establish the nature of the difference.

We next turn to applicability of our results to real systems. This hinges on two aspects of the calculation, the model which is implicit in the expression of the energy in terms of tetrahedral clusters in equation (5) and the tetrahedron approximationn of the C.V.M. It is important to distinguish what we assume in the model for the energy, which is couched in energies assigned to clusters, with the statistical problems of the basic clusters in the C.V.M. In this calculation we used energies of tetrahedra for the model and tetrahedra for the C.V.M. For obvious reasons the cluster in the C.V.M. must contain (be the same or larger than) the cluster in the model, unless one adds a Bragg-Williams approximation [20].

We have already noted that for fcc using clusters smaller than tetrahedra in the C.V.M. gives unrealistic phase diagrams, while using tetrahedral clusters in a near-neighbor pair wise energy model gives a quite realistic diagram in which there are three ordered phases which however have three congruent points δ almost the same temperature. The $\hat{\alpha}$ and $\hat{\beta}$ parameters represent four-atom near-neighbor interaction energies which create differences in congruent point temperatures. The small values used here were chosen to fit the CuAu diagram. They should not affect the qualitative conclusion reached here.

Because the model ignores the contribution of more distant neighbors to the interaction energy it exaggerates the anisotropy of the APB's. Our finding that σ(001) is identically zero is a direct result of a near-neighbor model. Introducing higher neighbor interactions would require an increase in the size of the cluster in the C.V.M. with a large increase in the computational effort.

The accuracy of the C.V.M. is usually tested by having some rigorous results available. For bcc APB's such results existed at T=0 and the critical temperature, and it was possible to show that the pair approximation gave quite adequate results. For fcc the results merge with the rigorous predictions at T=0.

The thermodynamic self consistency checks (Figs. 9 and 10) test neither the validity of the model nor the approximation in the C.V.M. but only checks that the calculations were performed consistently with both. It is surprising how many calculations on surfaces fail this check. It fails e.g. whenever there is an artificial constraint on the thickness of the boundary, which prevents it from equilibrating or whenever the boundary is between phases that are not in equilibrium.

Corresponding to this theoretical check is the experimental use of the Gibbs Adsorption equation as a true test for surface equilibria. An extreme case of a nonequilibrium surface between layers of water and sulfuric acid gives no detectable surface tension. For such miscible phases one would calculate a negative σ much as was done for an earlier theory of IPB's (23).

Some results of our calculation are completely model independent. The large difference in IPB energy on either side of the congruent point and the infinite value of $d\sigma/dT$ there follows directly from the Gibbs adsorption equation. It implies that the hysteresis in order-disorder kinetics due to nucleation will be quite different on the two sides of any congruent point. For the same reason, coarsening kinetics of ordered precipitates driven by reduction in surface area would be quite different on the two sides of the congruent point.

References

1. J. S. Koehler and F. Seitz, Appl. Mech. 14A, 217 (1947).

2. A. H. Cottrell, Seminar on Relation of Properties to Microstructure, ASM, p. 131 (1954).

3. K. C. Russell, Nucleation in Solids, Ch. 6 in Phase Transformations, ASM (1968).

4. J. D. Boyd and R. B. Nicholson, Acta Met. 19, 1379 (1971).

5. R. Kikuchi, J. Chem. Phys. 57, 4633 (1972).

6. N. Brown, Phil Mag. 4, 693 (1959).

7. P. A. Flinn, TAIME 218, 145 (1960).

8. J. W. Cahn and R. Kikuchi, J. Phys. Chem. Solids 20, 94 (1961).

9. R. Kikuchi and J. W. Cahn, J. Phys. Chem. Solids 23, 137 (1962).

10. J. W. Cahn and R. Kikuchi, J. Phys. Chem. Solids 27, 1305 (1966).

11. P. A. Flinn, Strengthening Mech. in Solids, ASM p. 17, (1962).

12. S. M. Copley and B. H. Kear, Trans. Met. Soc., AIME 239, 977, 984 (1967).

13. A. Lauley, J. A. Coll and R. W. Cahn, Transactions AIME 218, 166 (1960).

14. G. W. Ardley and A. H. Cottrell, Proc. Roy. Soc. 219, 328 (1953).

15. G. W. Ardley, Acta Met 3, 525 (1955).

16. N. S. Stoloff and R. G. Davies, AM 12, 473 (1964).

17. A. Gysler and S. Weissmann, Mat. Sci. and Eng. 27, 181 (1977).

18. D. P. Pope, Phil. Mag. 25, 917 (1972).

19. W. Shockley, J. Chem. Phys. 6, 130 (1938).

20. N. S. Golosov, L. Ya Pudan, G. S. Golosova, and L. E. Popov, Soviet Physics - Solid State 14, 1280 (1972).

21. R. Kikuchi and C. M. van Baal, Scripta Met. 8, 425 (1974).

22. R. Kikuchi and D. de Fontaine, Appl. of Phase Diagrams in Metallurgy and Ceramics, NBS Special Publication 496, C. G. Carter, Ed. p. 967 (1978).

23. W. J. Leamy, P. Schwellinger and H. Warlimont, Acta Met. 18, 31 (1970).

24. M. J. Richards and J. W. Cahn, Acta Met. 19, 1263 (1971).

25. L. E. Popov, N. S. Golosov, A. E. Ginsburg, N. V. Kodzemyakin and E. V. Kozlov, Ordered Alloys, B. H. Kear, Ed. et al Claytor Publishing, Baton Rouge (1970).

26. J. W. Cahn and R. Kikuchi, Unpublished research.

27. Intern. Tables of X-Ray Crystallography, Vol. 1, p. 330, 338, Kynock Press, Birminghan (1965).

28. R. C. Pond and W. Bollmann, Proc. Roy. Soc. (To appear) (1978).

29. D. de Fontaine and R. Kikuchi, ibid, p. 999.

30. R. Kikuchi, J. Chem. Phys. 60, 1071 (1974).

31. F. Larché and J. W. Cahn, Acta Met. 28 (1978).

32. J. W. Cahn, Seminar on Segregation in Metals and Alloys, ASM p. 3 (1978).

33. J. W. Cahn and R. Kikuchi, preceding paper.

34. M. J. Marcinkowski and L. Zwell, Acta Met. 11, 373 (1963).

35. E. Hornbogen and M. Roth, Zeitschr. Met. 58, 842 (1967).

36. H. Gleiter, Ordered Alloys, Proc. 3rd Bolton Landing Conference, B. H. Kear, et al, Eds. Claytor Publishing, Baton Rouge, p. 375 (1970).

37. M. J. Marcinkowski, R. M. Fisher and N. Brown, J. Appl. Phys. 31, 1303 (1960).

38. D. G. Morris and R. E. Smallman, Acta Met. 23, 73 (1975).

39. B. Widom, Phys. Rev. Lett. 34, 999 (1975).

40. P. R. Swann, W. R. Duff and R. M. Fisher, Met Trans 3, 409 (1972).

41. S. M. Allen and J. W. Cahn, unpublished research.

TABLE 1 Definition of the Pair Variables

Pair of Species	Probability variables
$i_{pn} - j_{Qn}$	$Y_n(i,j)$
$i_{Pn} - k_{P(n+1)}$	$V_{PPn}(i,k)$
$i_{Pn} - \ell_{Q(n+1)}$	$V_{PQn}(i,\ell)$
$j_{Qn} - k_{P(n+1)}$	$V_{QPn}(j,k)$
$j_{Qn} - \ell_{Q(n+1)}$	$V_{QQn}(j,\ell)$

TABLE 2 Definition of the Point Variables

Configuration of a Point	Probability variables
i_{Pn}	$x_n(i)$
j_{Qn}	$u_n(j)$

Figure Captions

(1) An antiphase domain boundary separates two domains of the same ordered phase. a) (100) projection of two Li_2 phases showing difference between (010) and (001) boundaries, b) (001) projection showing that (100) and (010) boundaries are quite similar. Excess of either species can be accomodated at the boundaries.

(2) The convention for defining the four sublattices I, II, III and IV, the planes (... n, n+1, ...), the layers (P,Q), and the tetrahedra.

(3) The unit cell at the center belong to one domain and the other three belong to another. The three-fold axis has been destroyed and two of the three four-fold axes have been reduced to two-fold axes. Only the (001) axis remains a common four-fold axis for both domains.

(4) The relationships among σ, the ground state energy of (100) APB's, the composition and the chemical potential is represented by a single curve. Its projection gives the relationships among any two of them. Thus, while σ is zero except at stoichiometry it is a continuous function of μ.

(5) The Cu_3Au phase diagram showing curves of constant μ's. Note the non-uniform convergence at n=0.25.

(6) σ of (100) antiphase boundaries as a function of temperature. Curves are either for constant chemical potential μ or constant composition x. A curve for a (110) APB at constant composition is also given.

(7) The reduced free energy σ of the interphase boundary between fcc and the Ll_2 structure as a function of reduced temperature for (100) and (110). The peak in σ does not occur at the peak temperature.

(8) The same free energy as Fig. 7 as a function of reduced chemical potential instead of temperature.

(9) Thermodynamic consistency by plotting for each temperature the calculated value of σ and the slope calculated from equation (18) for the (100) IPB. Compare with Fig. 7.

(10) Consistency with the Gibbs adsorption equation for APB's is demonstrated by giving for each temperature the calculated values of σ and its temperature coefficient. Compare with Fig. 6.

(11) The calculated profiles of the (100) APB and IPB at the congruent point shows that the APB has become two IPB's. The composition of each sublattice is given for each plane parallel to the interface. Note the portion where the two sublattices in each plane are equally occupied (a (2,2) or CuAu layer).

(12) There is a structural change in the core of (100) APB's between $KT/|w| = 0.90$ and 0.87.

(13) The excess entropy and adsorption of a (100) APB as a function of temperature shows that the transition at $KT/|w| = 0.882$ is second order.

(14) The ordering of atoms on the two sublattices of a given (100) atom plane as a function of temperature for one of the central planes (n=30) and the third plane from the center (n=28).
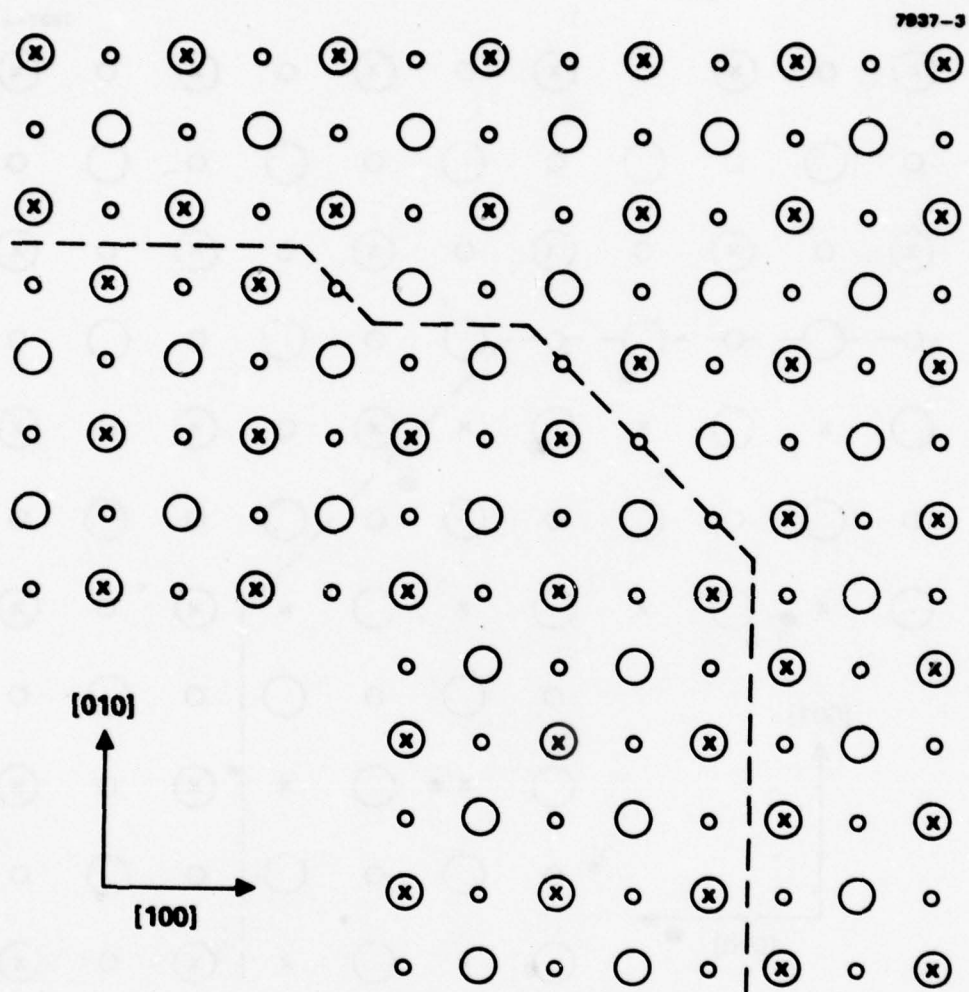
(15) The profile of a (110) IPB at the congruent point, to be compared with
      figure 11b.
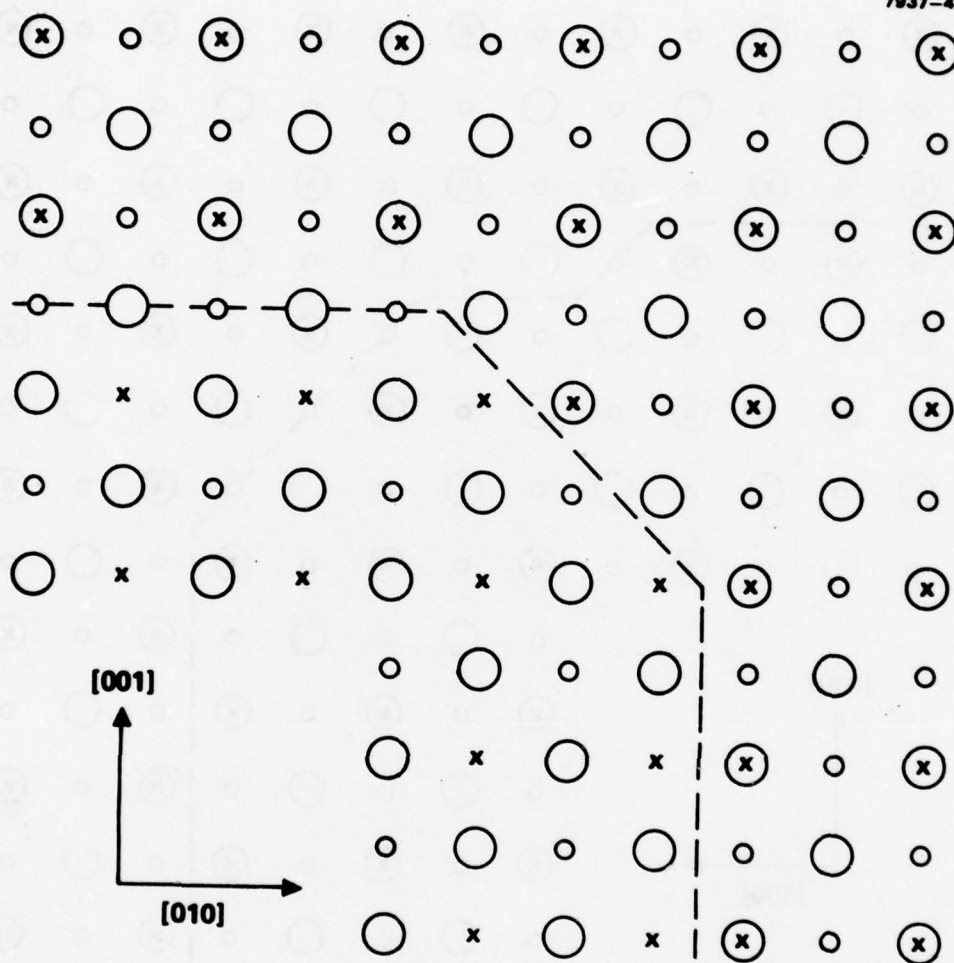
CROSSES INDICATE "B" SUBLATTICE POINTS

Figure 1a.
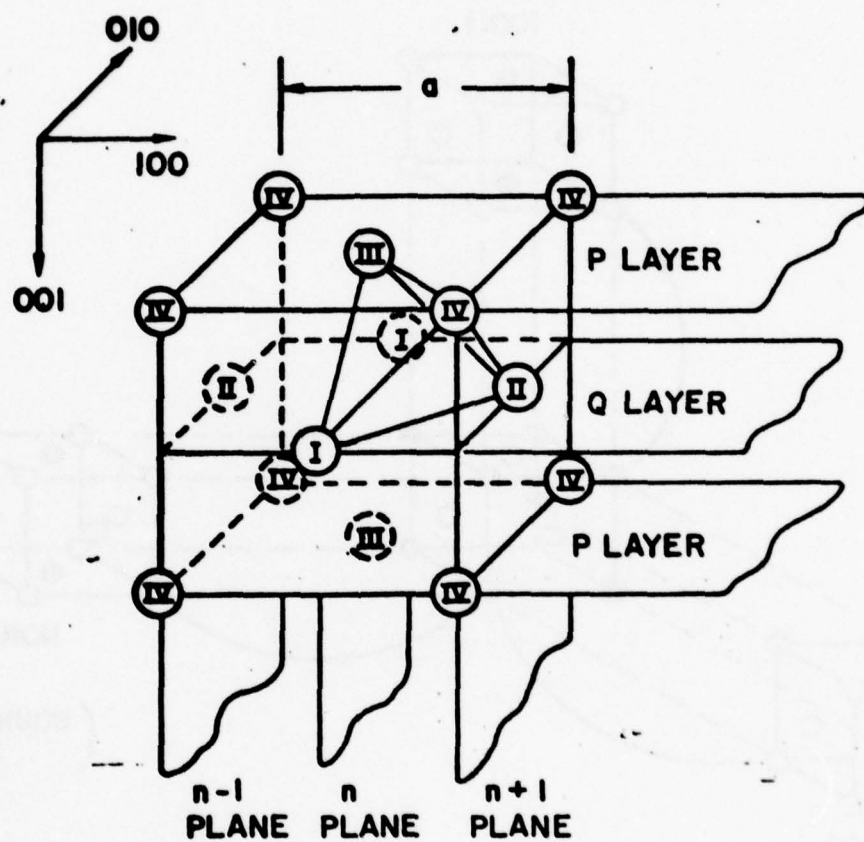
7837-3

CROSSES INDICATE "B" SUBLATTICE POINTS
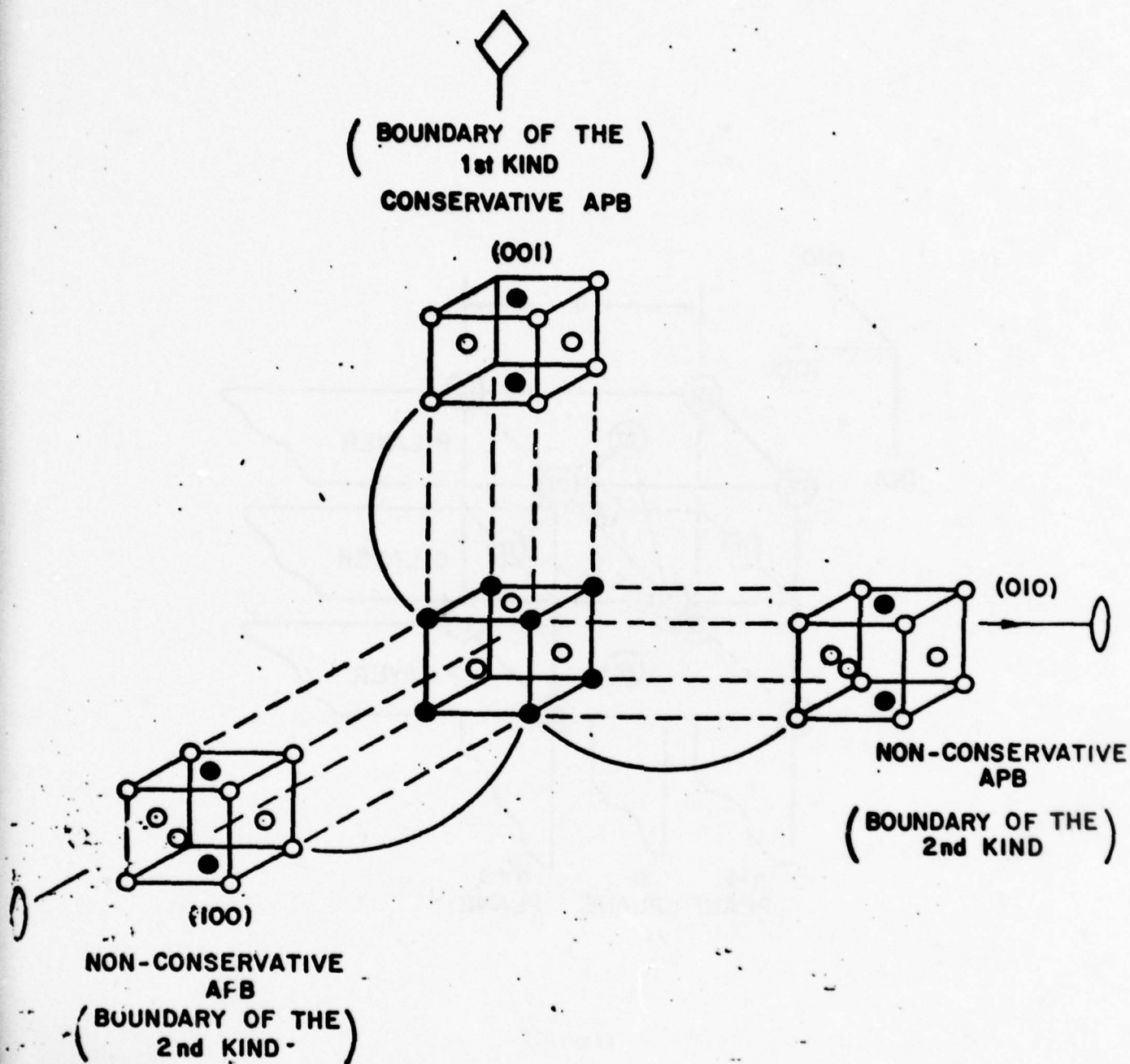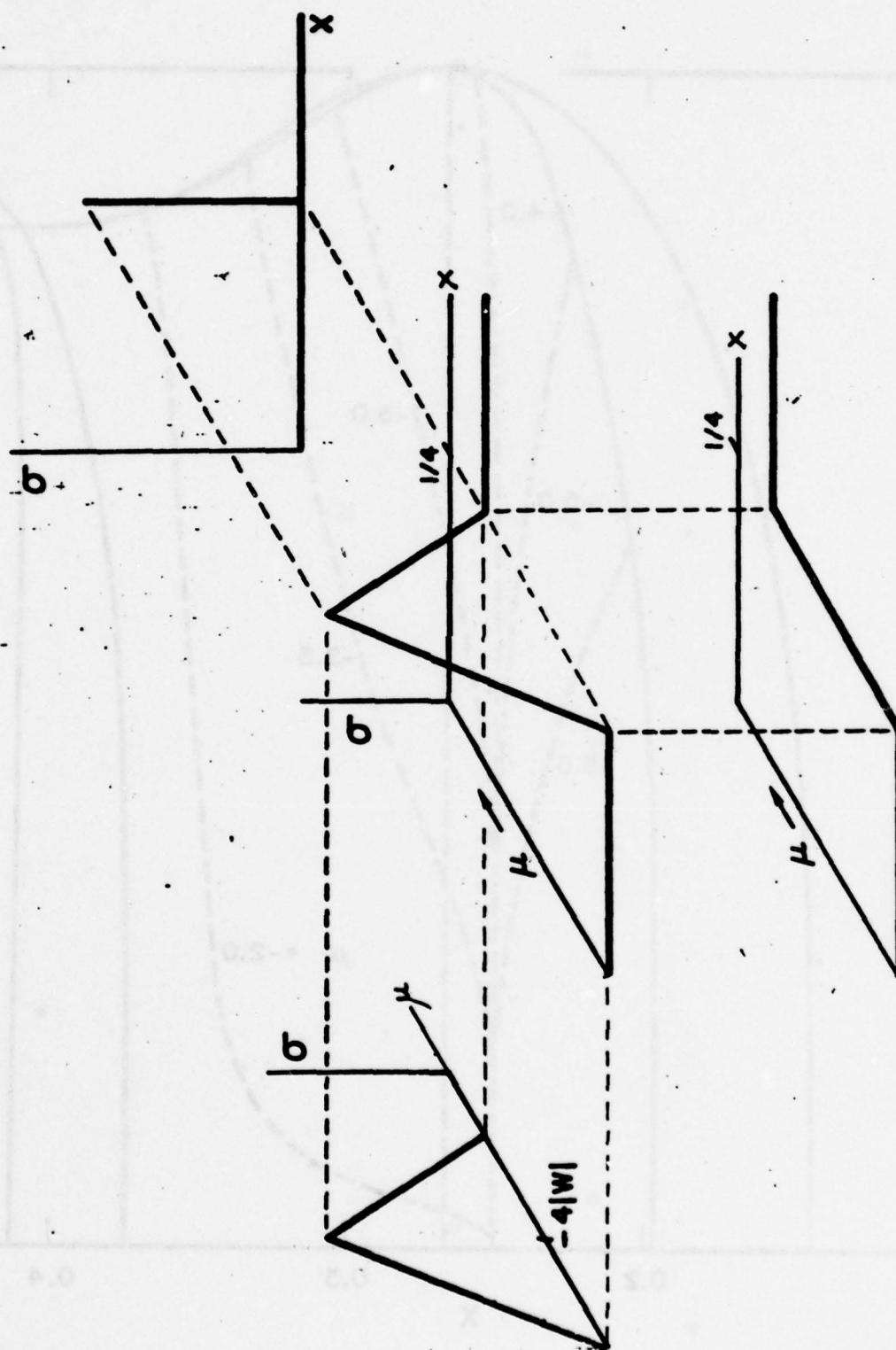
Figure 1b.

Figure 2.

BOUNDARY OF THE
1st KIND
CONSERVATIVE APB

(001)

NON-CONSERVATIVE
APB

BOUNDARY OF THE
2nd KIND

(010)

(100)

NON-CONSERVATIVE
AFB
BOUNDARY OF THE
2nd KIND

Figure 3.

Figure 4.

Figure 5.

APB

$\mu = -4.0$

$\mu = -3.758744$
at the peak of the
phase diagram

$\mu = -4.5$

$\sigma(100)$

$\dfrac{\sigma a^2}{|W|}$

2.0

1.0

APB $\sigma(110)$

$\chi = 0.266597$
$\left(\begin{array}{c}\text{the value}\\ \text{at the peak}\end{array}\right)$

$\sigma(100)$

0

0   0.4   0.8   1.2

$kT/|W|$
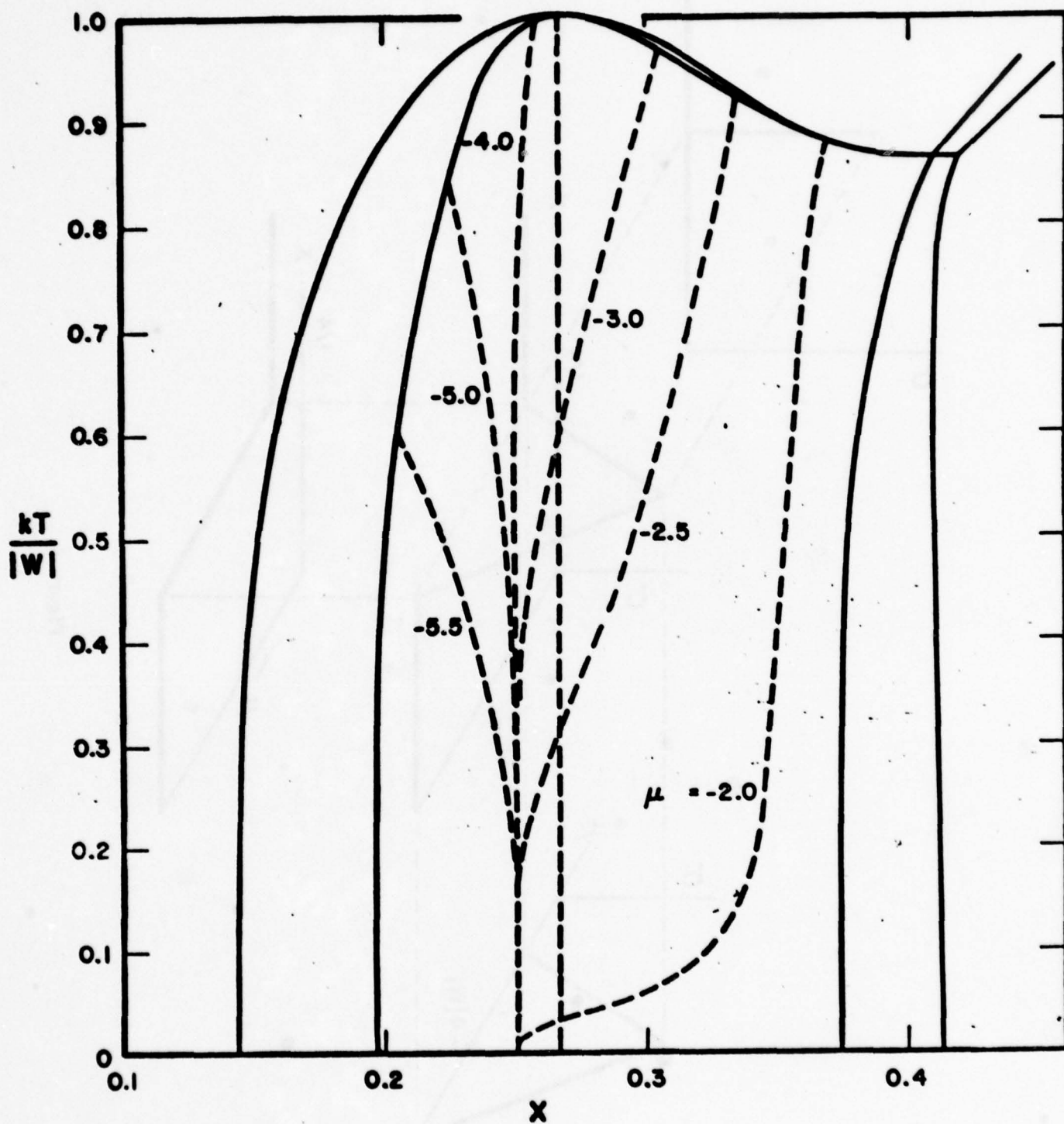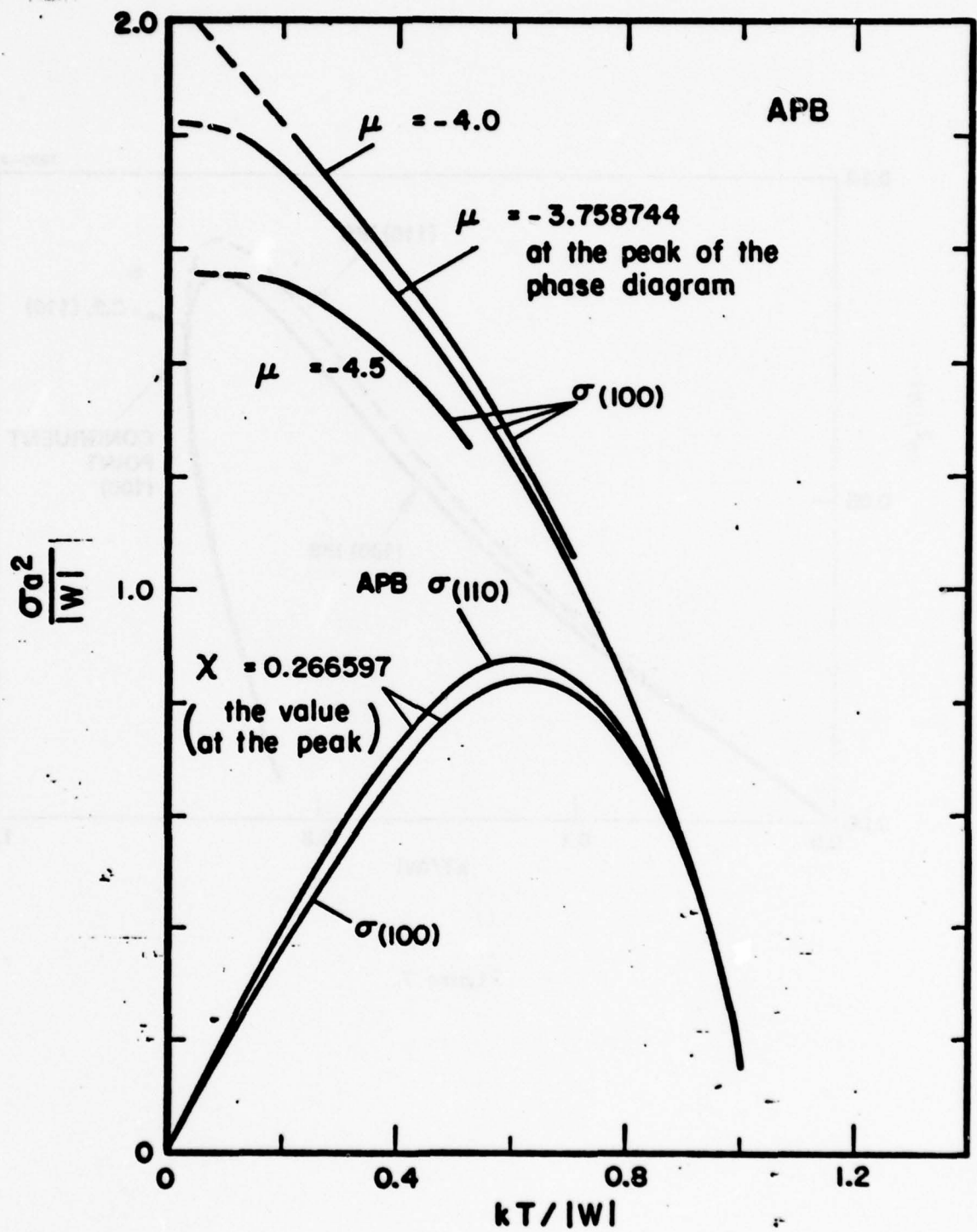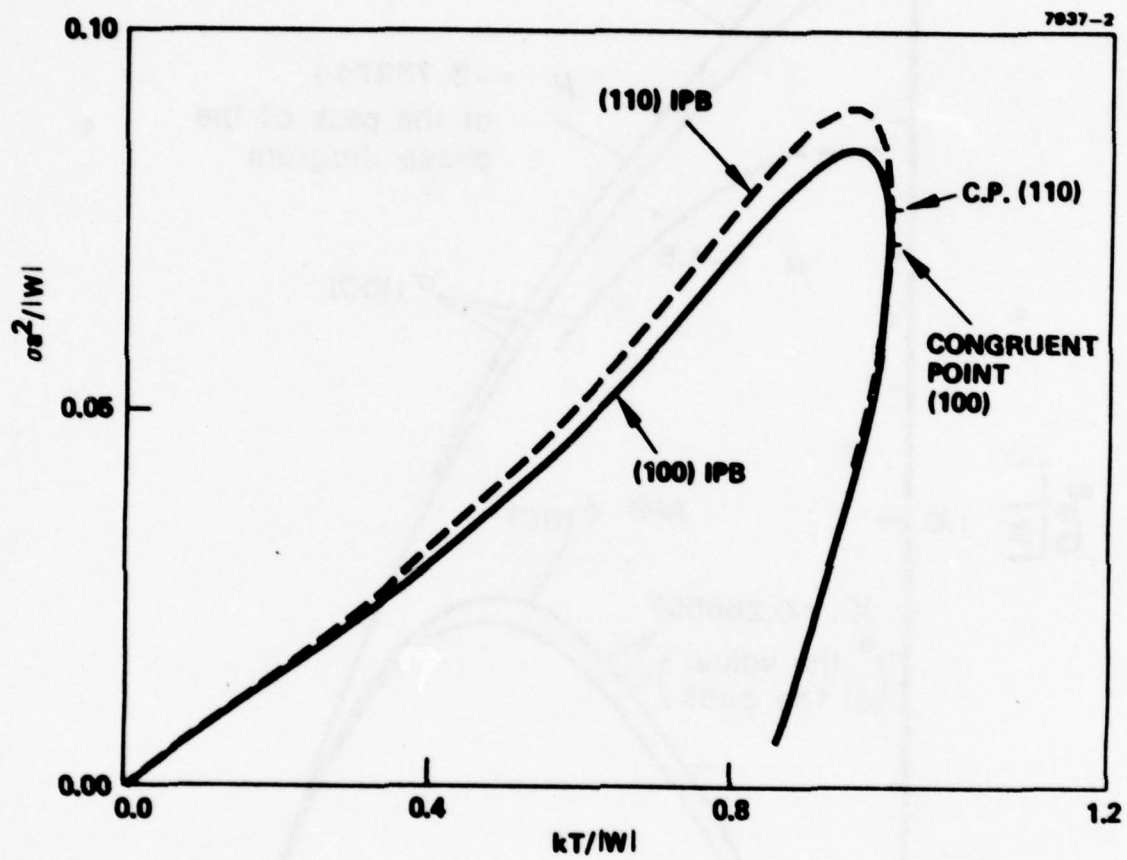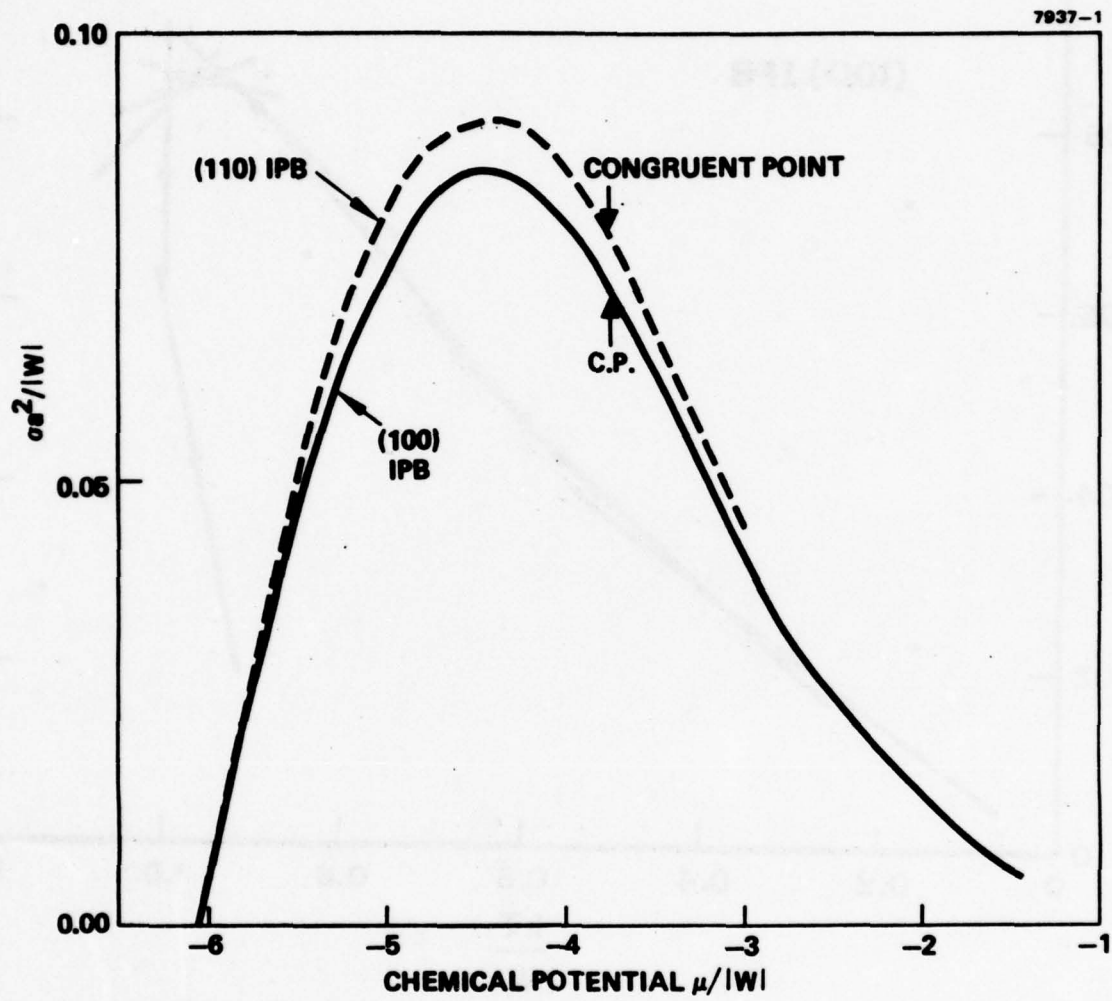
Figure 6.
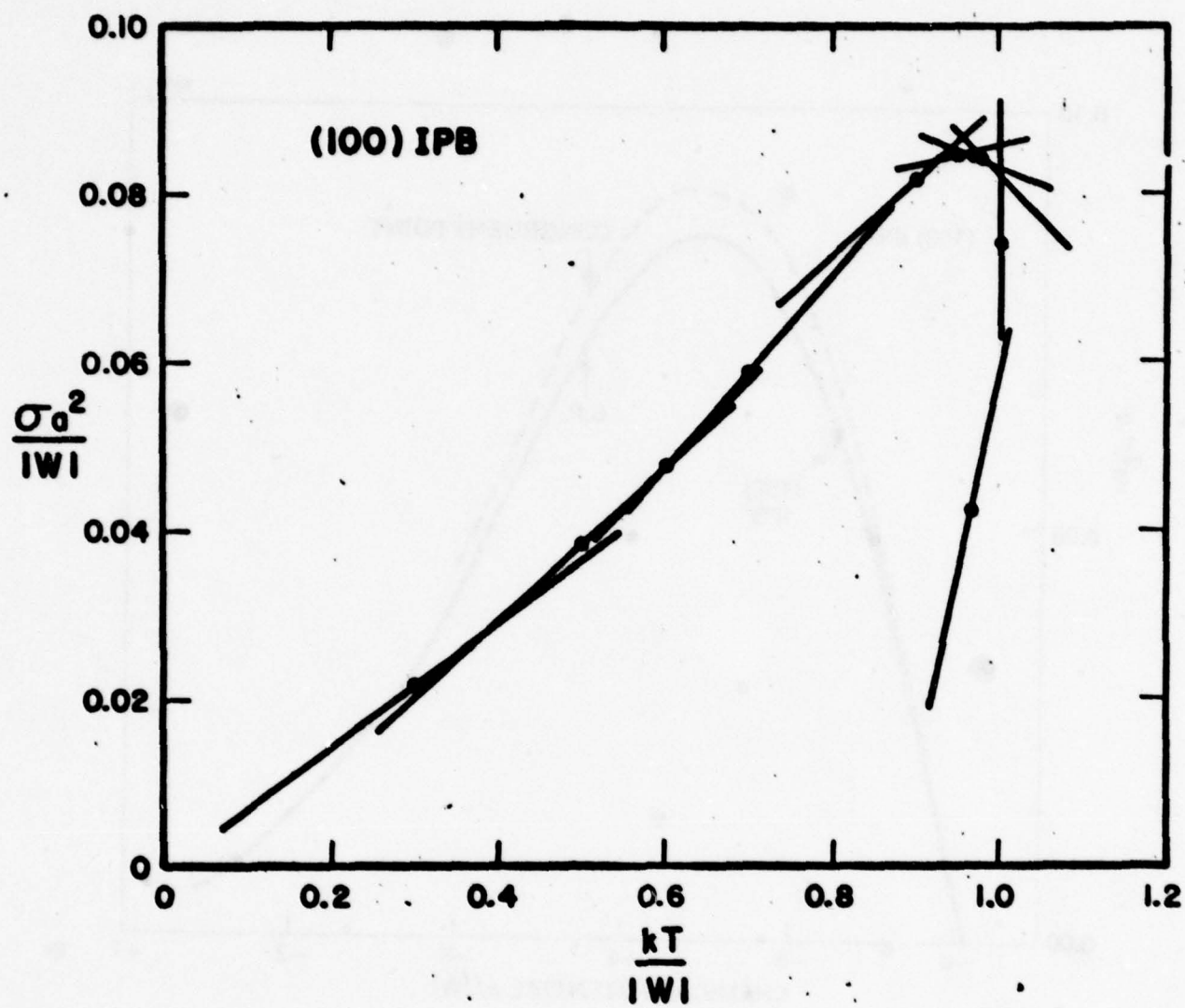
Figure 7.
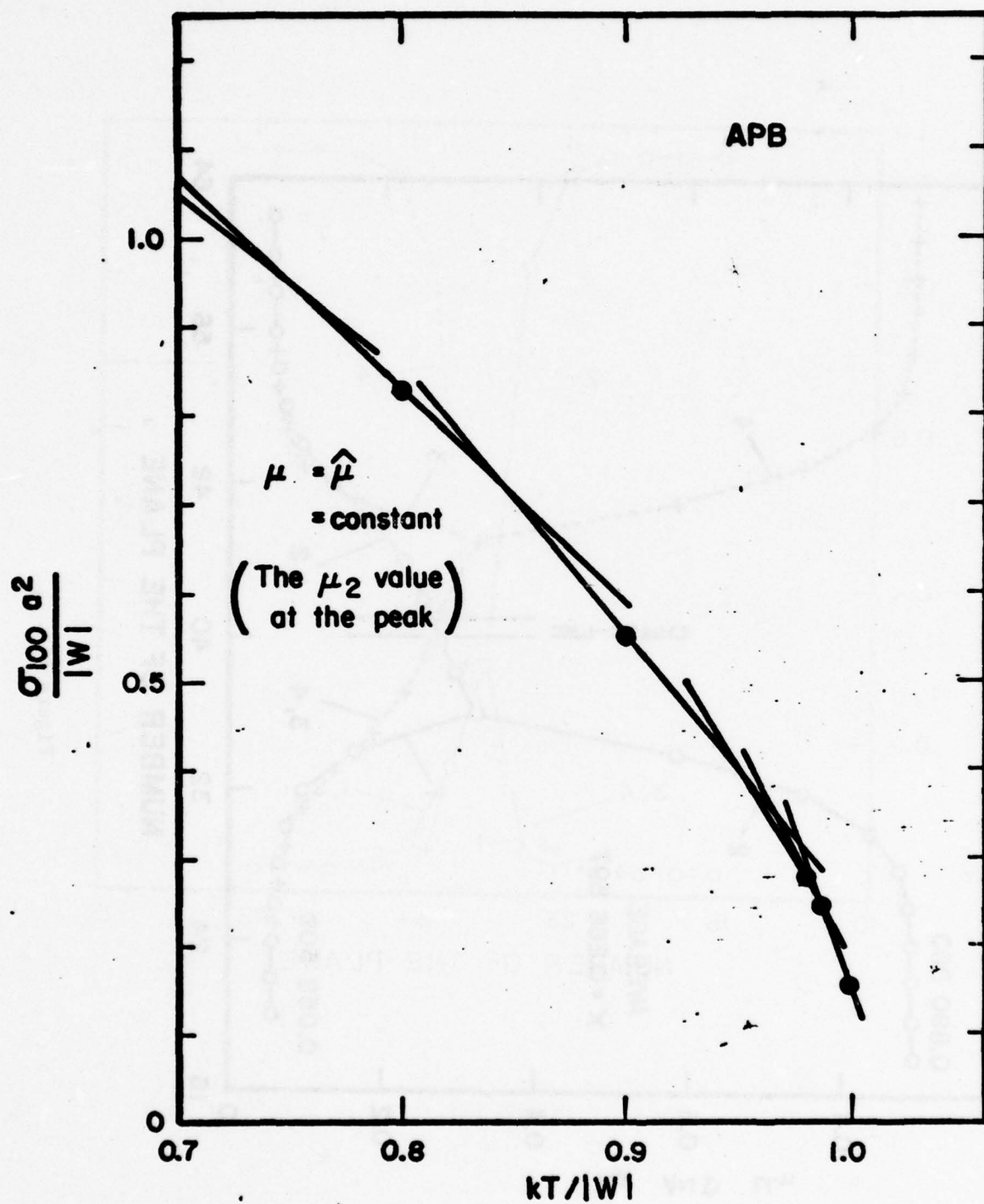
Figure 8.

Figure 9.

Figure 10.
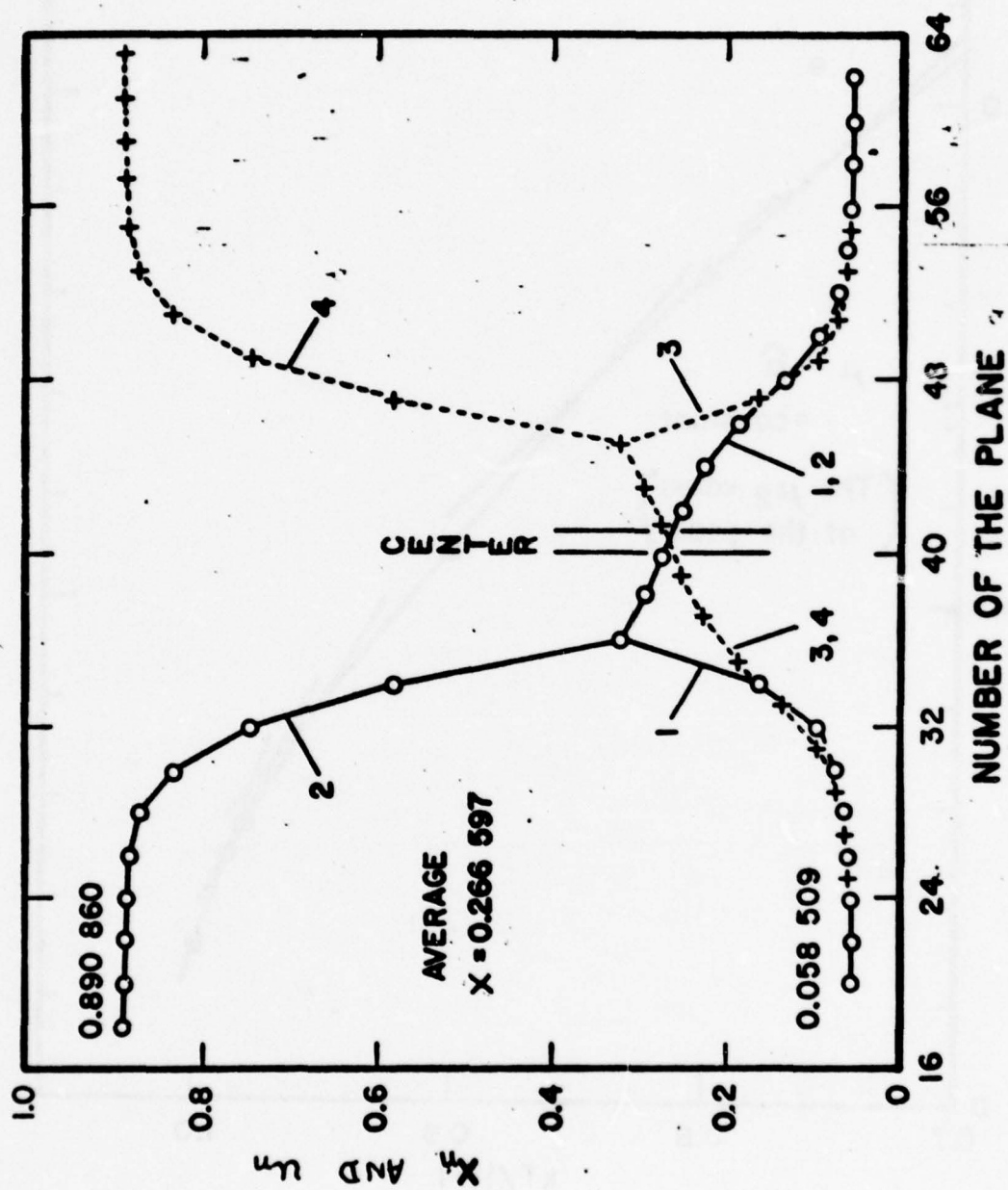
Figure 11a.
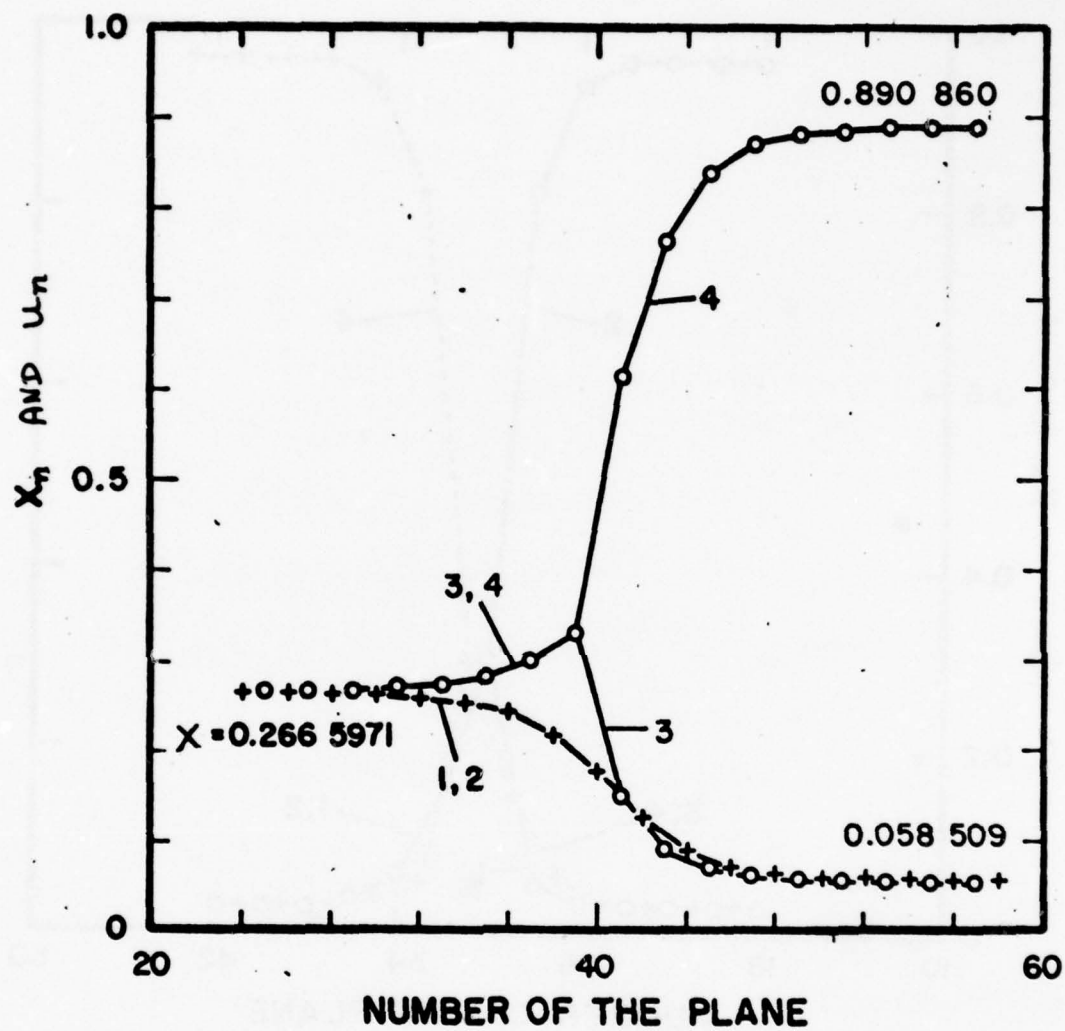
Figure 11b.
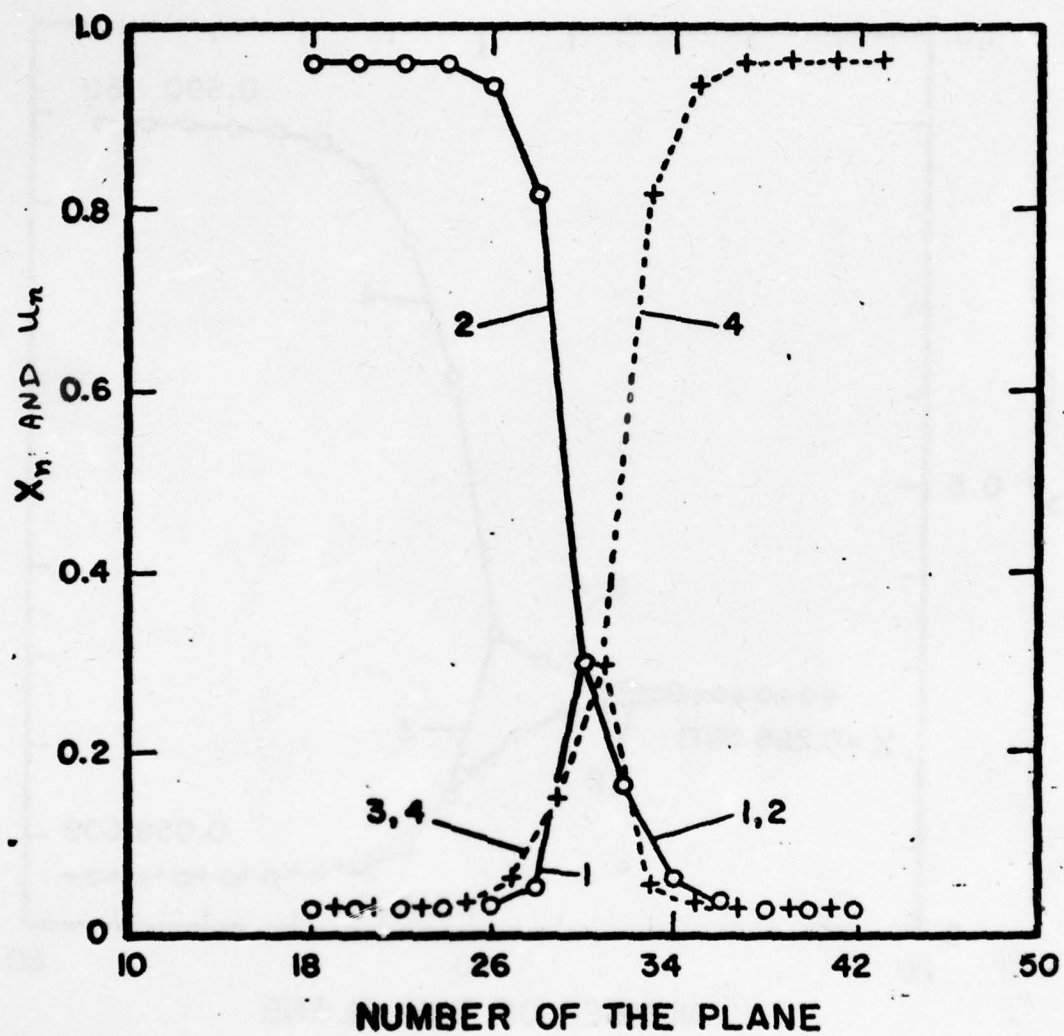
Figure 12a.
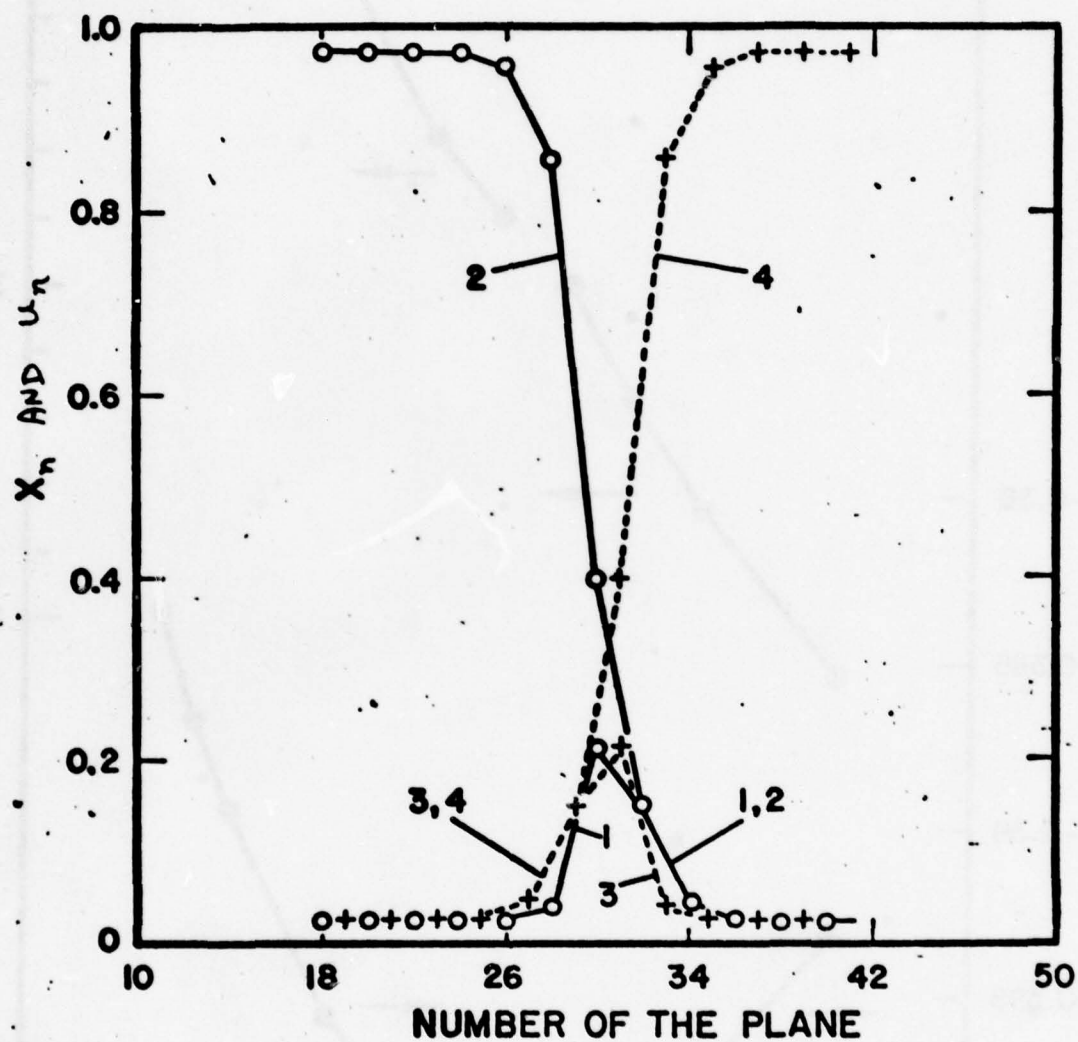
Figure 12b.
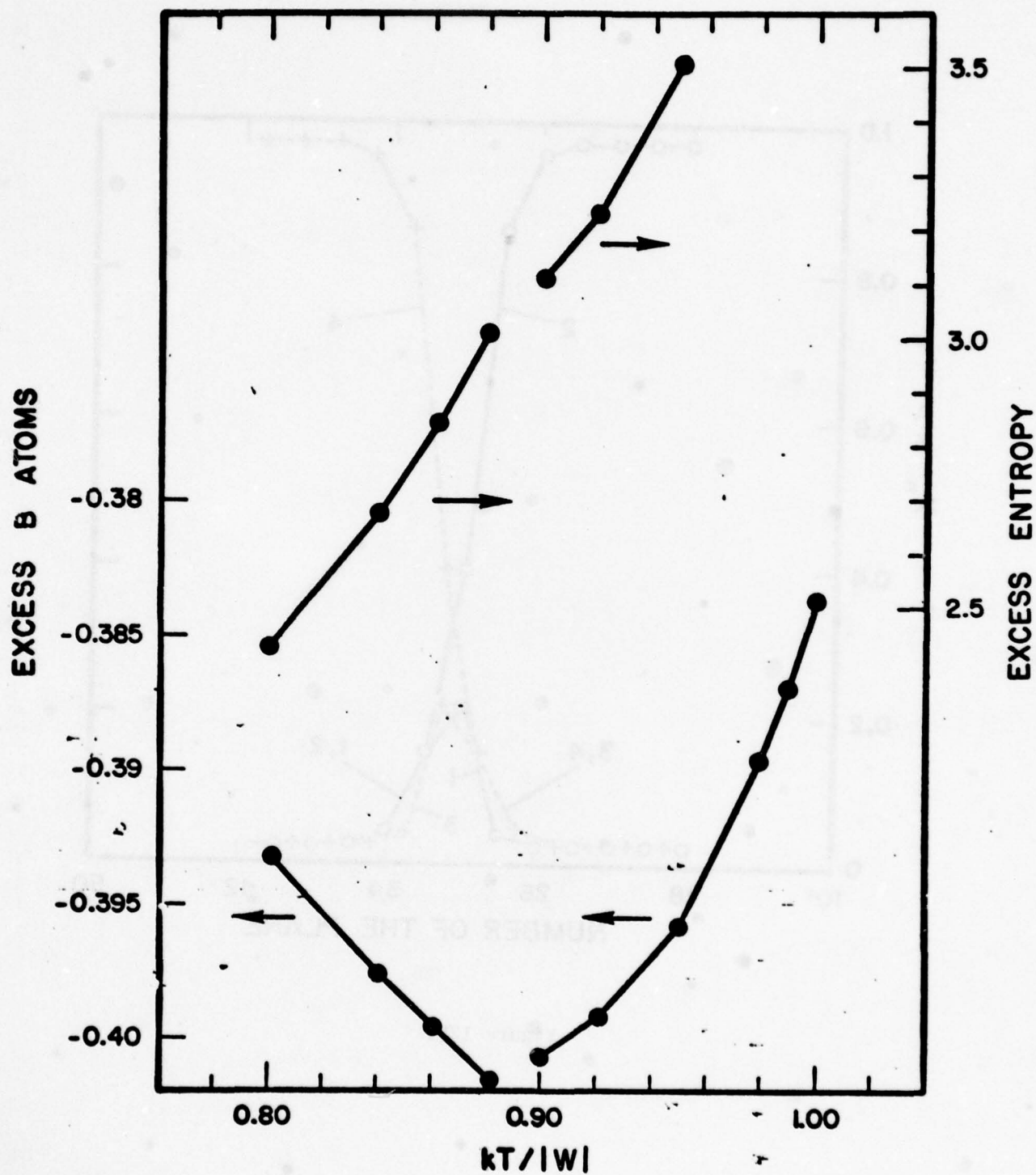
Figure 13.
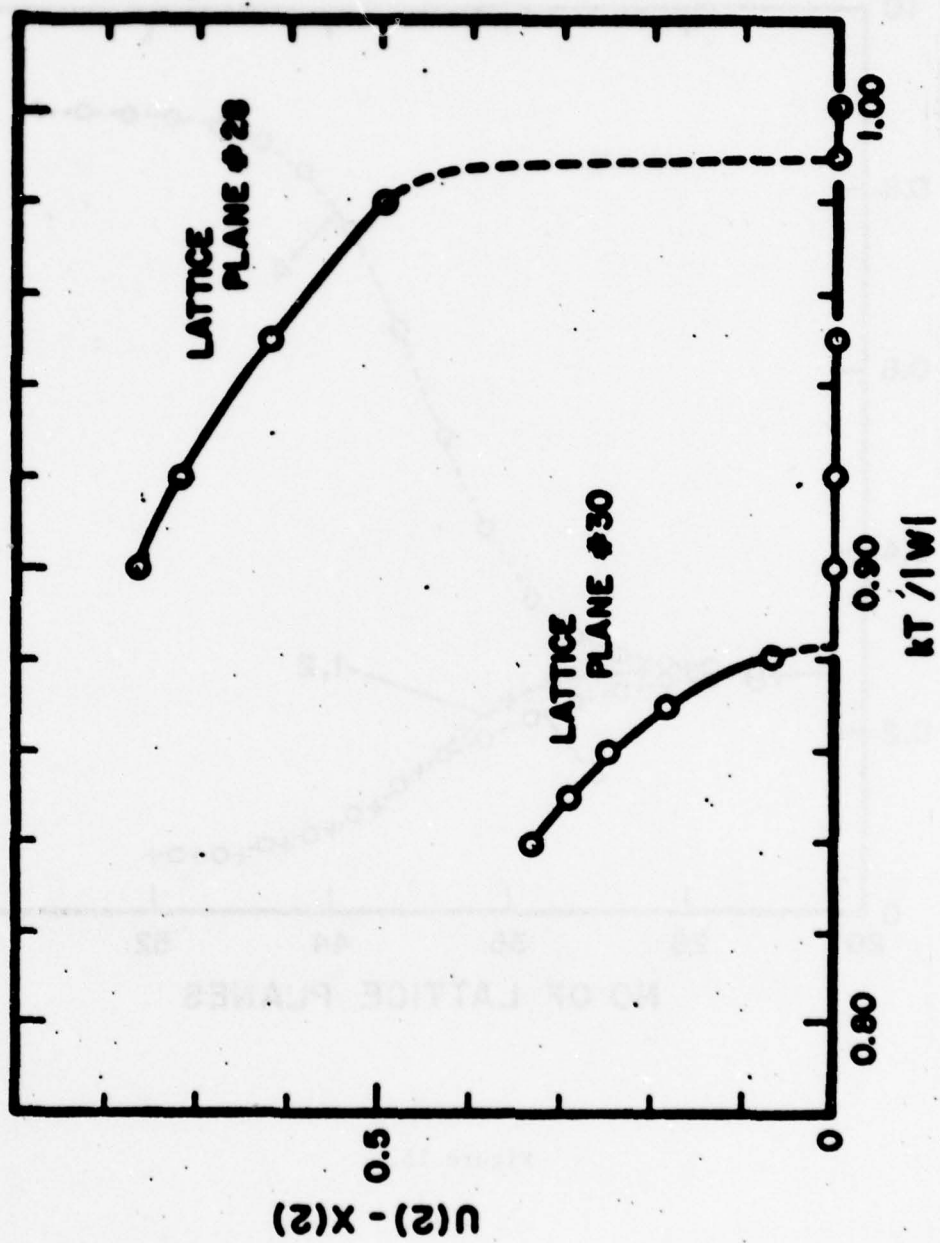
Figure 14.
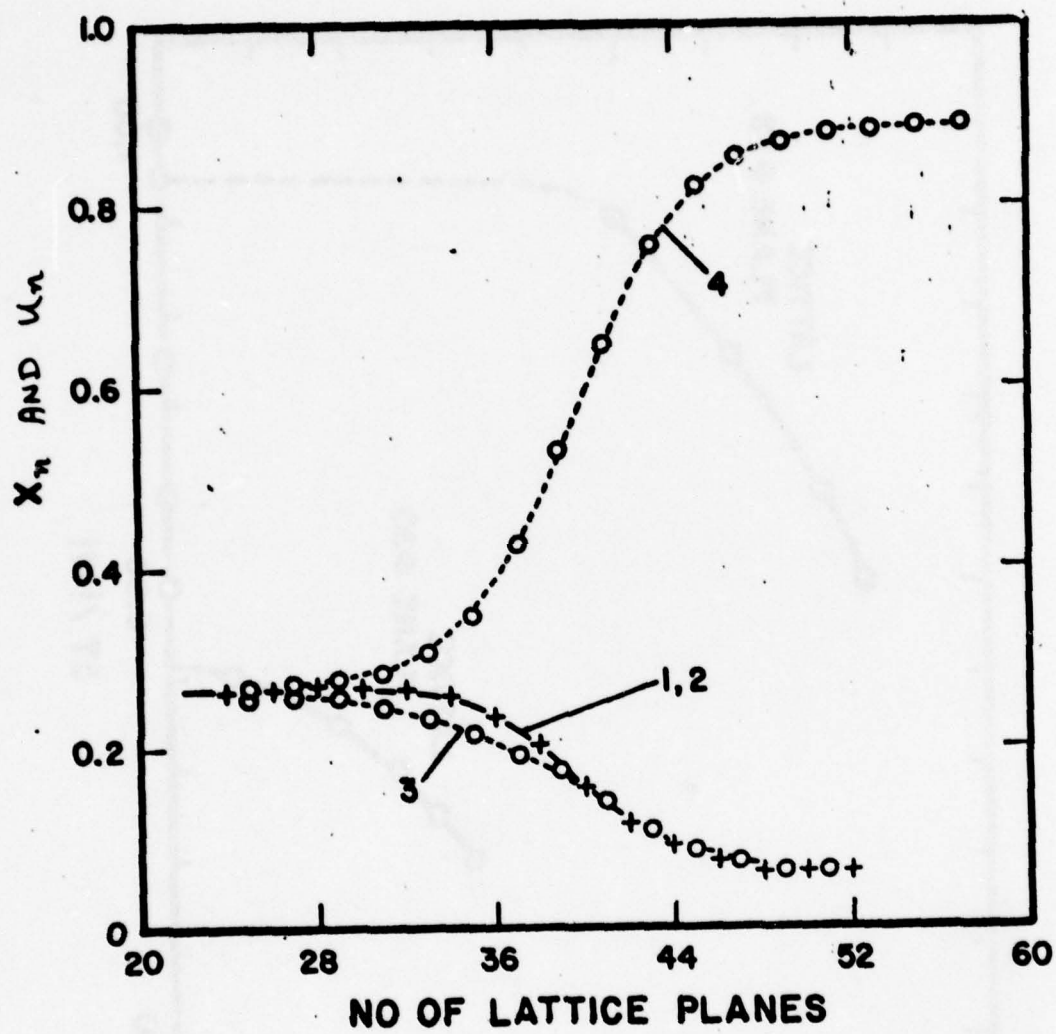
Figure 15.

APPENDIX 6

A TRANSITION IN GRAIN BOUNDARIES

(ANTIPHASE BOUNDARIES) IN A TWO-DIMENSIONAL

LATTICE-GAS MODEL

Ryoichi Kikuchi*

Hughes Research Laboratories
Malibu, California 90265

and

John W. Cahn

National Bureau of Standards
Washington, D. C. 20234

Recent calculations of a two-dimensional lattice gas model has led to vapor, liquid and crystalline phases.[1,2] In addition to permitting the phase transitions to be studied, such a model can be used in studying linear interfaces between all pairs of phases as well as the grain boundary between two crystals of the same solid phase differing in orientation (Figure 1). We report finding a gradual but well defined transition in the grain boundary structure well below the melting point of the crystal; as the transition region is passed, the grain boundary structure changes from its low temperature configuration into such a structure that there is a layer along the grain boundary whose thickness increases to infinity as the logarithm of the undercooling and that the properties of the grain boundary approach that of two solid-liquid interfaces separated by a liquid.

As the melting point is approached, the grain boundary shows a singular behavior in that the excess entropy and the excess specific heat due to the grain boundary (of a unit length) becomes infinite.

Our model is a two-dimensional square lattice gas with interaction potentials chosen to match a prior computer simulation[1]. We used the cluster variation method (CVM)[3] and natural iteration (NI)[4] to calculate the equation of state and the phase diagram. Figure 2 indicates that the phase diagram so calculated matches that obtained by the computer study. The properties of interphase interfaces and the grain boundary shown in Fig. 1 were calculated along the appropriate two-phase coexistence of Fig. 2 and for the grain boundary

between two solid state domains of different orientations as in Fig. 1; the CVM and NI were used as in our previous studies of anti-phase domains boundaries in ordered structures.[5-7] If we consider crystallization model to be an ordering of holes (V) and atoms (A) into a V_4A structure, the grain boundary is indeed a boundary between two ordered domains. It is also a model of domains in an adsorbate layer which can crystallize with a rotation with respect to the underlying substrate.[8,9]

The particular grain boundary in Fig. 1 is a symmetric tilt boundary. With this much tilt a $\Sigma = 5$ coincidence lattice exists in which one in five atoms (e.g., P and P') occupy a site that could belong to either crystal structure. The underlying lattice is known as the DSC lattice.[10] If we let a be the lattice constant of the DSC lattice, the lattice constant of the crystal (as marked by white or black circles in Fig. 1) is $\sqrt{5}$ a.

For the basic cluster in CVM, we used the nine-site cluster shown at the bottom of Fig. 1. Pair of atoms were not allowed closer than AB, the energy of pairs at distances AB and AC was assumed attractive, being respectively -1.2ϵ and $-\epsilon$.[1,2] There is no interaction between atoms further apart than the distance AC. We calculate the equilibrium state of the entire system including the boundary, and obtain the probabilities of encountering each of twenty possible arrangements of atoms on the nine-site clusters centered on each site in a strip of width PP' along the grain boundary and extending from

$j = 1$ to $j = 81$ (sometimes 61 or 41) into each grain. From these cluster probabilities we compute the excess (compared to an equilibrated single crystal) in the grand potential for this strip

$$\sigma = E - TS - \mu N_a \qquad (1)$$

where E is the excess potential energy, T is the absolute temperature, S is the excess entropy, μ is the chemical potential and N_a is the excess number of atoms in the strip of width PP'. We will define the unit length along the boundary to be the distance PP' $= 5\sqrt{2}$ a where a is the lattice constant of the underlying DSC lattice. Thermodynamic self-consistency requires that[11]

$$d\sigma = -SdT - N_a d\mu \qquad (2)$$

which is a useful test for equilibrium[7] and forms the basis for our extrapolation (v.i.).

Fig. 3 shows σ calculated as a function of temperature for $\mu/\epsilon = -1.5$. The low temperature behavior is readily understood by examining Fig. 1. The pair QQ' are forbidden and either site must be empty. For the unit length of the boundary this leads to $S = k \ln 2$, $N_a = -1$ and $E = 5\epsilon_{AB} - \epsilon_{AC}$ at $T = 0$. Hence for low σ

$$\sigma = 5\epsilon + \mu - kT \ln 2 \qquad (3)$$

which agrees with the curve for $kT/\epsilon < 0.3$.

The density profiles perpendicular to the boundary are shown in Fig. 4 for various temperatures. The low temperature W shape near the center of the boundary is consistent with the expectation that the layer on either side of center is half occupied. As the melting

point is approached a low density layer is formed near the center of the boundary and the thickness of the layer approaches our computer capacity. The excess quantities S and $-N_a$ tended to increase without limit as did $-\partial\sigma/\partial T$ as the melting point is approached.

Figure 5 plots S vs. $-\log(T_m-T)$. For $\mu/\epsilon = -1.5$, T_m is 0.71629 ϵ/k. It is observed that the curve in Figure 5 is made of two distinctly different portions. For low temperatures ($kT/\epsilon<0.20$), we see

$$S \simeq k \ln 2 \qquad (4)$$

for high temperatures ($kT/\epsilon>0.45$), S is linear in $\log(T_m-T)$ as

$$S = -3.681 - 4.1520 \ln(T_m-T) \qquad (5)$$

Making use of these relations for S in Figure 5, we can integrate $\int SdT$ to obtain the estimate of $\sigma(T)$ for the high temperature region:

$$\sigma_{HT} = 1.523 - (T_m-T)\left[-0.471 + 4.152 \ln(T_m-T)\right] \qquad (6)$$

This is shown as a solid curve in Fig. 3.

The good agreement between the solid curve σ_{HT} and individually computed σ values indicated by dots shown in Fig. 3 serves as a test of Eg. (2), the self-consistency of the formulation, but it also permits extrapolation of σ to the melting temperature where its value is 1.523.

We separately calculated the solid-melt interfacial properties for the orientation corresponding to that of our grain boundary. The value of its reduced σ was found to be 0.763, while its density profile closely matched that of either half of the grain boundary.

We concluded not only that the grain boundary has become a melted layer at the melting point, but that it behaves as if it is coated with a melted layer for a considerable temperature interval below the melting point. At some temperature near $0.35\epsilon/k$ there is a gradual transition in structure from the low temperature profile to a structure which with increasing temperature increasingly tends to resemble a melted layer and which exhibits a singularity as T_m is approached. Since the grain boundary is completely wet at T_m, it is legitimate to call the gradual transition near $T = 0.35\epsilon/k$ the wetting transition.

The possibility that a grain boundary would have a liquid layer at the melting point was first discussed by Gibbs.[12] Whenever σ for the grain boundary has a tendency to exceed twice the σ for the solid-liquid interface, the transition we found is expected to occur. Smith[13] attempted to formulate the temperature behavior of this transition by comparing two models of the grain boundary. The solid model was assumed to possess a known value of σ. The value of σ for the melted layer model was assumed to consist of three terms

$$\sigma_{ML} = 2\sigma_{SL} + \lambda\Delta S(T_m-T) + E(\lambda) \qquad (7)$$

where $2\sigma_{SL}$ is the contribution of the two solid-melt interfaces, $\lambda\Delta S(T_m-T)$ is the contribution of a melted layer of thickness λ, ΔS is the entropy of fusion, and $E(\lambda)$ is an unknown repulsive energy. If $2\sigma_{SL}$ was less than σ, the melted layer took over. Minimizing σ_{ML} with respect to λ at a fixed temperature we obtain a relation for λ

$$DE/d\lambda + \Delta S(T_m-T) = 0 \qquad (8)$$

When this relation holds, and when σ_{SL} and ΔS are assumed independent of temperature, we can further obtain

$$d\sigma_{ML}/dT = -\lambda \Delta S \tag{9}$$

Since this derivative is -S, our finding in Fig. 5 and Eq. (5) implies that λ linearly depends on $-\ln(T_m-T)$, and integration of Eq. (8) leads to an expression:

$$E(\lambda) = E(0) + C_1 \exp(-C_2\lambda) \tag{10}$$

This indicates the reasonable nature of the repulsive term in Smith's formulation (7). When we use these relations, we can write the temperature dependence of σ_{ML} in (7) in the form

$$\sigma_{ML} = 2\sigma_{SL} - (T_m-T)\left[C_3 + C_4 \ln(T_m-T)\right] \tag{11}$$

which has the name (T_m-T)-dependence as (6).

In the present paper, we used a two-dimensional lattice gas-liquid-solid model, and thus the grain boundary is essentially one-dimensional. This one-dimensional behavior is consistent with the nature of the gradual transition from the low-temperature behavior to the high-temperature behavior demonstrated clearly in Fig. 5. If we work on a three-dimensional system with a two-dimensional grain boundary, it is expected that the nature of the low- to high-temperature behavior may be a sharper one; for example, a second-order phase transition.

A melting transition in real metals has been observed[14] as a function of orientation difference and explained in terms of a dislocation model with liquid cores.[15] The temperature dependence of such a model might show several transitions.

References

1. J. Orban, J. van Craen and A. Bellmans, J. Chem. Phys. $\underline{49}$, 1778 (1968)

2. R. Kikuchi, J. Chem. Phys. $\underline{68}$, 119 (1978)

3. R. Kikuchi, J. de Phys. $\underline{38}$, C7-307 (1977)

4. R. Kikuchi, J. Chem. Phys. $\underline{60}$, 1071 (1974)

5. J. W. Cahn and R. Kikuchi, J. Phys. Chem. Solids, $\underline{20}$, 94 (1961); $\underline{27}$, 1305 (1966)

6. R. Kikuchi and J. W. Cahm, J. Phys. Chem. Solids, $\underline{23}$, 137 (1962)

7. R. Kikuchi and J. W. Cahn, "Theory of Interphase and Antiphase Boundaries in F. c.c. Alloys," Acta Met. (in press). The Appendix 5 in this report.

8. J. M. Blakeley, Chapter in "Interphasial Segregation," Am. Soc. Metals, Metals Park, Ohio 1977

9. M. G. Lagally, G.-C. Wang and T.-M. Lu, Critical Reviews and Solid State and Material Sciences $\underline{7}$, 233 (1978)

10. W. Bollmann, "Crystal Defects and Crystalline Interfaces," Springer Verlag, New York and Berlin, 1970

11. J. W. Cahn, Chapter in "Interphasial Segregation" Am. Soc. Metals, Metals Park, Ohio 1977

12. J. W. Gibbs, "The Collected Works," Vol. I, Footnote on p.320. Yale University Press, New Haven 1957

13. C. S. Smith, Trans. Am. Soc. Metals $\underline{45}$, 533 (1953)

14. M. E. Glicksman and R. Masumura, Met. Trans. $\underline{8A}$, 1373 (1977)

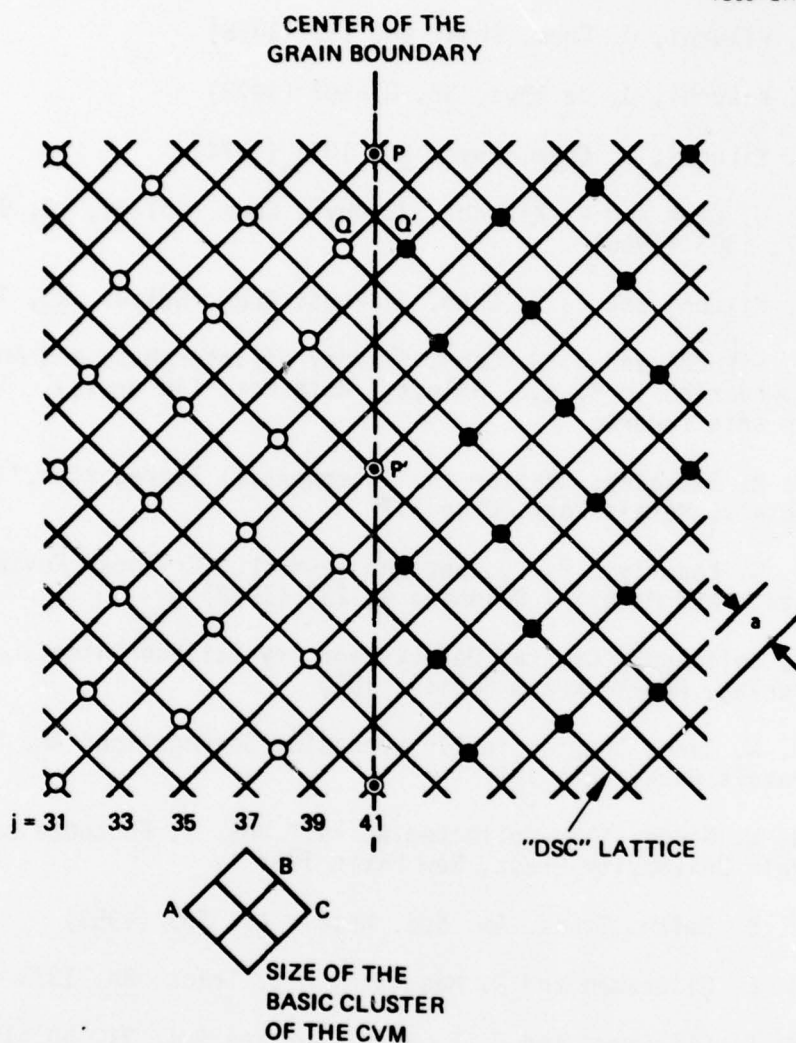15. M. E. Glicksman and C. E. Vold, Surface Sci. $\underline{31}$, 50 (1972)

Figure 1. A two-dimensional model of a grain boundary. Position of atoms in the crystalline state are shown by circles. This illustration is the unrelaxed state, and thus is schematic.
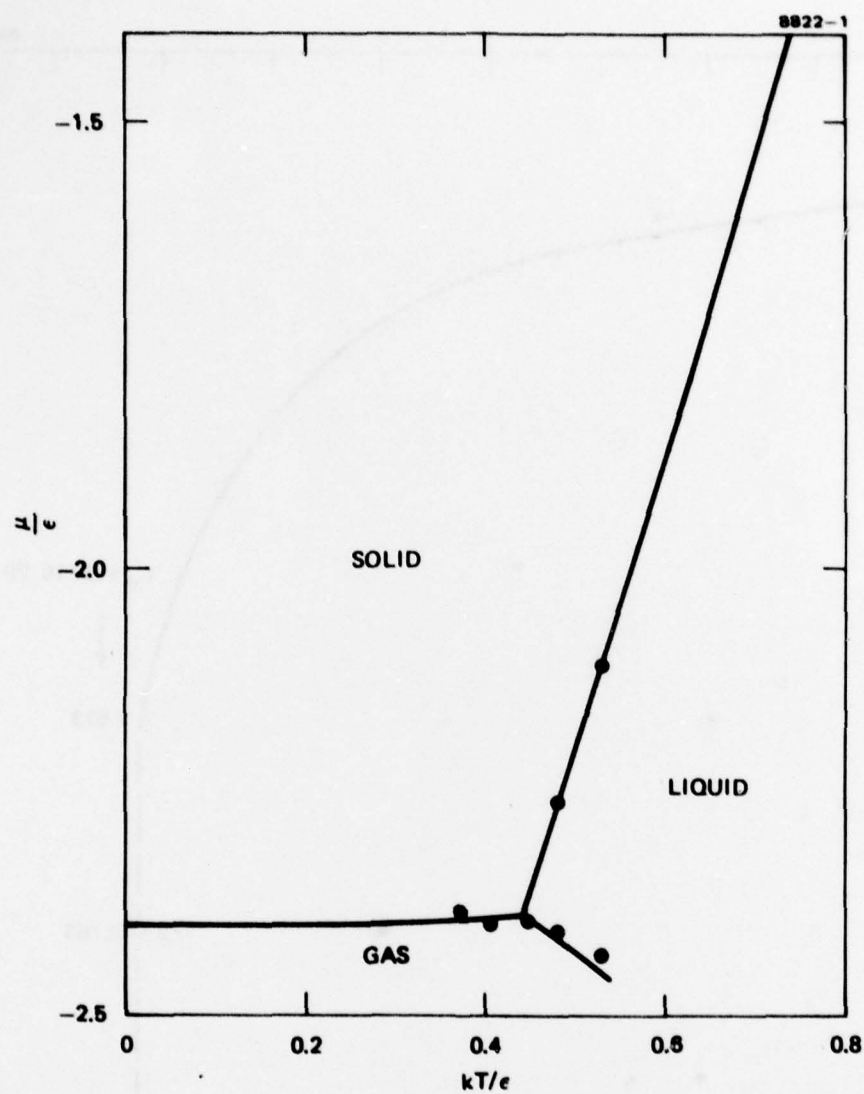
Figure 2.   The equation of state (μ versus T) of the homo-
geneous phases derived from the present model.
Black circles are the values obtained by the
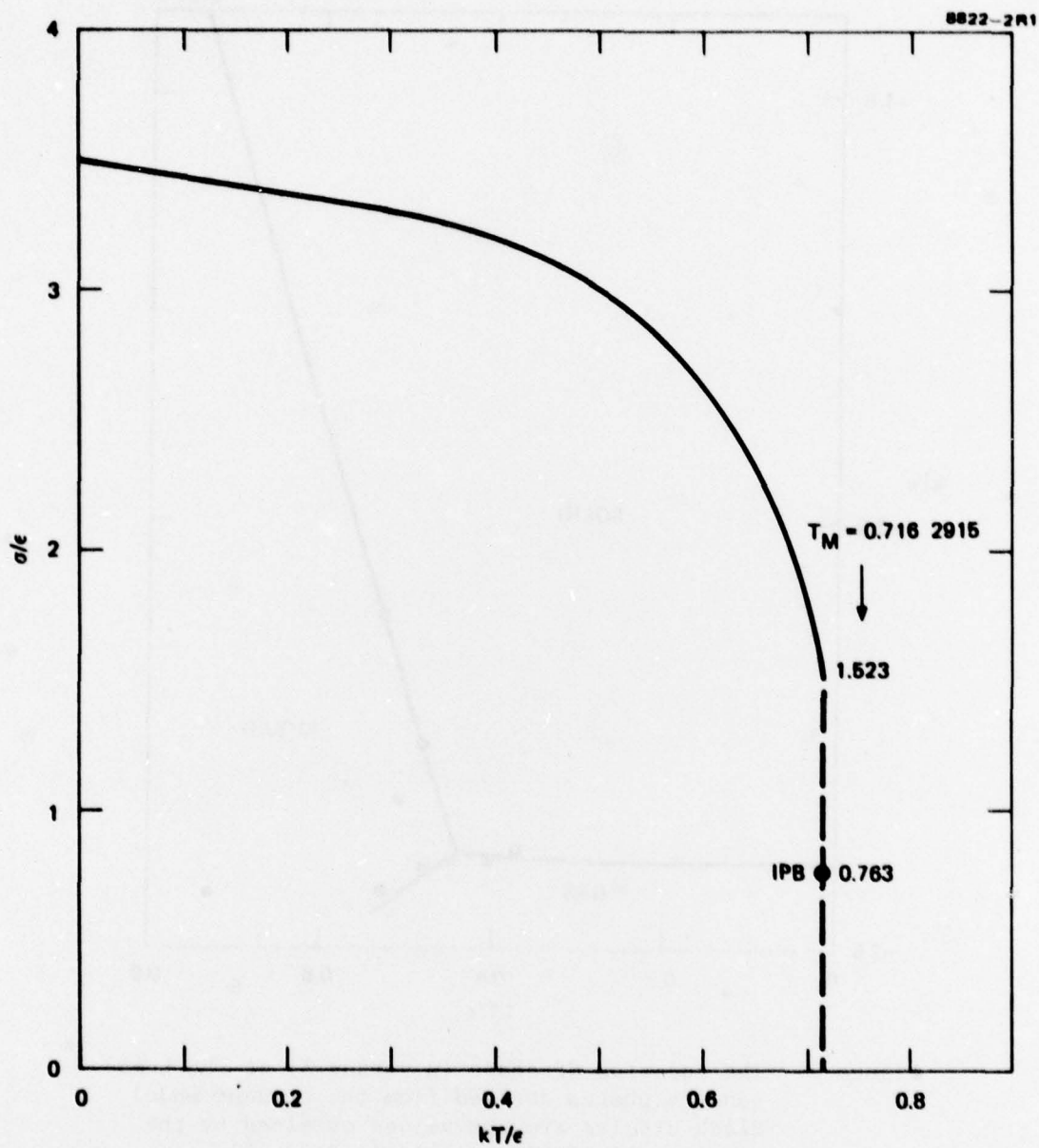computer simulation method in Ref. [1].

Figure 3. The σ versus T of the present work for μ/ε = -1.5. The point marked IPB is the σ for the solid-liquid inter-phase boundary at the melting temperature.

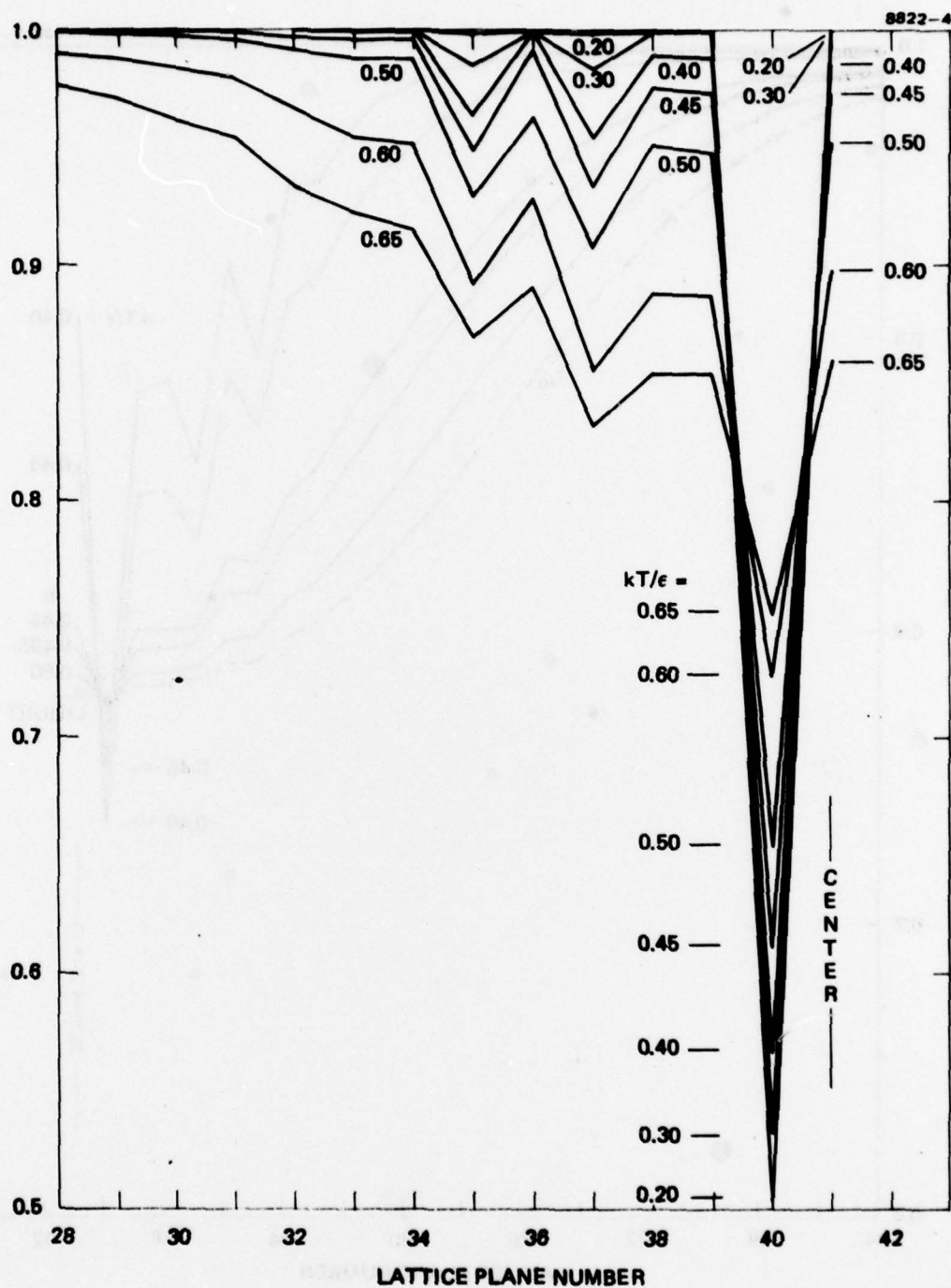Figure 4(a). Density profile across the grain boundary. The center of the boundary is chosen at the 41st lattice plane. The profile is repeated on the right of the 41st plane as a mirror image. $\mu/\epsilon = -1.5$ and starts from a very low temperature.
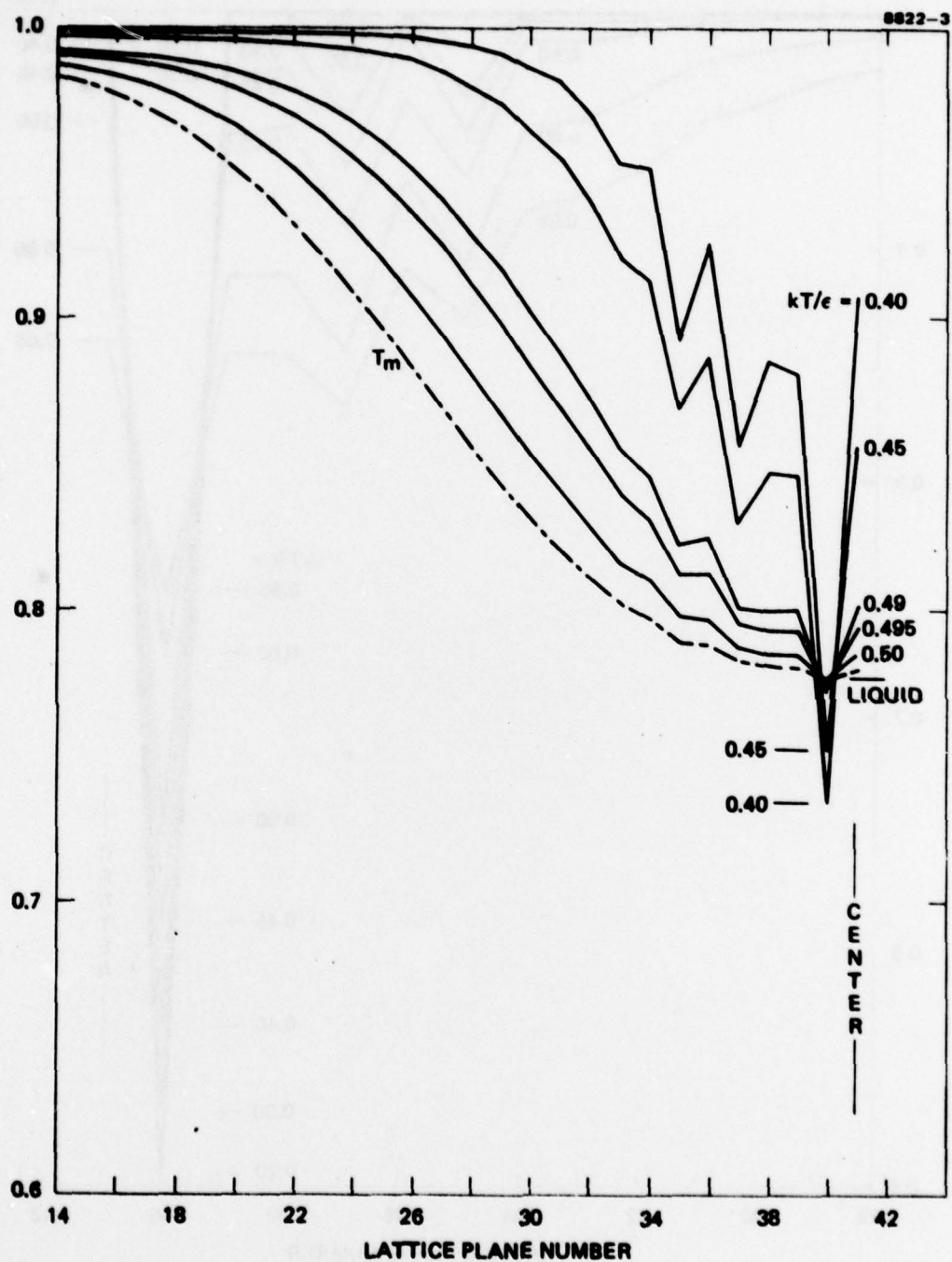
Figure 4(b). Density profile across the grain boundary. The center of the boundary is chosen at the 41st lattice plane. The profile is repeated on the right of the 41st plane as a mirror image. $\mu/\epsilon = -2.2$ and shows how the profile changes near the melting temperature ($T_m = 0.5031638$). The curve for T_m is for an intermediate stage of convergence.
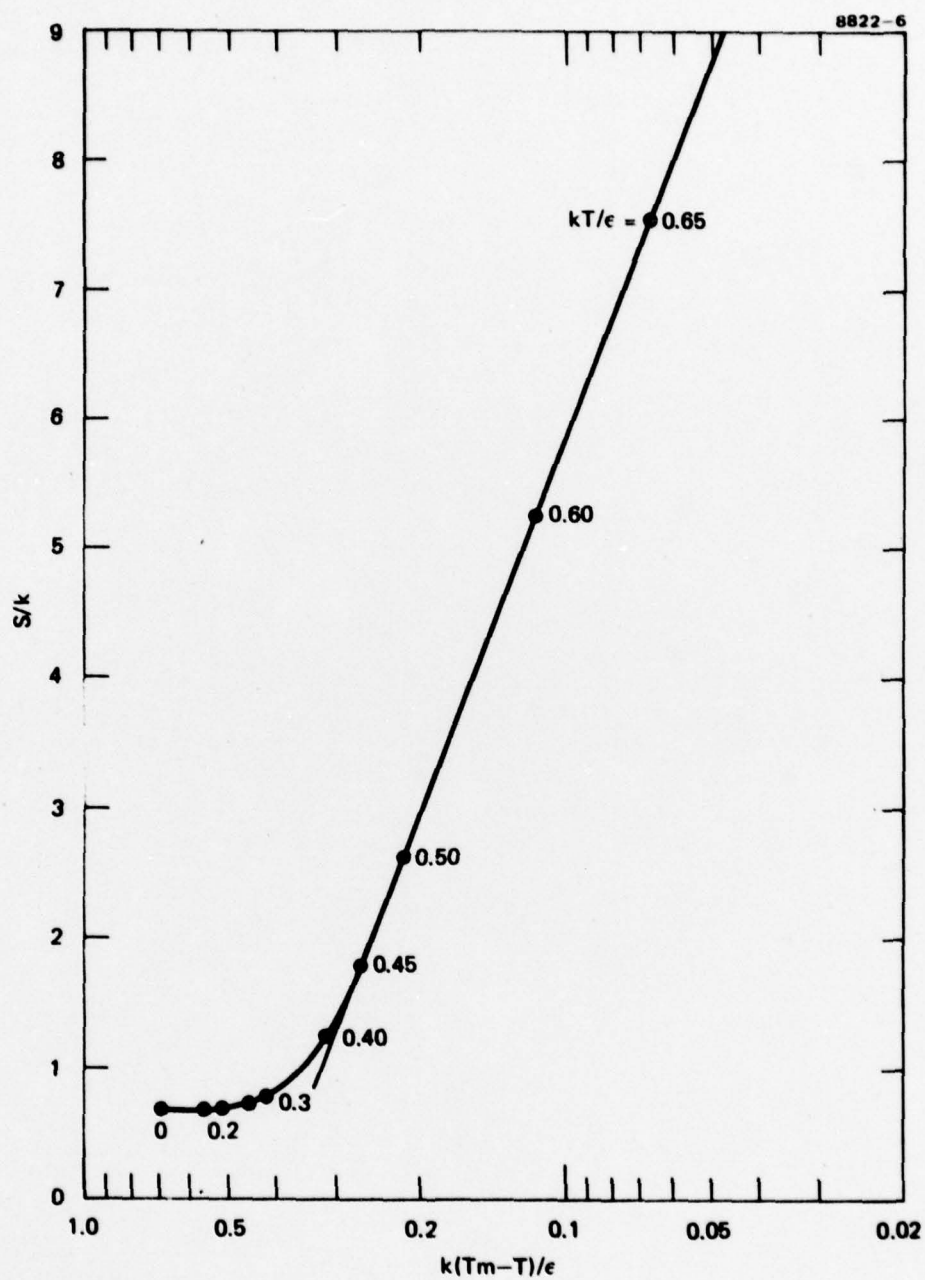
Figure 5. The excess entropy S of the present work plotted against $-\log(T_m - T)$.